Fabrication and Utilisation of Solid-phase Microdroplet Arrays for Nucleic Acid Detection and Other Applications

Department of Micro- and Nanotechnology

Marie Louise Laub Busk, March 2019

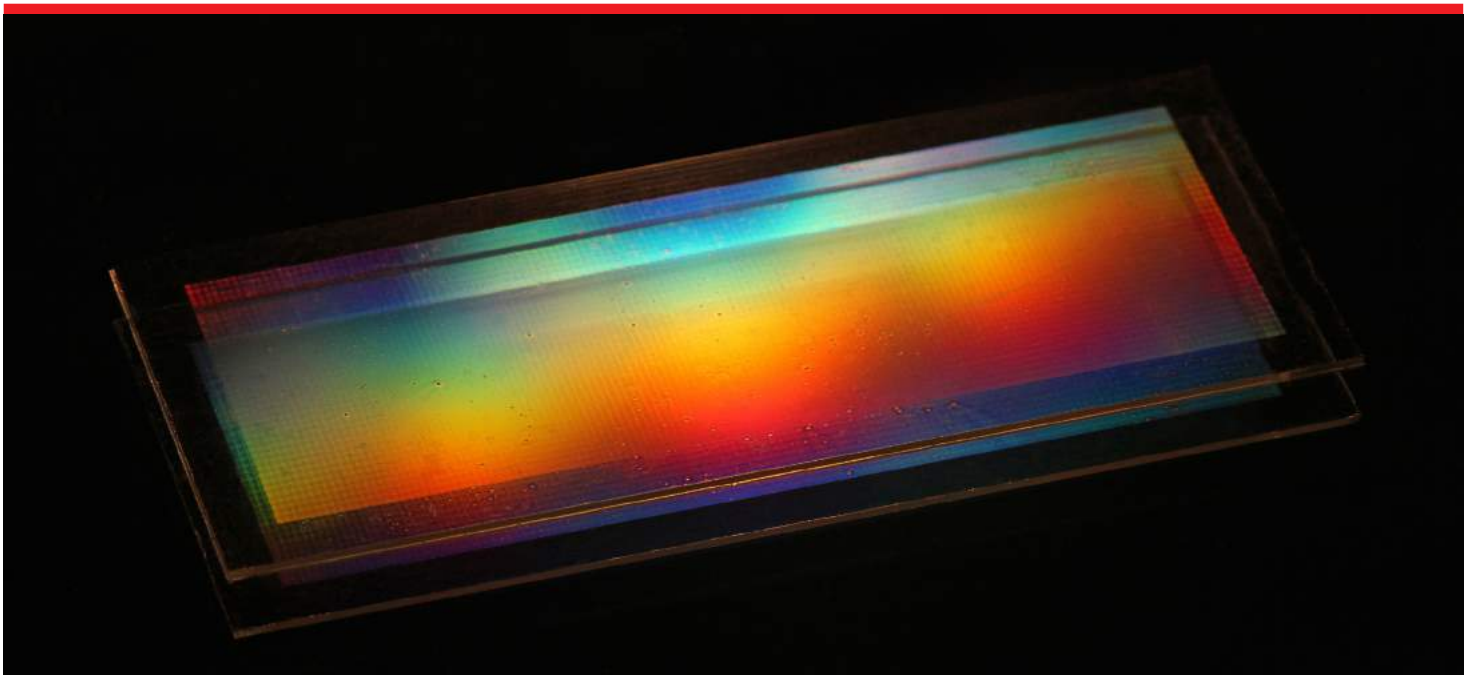

Supervisors:

Associate Professor Martin Dufva - DTU Nanotech

Andreas Kunding - SELMA Diagnostics ApS, DTU (former)

MD Inge Høgh Dufva - Herlev Hospital (former)

DTU Health Tech
Department of Health Technology

"If I have seen further, it is by standing on the shoulders of giants."

Sir Isaac Newton
Letter, February 5th, 1676

Front page figure:
Photograph of a micro droplet array fabricated using a fluorinated acrylate polymer.

Summary

Microdroplet arrays involves the compartmentalisation of biological or chemical reactions in hundreds of thousands of single compartments spatially distributed in 2D on a surface, for example a glass substrate. These compartments are so small that single molecules or cells can be encapsulated and interrogated. This can be used to study the heterogeneity of populations not possible by traditional methods. Reactions with single molecules in these droplets are detected, and precise quantification of the molecules can be achieved by counting the number of partitions eliciting a signal. This has, for example, enabled the sensitive detection of proteins by digital immunoassay, improving the limit of detection by three orders of magnitude compared to conventional, analogue methods.

This study concerned the development of a versatile microdroplet array platform. The thesis is comprised of three major parts.

The first part includes a numerical analysis of the hybridisation of DNA targets in low concentrations on planar biosensors, an overview of protein and DNA immobilisation on glass subtrates, the description of an optical detection set-up, as well as the design and fabrication of the liquid infrastructure surrounding the droplet arrays. The numerical analysis predicted a limit of detection of 2 aM for the detection of gene transcripts on MDAs, and showed that the process was highly diffusion limited, and that the greatest improvement to the number of molecules caught on the surface was seen by increasing the screened sample volume, something which is not possible or practical using current golden standard techniques for nucleic acid quantification.

The second part described the fabrication of a droplet array based on the deposition of the teflon-like, hydrophobic compound, FDTS. Microfluidics integrated arrays were capable of supporting 50 fL droplets surrounded by air for several hours with minimal evaporation, which greatly increase the number of possible applications of the platform. On this array, digital ELISA and cell-free protein expression was conducted. Digital ELISA reached a limit of detection around 10 fM, and was capable of splitting a patient cohort in two groups based on the concentration of Aβ_{1-42}, a biomarker for Alzheimer's disease. In the second example, proteins were directly synthesised from a single copy template DNA and immobilised in the droplets. Subsequent detection of the synthesised proteins was carried out by antibody recognition.

The third and last part of the thesis described the characterisation of the process parameters, and the fabrication of a droplet array by the direct patterning of a UV cross-linkable fluoropolymer. Immobilisation of streptavidin selectively in the droplet spots was demonstrated by binding fluorescently labelled proteins on the array functionalised with reactive epoxy groups. Secondly, streptavidin coated microspheres (beads) were immobilised on the spots and DNA hybridisation on the beads was demonstrated.

Resumé

Mikrodråbe arrays inddeler biologiske eller kemiske reaktioner i hundredetusindvis af enkelte partitioner fordelt på en todimensionel overflade, eksempelvis et glas substrat. Partitionerne er så små at enkelte molekyler kan fanges og undersøges i dråberne. Dette kan bruges til at studere heterogeniteten af hele populationer af molekyler, hvilket ikke er muligt med mange traditionelle metoder. Reaktionerne med enkeltmolekylerne i disse dråber detekteres og den præcise kvantificering af molekylerne opnås ved at tælle antallet af partitioner der fremkalder et signal. Dette har for eksempel gjort det muligt at detektere proteiner ved hjælp af digitale immunassays, hvilket har forbedret detektionsgrænsen tre størrelsesordener i forhold til den konventionelle, analoge metode.

Dette studie havde som mål at udvikle en alsidig mikrodråbe platform. Selve afhandlingen er inddelt i tre dele.

Den første del omhandler den numeriske analyse af hybridiseringen af DNA molekyler ved lave koncentrationer på plane biosensor overflader, et overblik over forskellige metoder til at immobilisere DNA og proteiner på glas, en beskrivelse af en optisk detektionsplatform, og designet og fabrikationen af mikrofluide komponenter til at håndtere væsketransport til og fra dråbe arrayet. Den numeriske analyse estimerede detektionsgrænsen for genetiske transkripter til at være 2 aM på dette dråbe array. Derudover viste analysen, at processen var diffusionsbegrænset, og at den største stigning i antal fangede molekyler kunne opnås ved at undersøge et større prøvevolumen. Dette er ikke ligefremt at opnå med konventionelle metoder.

Anden del omhandler fabrikationen af et dråbe array der er baseret på overflade deponeringen af det teflon-lignende kemikalie, FDTS. Dråbe arrays integreret i mikrofluide kanaler kunne understøtte 50 fL store dråber i mange timer i luft uden tegn på udbredt fordampning. Dette øger muligheden for anvendelserne af denne platform. Som applikationer blev digital ELISA og celle-fri protein ekspression demonstreret. Digital ELISA opnåede en detektionsgrænse omkring 10 fM, og kunne identificere to grupper fra patient prøver baseret på koncentrationen af $A\beta_{1-42}$, der er en biomarkør for Alzheimers sygdom. I det andet eksempel blev proteiner syntetiseret fra enkelte molekyler af kodende DNA og immobiliseret direkte i dråberne. Dernæst kunne proteinerne detekteres ved hjælp af antistofgenkendelse.

Den tredje og sidste del af afhandlingen beskriver karakteriseringen af proces parametrene og fabrikationen af et dråbe array baseret på den direkte strukturering af en UV krydslinkende fluoropolymer. Selektiviteten af protein immobilisering til den eksponerede glas overflade blev vist ved at immobilisere fluorescerende Streptavidin på arrayet der var funktionaliseret med reaktive epoxy-grupper. Derefter blev Streptavidin funktionaliserede mikrosfærer (beads) immobiliseret i dråberne og hybridiseringen af DNA til på disse beads blev demonstreret.

Preface

This thesis titled "Fabrication and Utilisation of Solid-phase Microdroplet Arrays for Nucleic Acid Detection and Other Applications" describes the results of a study carried out at the Technical University of Denmark, Department of Micro- and Nanotechnology in the Fluidic Array Systems and Technology research group in fulfilment of the requirements for acquiring the Ph.D. degree. The work was carried out in the period from March 2015 to January 2019. The Ph.D. study was interrupted for 9 months due to maternity leave in September 2016. The project was supervised by Associate Professor Martin Dufva (DTU Nanotech) in cooperation with Researcher Andreas Hjarne Kunding (DTU Nanotech, now SELMA Diagnostics ApS) and MD Inge Høgh Dufva (Herlev University Hospital Copenhagen).

The study was funded by the FP7 NAnosystems for early DIagnosis of NEurodegenerative diseases (NADINE) project for the first six months, and continued by financial support from the Technical University of Denmark.

Acknowledgements

First and foremost, I wish to thank my supervisor, Martin Dufva. It is solely due to his great mentoring that I embarked on this journey to begin with. It has been the greatest pleasure to take part in his interesting ideas and exciting work. Martin is always a supportive supervisor, in good times and when times are challenging, so thank you very much, it has been a pleasure.

Next, I would like to thank my co-supervisors, Andreas Kunding and Inge Høgh Dufva, who have helped shape the project. Andreas has been helpful introducing me to the concepts of solid phase droplet microfluidics in the lab, and Inge Høgh Dufva has provided me with an interesting medical problem to help overcome. This has made me feel that my work had a purpose. Thank you for inviting me to interesting talks at the hospital, it really gave me a perspective.

I would also like to thank everyone who has been in the FAST group during my studies. Each and everyone of you have been amazing colleagues, making sure that coming to work every day was a pleasure. In particular, I wish to thank Thomas Glasdam Jensen, who has helped me learning and improving my skills with LabView, and many other practical things, without whom I would never have come so far with my set up.

A very special thanks goes to my colleague Arianna Toppi. She is not just a colleague, she quickly became my friend, and working together with her has been the greatest motivation. She has made my last year and a half a very special time at DTU. So, grazie, sei un amore!

Additionally I would like to thank DTU Nanotech for supporting my studies, as well as the FP7 Nadine project for funding the first six months.

Last but not least, I wish to thank my family and friends for supporting me and always being here for me. I want to thank my mom for teaching me creativity, and my dad for inspiring my interests in science and engineering. Also, heartfelt thanks to my very dear friend, Freja. Thank you for your words of wisdom on the process of obtaining a Ph.D. degree.

And Mikkel. Thank you for always being by my side no matter what.

Contents

List of Figures

List of Tables

List of Abbreviations

Page	Abbreviation	Explanation
3	FEM	Finite Element Method
	ELISA	Enzyme-Linked ImmunoSorbent Assay
	PCR	Polymerase Chain Reaction
4	MDA	MicroDroplet Array
5	PDMS	PolyDiMethylSiloxane
	COC	Cyclic Olefin Copolymer
7	FISH	Fluorescence In-Situ Hybridisation
	CML	Chronic Myeloid Leukaemia
8	qPCR	Quantitative Polymerase Chain Reaction
10	SNP	Single Nucleotide Polymorphisms
11	ddNTP	Dideoxynucleotides
	dNTP	Deoxynucleotide
	NGS	Next-Generation Sequencing
15	HT-NGS	High-Throughput Next-Generation Sequencing
16	Ph (chromosome)	Philadelphia (chromosome)
	TKI	Tyrosine Kinase Inhibitor
	RT-qPCR	Reverse Transcription quantitative Polymerase Chain Reaction
24	PDE	Partial Differential Equation
40	EDC	1-Ethyl-3-(3-Dimethylaminopropyl)Carbodiimide
41	PEG	PolyEthylene Glycol
42	NTA	NitriloTriacetic Acid
	NHS	N-Hydroxysuccinimide
	PDITC	p-Phenylene diisothiocyanate
	PLL	Poly-L-Lysine
43	PBS	Phosphate Bufferes Saline
	MES	2-(N-Morpholino)ethanesulfonic acid
45	FDTS	Perfluorodecyltrichlorosilane
51	LED	Light Emitting Diode
54	PMMA	Poly(methyl methacrylate)
	PTFE	Polytetrafluoroethylene
55	(G)UI	(Graphical) User Interface
64	CNC	Computer Numerical Control
	PSA	Pressure Sensitive Adhesive
75	HMDS	Hexamethyldisilazane
76	TMAH	Tetramethylammonium hydroxide

	MVD	Molecular Vapor Deposition
84	HRP	Horseradish Peroxidase
	AFR	Ampliflu Red
86	CSF	Cerebrospinal Fluid
89	FFT	Fast Fourier Transform
94	HA	(Influenza) Hemagglutinin
	SOX2	SRY (sex determining region Y)-box 2
95	BSA	Bovine Serum Albumin
105	CAD	Computer-aided Design
	NMP	N-Methylpyrrolidone
109	SEM	Scanning Electron Microscopy
113	GFP	Green Fluorescent Protein
119	SSC	Saline sodium citrate
	TEG	Tetraethylene Glycol

List of Publications

Copies of each contribution can be found in Appendix D at the end of this thesis.

Peer-reviewed papers

1. Andreas H. Kunding, ***Louise L. Busk***, Helen Webb, Hans W. Klafki, Markus Otto, Jörg P. Kutter and Martin Dufva, *Lab on a Chip*, 2018 16, *Micro-droplet arrays for micro-compartmentalization using an air/water interface.*

Conference attendances

1. Poster presentation: A Multistep Cell-free Protein Expression and Detection Assay on Microdroplet Arrays, ***Louise L. Busk*** and Martin Dufva. Micro and Nanoengineering, 44th International Conference, Copenhagen September 24-27 2018.
2. Poster presentation: Cheap fabrication of solid phase droplet microfluidics chips for single molecule studies, ***Louise L. Busk*** and Martin Dufva. Lab-on-a-Chip and Microfluidics World Congress, San Diego, CA October 1-3 2018.

Part I

Introduction, Theory, and Technologies Surrounding Microdroplet Arrays

1 Introduction

The first part of this thesis aims at introducing the reader to the background and theory related to droplet microfluidics and digital assays. In Chapter 1, the motivation for droplet microfluidics and digital assays is presented, in particular as a tool for nucleic acid detection, ended by a presentation of the hypothesis of the thesis. In Chapter 2, nucleic acid hybridisation on biochips is discussed and substantiated through numerical simulations using the Finite Element Method (FEM). In Chapter 3, the immobilisation of biomolecules on glass substrates is discussed, which is commonly used to add specificity to the detection of target molecules. In Chapter 4, fluorescence detection and an optical platform for fluorescence detection is presented. Lastly, in Chapter 5, the fabrication of the microfluidic interface surrounding the microdroplet array is discussed, which enables the delivery of different regents onto the microdroplet array.

1.1 Droplet Microfluidics and Digital Counting

Compartmentalisation of reactions has been a useful tool in biology since the invention of the microtitre plate. Indeed, miniaturisation has been the hallmark of technological development. In electronics and computing, the rapid growth of the number of transistors per area has been described in Moore's law, which predict that the number of transistors in an integrated circuit doubles every 18 months. In chemistry and biology, reaction volumes has been decreased from millilitres in reaction tubes to micro-litres in microtitre plates, driving higher throughput, cost reduction, increased reaction speed, and greater sensitivity and specificity.[1, 2, 3]

Traditionally, quantification of molecules has been achieved by comparing the signal from a sample to a standard curve, where signal strength is proportional to target concentration. This has been used extensively in enzyme linked immunosorbent assays (ELISA). One issue, however, is the production of a standard which is purified and quantified while also retaining the function of the molecule and the ability to elicit a signal in the assay without inhibition from conformation or external molecules. Another issue to be addressed in molecular biology is the problem of detection limits or how many molecules it require to elicit a detectable signal. As an example, traditional ELISA has a detection limit around 1 pM.[4] In a 96 well plate, the typical volume of the reaction is around 100 μL, meaning that at least $6 \cdot 10^7$ molecules are required in order to detect a signal. On the other hand, quantitative Polymerase chain reaction (PCR) for the detection of DNA will undoubtedly produce a signal in case an intact target molecule is present in the sample.[5] However, the volume of sample analysed in a PCR reaction is small, 10 μL, and is taken from a larger sample. Ensuring that this one target molecule is reproducibly selected in the aliquot entering the reaction is the main issue, and in reality, the detection limit is rather around 5 molecules in

a 10 μL sample in order to ensure a low probability (p<1%) of obtaining a sample containing 0 molecules, calculated by the application of Poisson statistics.

For very sensitive applications, making compartments so small that single molecules are encapsulated individually improves the sensitivity of the detection. Examples of such applications could be in diagnostics, where biomarkers in some cases exist in very low numbers, for example in minimal residual disease cancer. By distributing the dilute samples in a way that single molecules are individually encapsulated in small reaction volumes, an increase in the sensitivity of detection is seen due to an increase in the effective concentration. As an example, one molecule in a 50 fL volume (one microdroplet) has an effective concentration of 30 pM. So in this sense, by encapsulation, a very dilute solution can be concentrated from a potentially undetectable level into an easily detectable one. The lower the initial concentration, the more compartments are required in order to reproducibly capture the single molecules. Essentially the same issue as described above for PCR. Typically, the signal from the single molecule is amplified for example by using specific enzymatic reactions due to the singular confinement of the molecules. This has spurred the development of digital assays, where the signal in one compartment is no longer limited by the original concentration of the target molecule. The distribution of the molecules in the partitions can be considered a Poisson process. Because the number of partitions far exceed the number of target analytes in the case of dilute samples, the probability of capturing more than one molecule in a partition is small. By counting the number of signal generating partitions, a relation can be made to the original concentration of the target, typically by the application of a standard curve generated by detecting the number of positive partitions for known concentrations of target.[4] This way of counting single molecules is considered binary or digital, as a positive signal is assigned the value 1 regardless of the signal intensity, and empty compartments are assigned the value 0.

The detection limit of digital assays are mainly limited by the number of compartments and the non specific binding of the signal amplification system. In practice, this means that even a sample containing no target will result in a small number of positive signals. The non specific binding can be reduced by engineering the properties of the capture surface, optimising the concentration of the labelling enzyme and buffer composition, as well as properly blocking reactive sites on the capture surface.[4] As an example, assume 100 droplets fluoresce in a negative control sample with a standard deviation of 10 molecules. The lowest number of molecules that can be reliably detected in a sample would be 130 molecules. If the nonspecific binding could be completely eliminated, in theory samples containing down to 5 molecules could be reliably detected. In the absence of non specific binding, the primary error contribution would be from Poisson noise.[4]

The physical compartmentalisation into microscopic droplets has generally been achieved in two ways. Either as emulsion droplets, where an aqueous phase is dispersed as droplet in another immiscible phase, typically an inert oil, or as aqueous droplets on a microstructured surface, here termed microdroplet arrays (MDA). Emulsion droplets are generated in microfluidic channels at rates approaching 15 kHz.[6, 7] Each individ-

ual droplet can be interrogated and manipulated in a sequential fashion, integrating active mixing,[8] temperature switching,[9] and sorting[10] as just some on-chip examples. Where emulsion droplets are manipulated and interrogated in a sequential manner, MDAs manipulate and interrogate the droplets in a serial manner, where an entire droplet array containing hundreds of thousands of droplets can be generated in mere seconds. The two methods cater different applications. The main difference being that the static MDAs perform the same action upon all the droplets simultaneously but is very fast, whereas the emulsion droplets allow manipulation of individual droplets, which in turn is a slower process.

For the interest of this thesis, the following section will introduce the microdroplet arrays and their applications in greater detail.

1.2 Microdroplet Arrays

Microdroplet arrays involve the encapsulation of a biochemical reaction in separate compartments spatially separated on a two dimensional substrate. Each compartment is typically on the micrometer scale, though examples of nanowells has also been demonstrated.[11] Microdroplet arrays has been realised in several forms, commonly applying some form of microfabrication technique to realise the microscopic compartments. Some examples include microfabricated wells in polydimethylsiloxane (PDMS) relying on soft lithography,[12, 13] etched optical fiber bundles,[14, 15, 16, 17] and patterned bi-philic surfaces utilising hydrophobic polymers, relying on photolithographic patterning.[11, 18, 19, 20] A commercially available platform has been realised by Quanterix, who designed a DVD format chip using physical wells in cyclic olefin co-polymer (COC) as well as an instrument, the Simoa (SIngle MOlecule Array) HD-1 analyzer, mainly for digital ELISA applications.[21] The Simoa platform has since then also been adopted to nucleic acid detection, detecting miRNAs in the low fM range.[22]

The applications of MDAs range from single cell studies to single molecule quantification and evaluation. Common to many applications is the utilisation of enzymatic signal amplification. Based on the work of Rotman[23], studies of the activity of single enzymes were conducted by utilising a substrate which fluoresced after conversion by an enzyme.[12] This study paved the way for single molecule ELISA, which rely on the enzymatic amplification of the fluorescent signal.[13, 24, 25] The digital ELISA seems the most common application of the MDAs, based on the number of publications. Furthermore, the single molecule ELISA has been multiplexed for the simultaneous detection of up to six biomarkers.[26] Other applications which have been realised on the MDAs include single-cell assays exploring the efflux system in bacteria,[19] drug combinatorial screening,[27] and DNA detection.[16, 22] A similar technology has also been used for genome sequencing, however applying larger compartments.[28, 29]

Common to many of these examples using MDAs is the use of magnetic beads for sample preparation and analyte capture. The use of beads has the advantage of an increased capture area, and the mobility of the beads may increase the chance of bead-target collision.[4] This makes the reaction kinetics of bead based assay more

similar to a solution reaction than a surface reaction. Another advantage to using beads, it that beads with different surface functionalisation is commercially available, possibly increasing the robustness of the capture molecule immobilisation needed for many bioassays. On the other side, using beads typically involve bulk reaction in a reaction tube and several washing steps performed out side of the chip, thus making the whole process more complex. Beads have been used in total analysis systems, such as the electro-wetting on dielectric (EWOD) systems, as an example for mRNA purification,[30] however, the fabrication of such systems are much more complex and involves integrated electronic circuits to be built into the chip.

Another common feature is the use of a mineral oil to displace the aqueous phase, preventing droplet evaporation. This is most often used in the case where droplets are generated on a bi-philic surface,[19, 27] but also in MDAs relying on physical wells.[4] In the case of microfabricated structures, the use of a sealing gasket has also been used to prevent evaporation of the small volumes.[12, 15] It has been observed that the mineral oil cover in some cases do not form a diffusion barrier to a range of molecules, and particularly hydrophobic molecules are prone to partition into the oil phase. One study showed the slow leakage of fluorescein, a commonly used fluorophore,[18] while another study investigated the partition of water into the oil phase.[31] Thus, one has to take care when using the oil cover that no cross talk occurs between the droplets. This can be avoided completely when displacing the aqueous phase with air.[11, 32] This is particularly practical in systems utilising microfluidic systems for the liquid transport, where the introduction of air is a common issue.

1.3 Nucleic Acid Detection

Both emulsion droplets and MDAs have been applied for the sensitive detection of nucleic acids, however, other methods for nucleic acid detection exist as well. In the following, a range of different methods will be described. These methods are used clinically or commercialised.

Nucleic acids is a very diverse group of biological molecules, and they range in size from some hundreds of bases to entire chromosomes several millions of bases long, and all sizes have an impact on the healthy function of the cells in our bodies. The detection methods and information that can be gained depends on the size of the nucleic acid to be investigated, as DNA contain many levels of information, from the placement of genes on the chromosomes to specific sequences. This short review will explore which diagnostic information can be gained and how from these different levels.

1.3.1 *Cytogenetic Approaches*

Starting from the condensed chromosome, G-banding is a method used to identify chromosomes. The chromosomes are fixed in metaphase, where the chromosomes are condensed in the well known X shape and stained using Giemsa stain. AT-rich regions stain more with Giemsa, producing dark bands, whereas GC rich regions appear bright. This pattern of dark and bright stripes on the chromosome is specific to each

chromosome, allowing their precise identification.[33] An example of Giemsa stained metaphase chromosomes from the human genome is shown in Figure 1.1 A. G-banding also reveals larger structural changes to the chromosomes, such as large deletions, insertions or translocations.[34] For more detailed chromosomal analysis, fluorescence in-situ hybridisation (FISH) may be used. This method utilise the hybridisation of fluorescently labeled probes to identify the position of specific sequences on the chromosomes.[34] An example of metaphase FISH is shown in Figure 1.1 B, where two fluorescently labelled probes show the position of the genes BCR and ABL. The co-localisation of these genes confirm the presence of the Philadelphia chromosome, a genetic marker for chronic myeloid leukaemia (CML). FISH allows the identification of more complex chromosomal changes compared to G-banding.[34] FISH can also be used to count the fraction of mutated alleles and can as such be considered a single-molecule counting method. Studying chromosomes in metaphase is cumbersome, requiring cell culture and fixation at the right time when the cells undergo mitosis. Methods to study the chromosomes in interphase has also been developed, as an example, interphase FISH. This is particularly useful in cases of minimal residual disease or early stages of cancer, where cells bearing disease indicators are rare and difficult to pick for cell culture and subsequent metaphase spreads.[34] The basepair resolution of the FISH methods span from around 5 Mbp in metaphase FISH down to 50 kbp in interphase FISH, and the even more sensitive fibre FISH, where the fluorescent probes are bound on chromatin fibres from expanded chromosomes where the histones have been removed. This method provide resolution down to 1 kb.[34] These cytogenetic methods are typically conducted in a very manual matter, and the throughput is very limited. However, the methods are still used since they may complement the genome wide analysis by sequencing in regions of the human genome which are difficult to sequence.

1.3.2 *Polymerase Chain Reaction*

For nucleic acid detection on the sequence level, PCR is one of the most popular techniques in the age where whole genome sequencing of many species has been undertaken. A specific, known DNA or RNA sequence 100 bp to 10 kbp long is multiplied exponentially using a polymerase enzyme, and subsequently detected. The specificity of the PCR reaction arise from the PCR primers which are designed to bind to one specific sequence of DNA, ensuring amplification of the target sequence alone. Figure 1.2 A shows the working principle of PCR. The target DNA is denatured by heating the sample, and the forward and reverse PCR primers are allowed to anneal to the template strand as the temperature is reduced. Next, DNA polymerase begin extending the strand by incorporating nucleotides base by base (2). This process is repeated through many cycles (3), resulting in an exponentially growing population of DNA copies containing the target sequence (4). Traditionally, the amplified DNA was separated on an agarose gel using electrophoresis where the mobility of the DNA depends on the size of the amplified fragment. In this way, the presence or absence of the target sequence in the sample can be determined.[35] An example of a gel electrophoresis separated PCR reaction in shown in Figure 1.2 B. The second and third

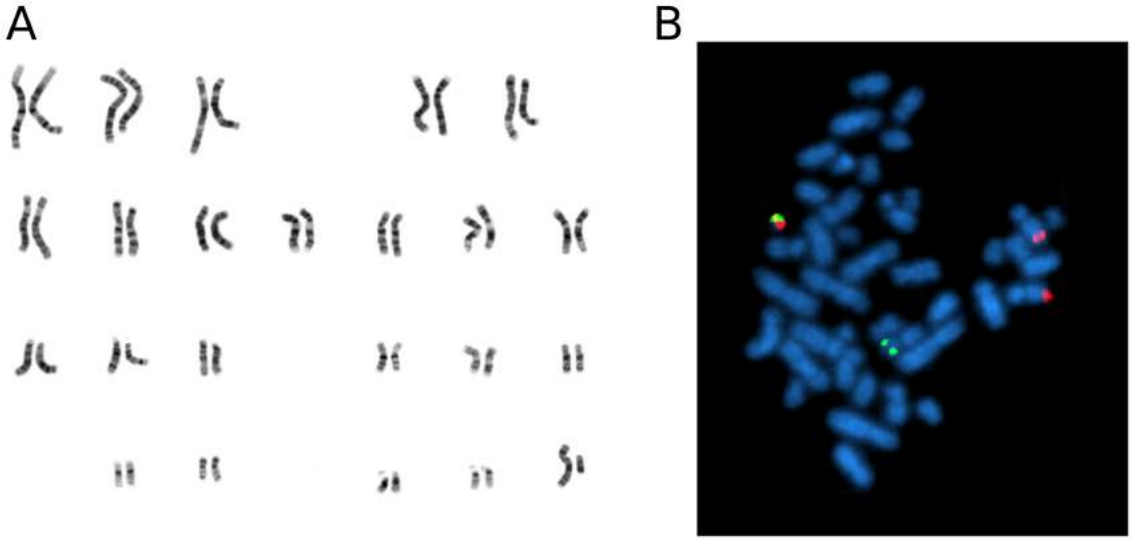

Figure 1.1: A) Giemsa stain of the human genome shows a distinct pattern of dark and bright stripes. From [1]. B) Fluorescence in-situ hybridisation. Methaphase chromosomes hybridised with fluorescently labelled probes for the genes BCR and ABL (red and green). The co-localisation of the probes indicates the prescence of the Philadelphia chromosome, a genetic marker for chronic myeloid leukaemia. From [2].

sample contain the target amplicons, while the first sample is negative. Separation of the PCR product on a gel does not determine the amount of target DNA in the sample. For quantitative detection, real time or quantitative PCR (qPCR), was developed. It relies on a fluorescent marker for the detection of the amplified DNA. The fluorescent marker can be an intercalating dye or quenched, fluorescently labelled complementary probes, which only fluoresce as the fluorophore is released from the vicinity of the quencher as the strand is elongated. As the amount of DNA increase for each cycle, the fluorescence intensity increase. Based on the speed of the rise in intensity, it is possible to determine the starting concentration of the DNA target. An example of a qPCR curve is shown in Figure 1.2 C for five samples with concentrations varying from high (green line) to low (light blue line). The concentration can be determined by comparing the cycle which result in a fluorescent signal above the chosen threshold (C_T) to samples of known concentration for absolute quantification.

The limitation of qPCR is that it has difficulties in determining differences in gene expression and copy number variance. For this purpose, digital PCR was invented. This method allows the quantification of mutant alleles present in less than one copy in thousands of wild type allele DNA strands.[36, 37] Originally, the PCR sample was

[1] https://commons.wikimedia.org/w/index.php?curid=583512
[2] https://commons.wikimedia.org/wiki/File:Bcrablmet.jpg#media/File:Bcrablmet.jpg
[3] https://commons.wikimedia.org/w/index.php?curid=17271079
[4] https://commons.wikimedia.org/wiki/File:Qpcr-cycling.png#media/File:Qpcr-cycling.png

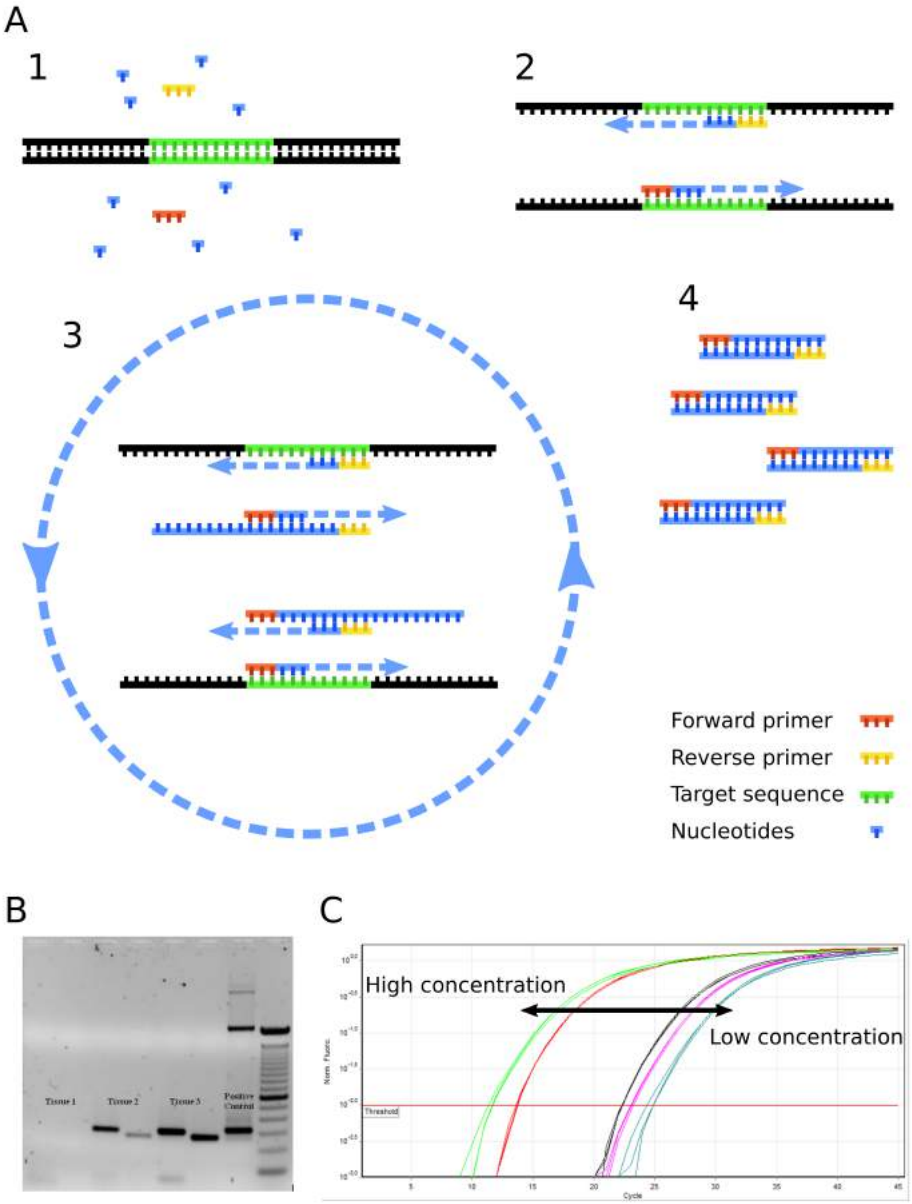

Figure 1.2: A) Working principle of PCR: 1. The target is flanked by the forward and reverse primers. Nucleotides allow the synthesis of new DNA strands by the enzymatic activity of DNA polymerase. 2. The target DNA is denatured by heating the sample, the primers bind as the sample is cooled down, and the DNA polymerase extends the PCR primers along the target strand. 3. The process is repeated many times (cycles), resulting in 4. the replicated target sequence. B) Size separation of PCR products on an agarose gel by electrophoresis. From [3]. C) Accumulation of target product in real time PCR is measured as an increase in fluorescence intensity after each cycle. Higher concentrations of target rise in intensity faster than samples with low concentration. From [4].

spread out in well plates to concentrations of target less than one copy per well.[5] This, however, is impractical due to the enormous amount of reagents required to perform such an assay, and microfluidic methods for the encapsulation was applied.[37] By encapsulating the PCR reaction in water in oil emulsions, millions of individual droplets could be analysed in one run. The greater the number of partitions, the better the resolution of the quantification and the larger the dynamic range.[36] Digital PCR is also less sensitive to PCR inhibitors and differences in amplification efficiency, as it relies on a binary end point measurement for the quantification.[36] From the fraction of positive partitions, the number of copies can be calculated using Poisson statistics. This is exemplified in Figure 1.3, showing how the number of positive droplets increase with concentration. Initially the relationship between the concentration and the fraction of positive droplets is linear, as the average number of target molecules per droplet is below one. As the concentration increases, the chance of obtaining droplets containing more than one target increases as well, and a deviation from the linear relationship is observed (see Figure 1.3 B). The average number of molecules per droplet (λ) is calculated as $\lambda = V_{drop} c N_A$, where V_{drop} denotes the volume of each droplet, c denotes the target concentration, and N_A is Avogadro's number ($6.022 \cdot 10^{23}$ mol^{-1}). The Poisson distribution describes the percentage of droplets containing n molecules, ($n \in \mathbb{N}_0$) by the distribution:

$$P(n) = \exp(-\lambda) \cdot \frac{\lambda^n}{n!}. \tag{1.1}$$

As the droplet volume is constant in one assay, λ is directly proportional to the initial concentration, and the distribution of targets in the positive droplets can be determined directly by the expression:

$$P(n > 0) = 1 - \exp(-\lambda), \tag{1.2}$$

as seen plotted in Figure 1.3 B.

1.3.3 *DNA Microarrays*

PCR is capable of detecting a few different sequences by multiplexing.[37] In the case where you need to evaluate the gene expression of many different genes, DNA microarrays are employed.[38] DNA microarrays rely on surface bound capture sequences which are complementary to the sequences of interest, and one single array may contain thousands of different probes. Each probe binds a specific DNA target, which is first amplified, labelled, and then allowed to hybridise with the surface bound probes. By mapping the signals to the probe sequences, the DNA contents of the sample can be examined.[39] The highly parallel fashion of the DNA microarrays is very powerful, however, the need to amplify the material before detection has the risk of introducing bias to the result.[39] Examples of the applications of DNA microarrays include gene expression, for example comparing the gene expression of two cell populations such as cancer cells and normal cells, single nucleotide polymorphisms (SNP) detection and mutational analysis, among others.

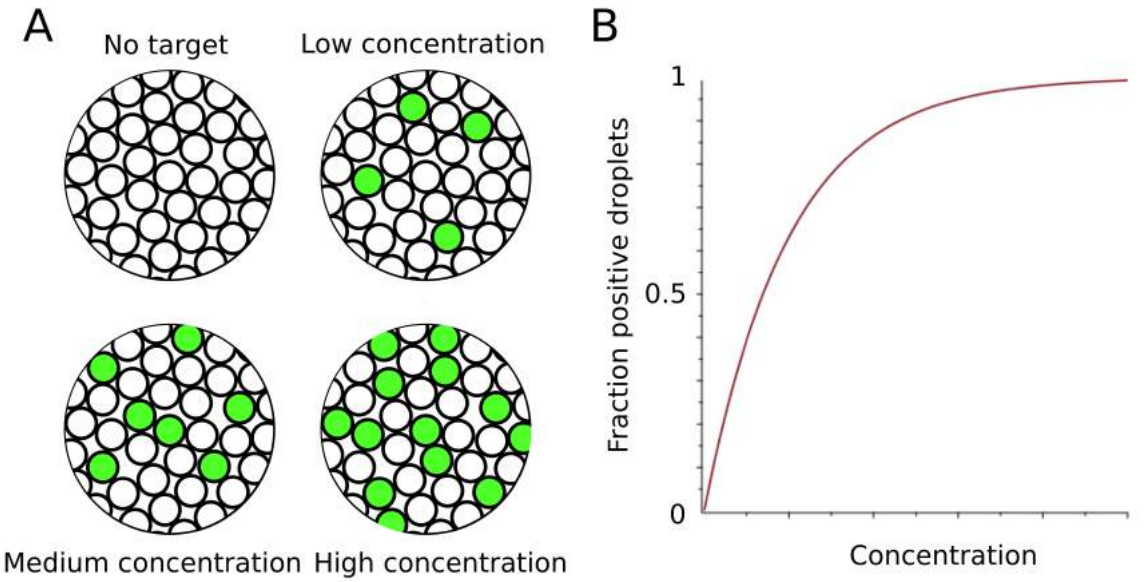

Figure 1.3: A) The number of droplets eliciting a fluorescent signal from droplet PCR increase with increasing concentration. B) The relation between the initial target concentration and the fraction of positive droplets in digital PCR. The relationship is initially linear, however, as the fraction of occupied droplets increase, the likelyhood of each droplet containing more than one target increase as calculated by Poisson statistics.

1.3.4 *DNA Sequencing*

The highest level of information obtained from DNA is its sequence. The most well known method of obtaining sequence information from DNA is by Sanger sequencing, first described in the 1970s.[40] The method utilises DNA polymerase activity to generate copies of the DNA to be sequenced. Copies of different lengths are generated by utilising di-deoxynucleotidetriphosphates (ddNTPs), which terminates the polymerase base extension activity, as they lack the 3' -OH group used to form the phosphodiester bond in the backbone between two nucleotides. The process is sketched out in Figure 1.4. 1. Four parallel reactions are carried out, each containing the DNA target, DNA polymerase, an extension primer sequence (similar to PCR), dNTPs and one of the four ddNTPs each. The dNTPs are added in 100-fold excess to ensure the generation of longer sequences. The copies of the target are labelled radioactively or by a fluorescent marker, either by labelling the ddNTPs or by incorporating labelled deoxynucleosidetriphosphates (dNTPs) until the sequence is terminated. 2. This generates copies of the target of different lengths. Each of the four reactions are evaluated by 3a. gel- or 3b. capillary electrophoresis, which allows the separation of the sequence copies down to one base resolution. Comparing the four samples reveals the sequence of the target strand.

One drawback of Sanger sequencing is the throughput. A group of new sequencing methods were developed, which increased the sequencing throughput 100- to 1000-fold. These methods were named Next Generation Sequencing (NGS).[41] Three meth-

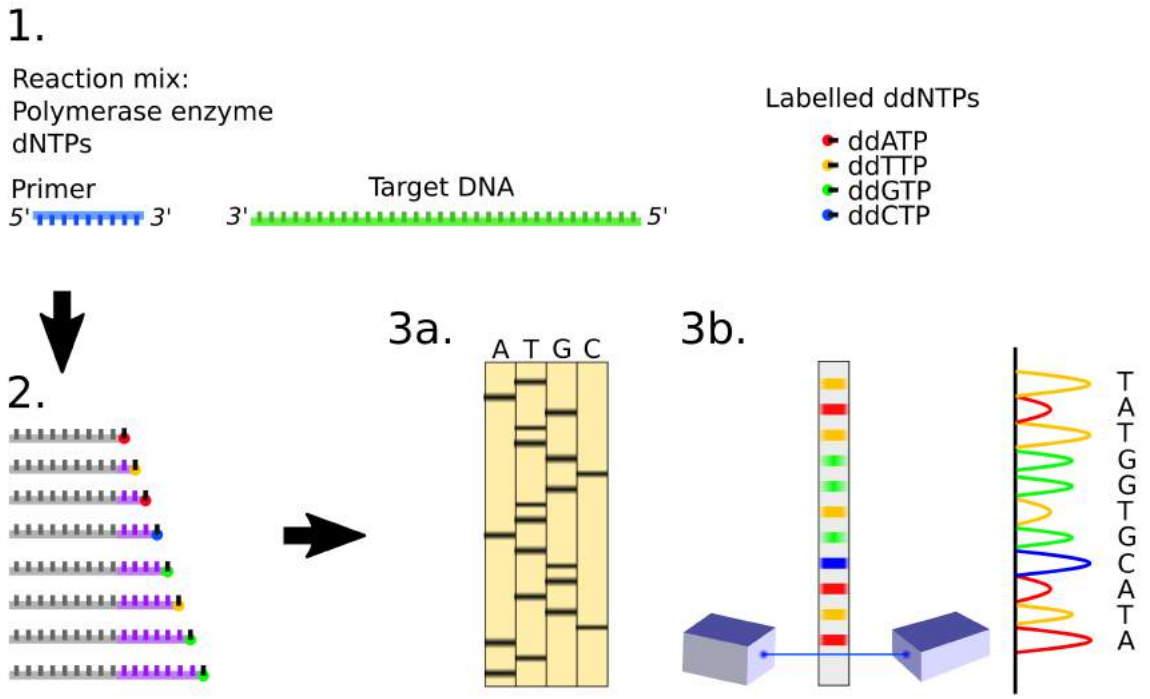

Figure 1.4: The concept of Sanger sequencing. 1. Four tubes are assembled containing DNA polymerase, dNTPs, Primer and target DNA. To each tube is added one of the four ddNTPs. 2. By activity of the DNA polymerase, copies of the target are produced. Upon incorporation of a ddNTP, the replication is terminated. 3a. Copies are separated on a gel, and the sequence can be interpreted. 3b. The copies are separated by capillary electrophoresis and the sequence read.

ods were commercialised: Roche's 454 pyrosequencing method, the Illumina Solexa platform, and Life Technologies' ABI SOLiD platform. Several great reviews exist which compare these three methods,[41, 42, 43] why only a brief explanation of the working principle, strengths, and drawbacks of these methods will be described here.

454 Pyrosequencing

The Roche 454 pyrosequencing method works by incorporation of each of the four bases individually in a sequential manner. The incorporation of one or more bases results in the emission of a signal.[44] Here, the target preparation involves the generation of dual-tagged target fragments. Single stranded fragments are ligated to adapter sequences in either end, which serves as a binding sequence and a polymerase initiator respectively. The library is purified and added to a mixture containing agarose beads carrying the complimentary, 454 specific binding sequence in a way that each bead is associated with a single library fragment. The beads are then isolated in individual water in oil partitions and PCR amplification of the surface bound library fragment produce approximately one million copies which all bind to the surface of the agarose bead.[44] The emulsion is broken and the beads are distributed in spatially separated micron-sized wells one by one. In this way, the location of the signal from each bead is well defined. Next, the wells are filled with small beads containing Sulphurylase and Luciferase, which catalyse the signalling reaction upon incorporation of the bases. Lastly, the pure nucleotides are flushed over the wells in a sequential fashion,[44] and upon incorporation by a polymerase enzyme, a pyrophosphate is released, allowing the conversion of adenosine 5' phosphosulfate into adenosine tri-phosphate (ATP), which acts as a substrate in the conversion of Luciferin by Luciferase, which results in the emission of light. The strength of the emitted signal is proportional to the number of bases incorporated up until sensor saturation.[42, 44] Therefore, in the case of long homopolymeric sequences, base calling is prone to error. Contrarily, substitution errors are rare, as the bases are incorporated one nucleotide at a time.[44]

Illumina-Solexa

The Illumina sequencer works in a sequencing by synthesis fashion, where one base is incorporated at a time. The target preparation is similar to that of the pyrosequencing method, in that the genomic material is randomly fragmented and ligated to Illumina specific adapter sequences in both ends. The amplification method in this case relies on bridge amplification on a solid support. The library fragments are spread on to a silica surface where the complimentary adapter probes are bound. The target fragments are separated from each other by random probability. Amplification occurs only when the free end of the target fragment binds to the second complimentary adapter on the surface (forming a "bridge" between the two probes), which acts as a Polymerase initiator. The double stranded fragments are denatured, and the process repeated until clusters of equal sequences has been generated on the surface. Next, individually labelled NTPs with the 3' OH group chemically blocked are added simultaneously. The chemical blockade of the 3' end ensures that only one base is incorporated. After flushing the excess bases, the surface is imaged, and each cluster

will elicit a fluorescent signal with a wavelength specific to the nucleotide incorporated. The 3' group is un-blocked, and the process is repeated.[44]

ABI SOLiD

The last NGS platform described here is the SOLiD platform. Similar to the 454 pyrosequencing platform, the template library is formed by ligating adapter sequences to the genomic DNA fragments and amplification occurs on small magnetic beads in an emulsion PCR system. Contrary to the other two NGS methods, the SOLiD method relies on DNA ligase to read off the sequence. First a universal primer is hybridised to the adapter sequence. This primer ends at the very last base of the adapter. Next, fluorescently labelled probes (di-base probes) are hybridised onto the target sequences and ligated to the primer. The first and second base of the probe defines the colour of the fluorescent label, hence the name di-base probe. A cleaving agent removes the fluorescent label after imaging, leaving the primer extended by five bases. This ligation reaction is repeated a number of times, reading the fluorescent signal after each cycle. Then, the primer is reset by melting off the extended primer and hybridising a new primer, which is offset by one base compared to the first primer. The ligation process is repeated. This cycle of off-set primer binding is repeated five times until each position has been interrogated twice. The double coverage of each base results in the unique identification of each base.[44]

When comparing sequencing methods, particularly three parameters are important: (I) Read length, i.e. the number of consecutive bases identified, (II) throughput, i.e. the number of bases identified per hour or the total number of bases identified per run, and (III) the base calling accuracy. The read length is important, particularly in de novo assembly of genomes which is the identification of a sequence without the use of a reference genome. The longer the overlap between sequences produced by the sequencing, the more likely the overlap is unique. Automated Sanger sequencing produce reads with an average read length of 900 bases.[41], where the NGS methods produce quite shorter reads. The Roche pyrosequencing method and the newest Illumina sequencers[1] produces the longest reads, on average 200-400 bases, whereas the SOLiD methods produce reads of just 75 bases[2].[41, 43] The throughput determine how fast a genomic sequence can be identified. Sanger sequencing traditionally produce 0.03-0.07 Mb per hour. The NGS methods improve the throughput up to 1000-fold, producing 10-30 Mb per hour, and up to 20 Gb per run.[43] This is an immense amount of data, and the applications are countless. One example is in diagnostics, where resequencing of the genomic material may help identify mutated genomic material. Particularly identifying single nucleotide variations can be difficult. Some of the drawbacks of the NGS methods include the total cost per run. One run costs $ 8000 or more,[43] which limits the routine use of sequencing in diagnostics. Another drawback is that the NGS methods rely on target amplification by PCR, which in-

[1] Illumina company website. https://www.illumina.com/systems/sequencing-platforms.html.

[2] Thermo Fischer Scientific company website. https://www.thermofisher.com/dk/en/home/life-science/sequencing/next-generation-sequencing/solid-next-generation-sequencing/solid-next-generation-sequencing-systems-reagents-accessories.html

herently introduce an uncontrolled bias. This is due to differences in amplification efficiency based on the template sequence.[45] Another drawback is that the short read methods require a larger library of targets with defined adapter sequences, increasing the cost and labour required for the generation of the library. Thirdly, the error rate of DNA polymerases are substantial considering that the libraries are generated from single molecules. The Taq DNA polymerases' error rate is 1 in 10000, meaning that for each 10000 nucleotides incorporated, one nucleotide substitution has occured.

The next evolution in sequencing occurred when single molecule sequencing was developed. These were termed third generation sequencing or high throughput next generation sequencing (HT-NGS). These methods do not rely on the error prone PCR amplification and are capable of producing reads thousands of bases long. Particularly the single molecule sequencing methods commercialised by Pacific Biosciences and Oxford Nanopore Technologies are of great interest.

Pacific Biosciences' single molecule real time (SMRT) sequencer

The SMRT technology from Pacific Biosciences utilises zero-mode waveguides (ZMW)[46] and a real time sequencing by synthesis approach. The ZMW contain an array of zepto-litre wells each containing a single DNA polymerase. Due to the extreme reduction in observation volume, the ZMW is capable of observing the fluorescence from single fluorescently labelled nucleotides as these are incorporated. Because of the small observation volume, by probability, only the incorporated nucleotides are detected, and upon incorporation, the fluorophore is cleaved and diffuse quickly out of the detection volume.[42, 43] The error rate of the SMRT sequencer reaches up to 15%, however the errors occur at random, and thus very precise reads can be obtained by resequencing, increasing the read depth.[47]

Oxford Nanopore Technologies' Nanopore DNA sequencer

In stark difference to the previously mentioned techniques, the nanopore DNA sequencer does not rely on signals generated by the incorporation of nucleotides by a DNA polymerase. Alternately, this method relies on the specific modulation of current passing through a nanopore, here an α-hemolysin protein, as the DNA passes through the pore.[43] The pore diameter is comparable to the size of single stranded DNA. The proteins are incorporated in a membrane separating two small chambers connected to the anode and the cathode of a patch clamp amplifier, which measures the current through the pore.[48] The current modulation is characteristic for each base, and as each base pass through the pore, the sequence can be read. The reading of the bases, however, is error prone just as the SMRT sequencer although the errors are less random in occurrence than the SMRT. This means that increasing read depth cannot compensate for the error alone.[49]

Other emerging technologies are being developed as well, as cheap and broadly available sequencing is an immensely powerful tool in e.g. diagnostics. Levy and Myers mention some of these emerging technologies in their recent review [50], and gives a good overview of the current commercially available technologies.

One example where NGS has been applied for a more sensitive mutational analysis compared to Sanger sequencing is in the monitoring of chronic myeloid leukaemia. Using the Roche pyrosequencing platform, a mutation load down to 3% were routinely measured in a multi-lab study. In another study, the SMRT third generation sequencing platform improved this detection limit by 1-2 percentage points.[51]

1.4 Chronic Myeloid Leukaemia: A Good Model Disease with Therapeutic Challenges

In order to put the work presented in this thesis into perspective, chronic myeloid leukaemia and the challenges in therapeutic decision making and monitoring is chosen as a model disease, where the solid phase droplet array technology may overcome some of the challenges faced today.

Chronic myeloid leukaemia occurs due to the translocation of genes between chromosome 9 and 22 in the haematopoietic stem cells. The translocation results in the fusion gene BCR-ABL on chromosome 22, which is transcribed and translated into a protein in the diseased cells.[52] The altered chromosome 22 is referred to as the Philadelphia chromosome (Ph chromosome). Hence, Detecting mRNA containing sequences of both the BCR and the ABL gene provide solid evidence of the presence of this specific translocation, and can be used as a singular biomarker for disease detection. The BCR-ABL protein is a constitutively active tyrosine kinase signalling protein which results in a disruption in the regulation of the cell cycle through several known mechanisms.[52] The development of tyrosine kinase inhibitors (TKIs) presented curative treatment of CML. The response to treatments is divided into: (I) Haematologic response, where a normalisation of blood count is achieved and no immature blood cells are observed in peripheral blood. (II) Cytogenetic response, where a reduction in Ph positive cells are observed in bone marrow metaphases. Complete cytogenetic response is defined as no Ph-positive metaphases observed, typically measured by FISH. (III) Molecular response is defined as the a reduction in BCR-ABL mRNA compared to a control gene, typically ABL, as detected by real time reverse transcriptase PCR (RT-qPCR). The reduction is measured on a logarithmic scale and compared to the cancer load at diagnosis. A 3-log reduction (0.1% of cells in the cell population contain the BCR-ABL transcript[53]) is defined as major molecular response, and complete molecular response is defined as the inability to detect BCR-ABL by RT-qPCR.[54] More and more patients achieve prolonged complete molecular response on TKI treatment, and ultimately TKI stop trials have been conducted.[53] A three-year evaluation of one stop trial conducted in Japan revealed that 44% of patients in the trial remained on treatment free remission three years after discontinuation of the TKI treatment.[55] For relapsing patients, the rise in BCR-ABL transcript detected by RT-qPCR was used as the indicator for restarting the treatment with TKIs. An interesting unanswered question is what happens with the cancer load in the patients with complete molecular response, where the levels are undetectable by RT-qPCR. If a more sensitive method is applied would it be possible to detect relapse at an earlier stage?

Another challenge in the monitoring of CML is the monitoring of mutations occurring after the initial translocation. It is believed that genetic instability of the translocated chromosome may be responsible for further mutations of the genes[56] and may be involved in the advancement of the disease or result in resistance towards the TKI treatment.[56, 57] Point mutations are detected in around 50% of patients developing drug resistance as measured using Sanger sequencing.[58] During treatment drug resistant mutations are selected and any relapse occurring during treatment should be investigated by mutational analysis.[59] After relapse on TKI treatment, the choice of treatment should be guided by the mutational analysis, as the specific mutation have a large impact on the possible treatment options, as shown by O'Hare et al.[59] This report lists the most common point mutations observed in relapsing patients and indicate which treatments options are more or less efficient depending on the specific mutations. The mutational analysis is performed by Sanger sequencing, however more sensitive NGS platforms emerge to detect lower levels of mutations.[58] Studies using ultra deep sequencing methods have revealed a more complex mutational landscape compared to what was observed using Sanger sequencing. Mutational frequencies were detected down to 1% mutation frequency compared to 10% by Sanger Sequencing.[60] Ultra deep sequencing revealed how populations harbouring different mutations would rise and fall depending on the therapeutic intervention, however the data are still too insufficient to interpret the clinical relevance.[58] As it is now, mutational analysis is only recommended if the patient does not respond to initial treatment (considered if there is no response at 3 or 6 months follow up and recommended if there is no response at 12 to 18 months follow up) or if relapse occurs.[54] This is most likely due to the low availability of NGS locally, and the question can be raised if decision making in therapy could be improved by early mutational analysis if this was easier to conduct and more generally available, and what could be learned if the detection limit of mutated alleles were reduced even further.

1.5 Hypothesis

The research in this thesis involved the development of a versatile platform based on hydrophilic-in-hydrophobic microdroplet arrays. To increase the versatility of this platform compared to other MDA platforms presented in current literature, the target capture was performed directly on the surface of the MDA spots. This should allow multiple interrogations of the same molecule, as they will remain in the same position even after washing the MDA. In addition, the use of an oil phase was avoided in order to reduce the complexity and improve the ease of using the platform. By using air to displace the water phase, the issue of intoducing air in the microfluidic channel was eliminated, which is a common issue encountered when working with microfluidics. This thesis presents the foundation on which a range of more complex assays can be built, which spans from applications in diagnostics into high throughput screening applications. In practice, the work can be divided into the following problem statements:

- As beads are often used for target immobilisation, a numerical model exploring

the hybridisation of nucleic acids on a planar capture surface should be conducted to validate the feasibility of omitting the beads in the MDA assays. The numerical model should be based on relevant literature on the kinetics of DNA hybridisation and should explore how the different assay parameters could affect the binding of the target molecules.

- Part of the work conducted in the FP7 NADINE project involved the construction of a detection platform, including hardware and software development. The price of the platform should be kept low as an alternative to the purchase of inverted fluorescence microscopes. The platform should also hold the possibility of automating assay procedures on the MDA including liquid actuation and chip imaging.
- A robust method for the fabrication of MDAs should be developed which rely on hydrophilic-in-hydrophobic spots and using air to displace the aqueous phase rather than oil. A method to prevent the droplets from evaporation should be incorporated, as well as infrastructure to transport the reagents across the MDA surface. This could be incorporated by a microfluidic system. The microfluidic system should also consider the easy interfacing with liquid actuation and reagent addition.
- Relevant bioassays should be conducted on the MDA platform showing the versatility of the platform. First, digital ELISA should be demonstrated for sensitive detection of biomarkers related to the diagnosis of Alzheimer's disease as part of the FP7 NADINE goals. Secondly, to demonstrate the feasibility of multistep assays on the MDA, transcription and translation of proteins and in situ immobilisation followed by antibody labelling and detection was to be conducted. Thirdly, as a promising platform for the combined quantification and SNP detection of nucleic acids, DNA/RNA hybridisation should be shown on the platform, and preferably SNP detection by single base extension should be demonstrated as well. The realisation of the sensitive quantification of nucleic acids combined with SNP detection on one platform could increase the availability of mutational analysis in the diagnosis and monitoring of e.g. chronic myeloid leukaemia, currently undertaken using several different procedures such as NGS, which is still somewhat expensive for routine use.

2 | Finite Element Modelling of DNA Hybridisation

The contents of this chapter is omitted for confidentiality reasons.

3 Immobilisation of Biomolecules on Glass Substrates

The immobilisation of biomolecules on sensor surfaces is essential in many applications, including DNA microarrays and protein arrays. MDAs have primarily been using beads to bind capture molecules and capture targets, however, some benefits come from immobilising the molecules directly on the surface of each drop. For this reason, surface chemistry and biomolecule immobilisation was a major part of this study. In the following sections, traditional methods for the immobilisation of DNA and proteins is discussed in addition to the observations made during this study.

3.1 Introduction

Different chemistries and surface modifications can be used to create interactions between (bio)molecules and sensor surfaces in order to detect specific targets in a sample. As an example, antibodies may be immobilised on a sensor in order to specifically detect the protein which is an antigen to that specific antibody, or a short DNA probe can be constructed to bind a unique complementary strand of target DNA or RNA. This allows highly specific detection of e.g. nucleic acid or protein biomarkers in diagnostics. The degree of specificity of nucleic acid hybridisation depend on the assay conditions, but optimised assays has been able to distinguish single pair mismatches.[76] The specificity of antibodies is also a question of optimisation, and protein arrays has been used to explore highly specific antibodies for diagnostics and therapeutics, where a high degree of specificity is essential.[77] Many nucleic acid and protein sensors rely on these specific interactions, and the droplet microarrays as well.

3.1.1 *Immobilisation of DNA*

The binding of DNA on solid supports has been widely investigated through the fabrication of DNA microarrays. The first report on the computerised analysis of arrayed nucleic acid hybridisation came out in 1983[78], and since a huge effort has been put into optimising the immobilisation and hybridisation of DNA on solid supports. Several reports show that the immobilisation strategies impact the density and availability of the immobilised DNA, and thus the signal strength achieved. In the case of single molecule detection using MDAs, signal strength is not achieved through a high degree of binding to the surface, however, a high binding affinity will affect the limit of detection in a positive way. A review of traditional and novel immobilisation strategies will give a broad picture of the immobilisation strategies relevant for the binding of DNA probes onto the MDAs. Here, immobilisation onto glass substrates will be the main focus.

The immobilisation strategies of DNA on glass range from the simple, using unmodified glass substrates, to the more complex, where branching, three dimensional chemistries are used to increase the effective binding area. However, the most common strategies involve functionalisation of the glass using silanes, which produce a two dimensional, chemically active substrate for the immobilisation of the DNA. Besides creating functional groups on the glass substrates, several binding strategies require functionalisation of the DNA probe as well.

The simplest combination involves immobilisation of unmodified DNA probes onto unmodified glass. In one report, hydrogen bonds and electrostatic interactions are suggested as the responsible mechanisms of the attachment of unmodified oligonucleotide probes on glass slides washed in an acid bath. The hybridisation efficiency of the bound unmodified probes is compared to amine modified DNA probes on an epoxy functionalised slide, and even though the signal is less strong, the method should produce sufficient signal to perform a DNA microarray assay.[79] In another report, DNA oligonucleotides are bound on unmodified glass by drying the spots of DNA solution and exposing the slide to UV light. The oligonucleotides contained a poly(10) T poly(10) C tail (TC tag) but were otherwise unmodified. The thermal stability studies in this case indicated that the probes became irreversibly bound on the glass surface, as no signal loss was observed after boiling and rehybridising the slide. This is not even seen with modified probes on commercial amino silanised slides, as a 60-70% signal loss is observed after boiling, which is attributed to a delamination of the surface coating between the glass and the silane. The detection limit in a microarray assay using the TC tag was at least as good as that obtained on commercial slides using amino modified probes.[80] The biggest benefit of using unmodified DNA probes is the price reduction, as the price per oligo increases drastically when modifications are incorporated. Commercially available glass slides with functional coatings also present a very high cost compared to unmodified glass slides, however, the cost of functionalising the slides in house is minimal.

The most commonly used surface modifications for immobilising DNA probes are the epoxy, the aldehyde and the amine modified glass. The epoxy and aldehyde modifications are highly reactive and allows the direct binding of amino modified DNA probes. In order to bind amino modified DNA probes onto amine functionalised glass, a cross linker such as glutar aldehyde is used.[81] Phosphate functionalised DNA also binds to amine modified glass through an intermediate reaction with imidazole and 1-Ethyl-3-(3-dimethylaminopropyl)carbodiimide (EDC).[82] Lastly, disulfide modified DNA probes were bound to mercapto silanised glass slides, presenting a thiol functional group resulting in a covalent attachment of the DNA probe through a disulfide thiol exchange reaction.[83] The reason why these immobilisation strategies are preferred, is because the specific reactions between the end functionalised probes and the modified glass result in a higher fraction of probes available for hybridisation compared to the nonspecific interactions between unmodified DNA probes and the substrate.[83] However, reports have also shown that nonspecific attachment and nonspecific hybridisation occur on both amino and epoxy modified glass, but not with the thiol-disulfide immobilisation.[83] The hybridisation efficiency on these types of

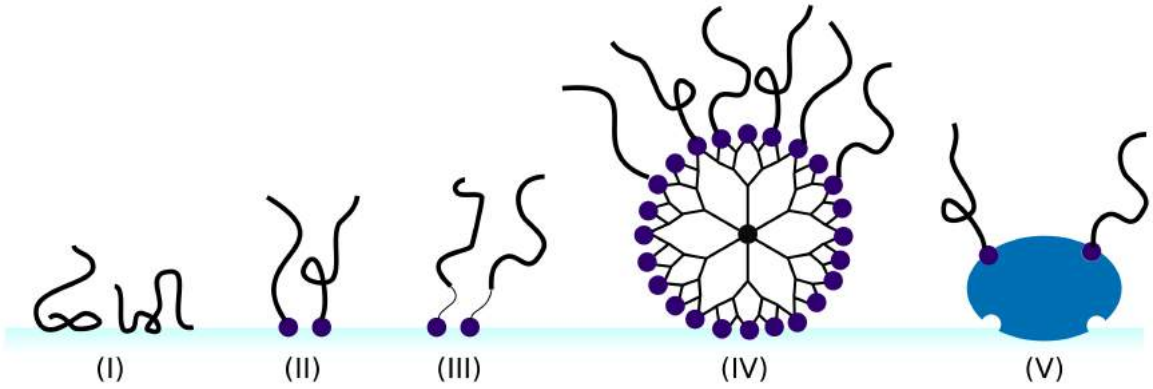

Figure 3.1: (I) Randomly immobilised DNA. Only some will be able to participate in hybridisation. (II) End tethered DNA probes reduce the risk of random intra chain bonds. (III) End tethered probes using a spacer increase the availability of the DNA probes. (IV) Dendrimeric spacer lifts the DNA probes avay from the negatively charged glass substrate. The number of binding sites is increased by the 3D structure of the dendrimers. (V) Binding by avidin. The avidin protein effectively shields the charges from the glass substrate.

immobilised probes is quite similar.[84]

One issue of hybridisations close to the glass substrates is that the negatively charged glass surface repels the negatively charged DNA. This affect both hybridisation to the DNA probes immobilised directly on unmodified glass, but also to end tethered DNA as described directly above. To prevent the repulsion from the glass, the use of long spacers may prove beneficial. Such spacers may be dual functional polyethylene glycol (PEG) molecules, avidin, or dendrimers. Reports on the use of dendrimers report that saturation of the array is reached at 10 μM which is comparable to that of commercially available slides for end tethered capture probes, however, the detection sensitivity was 10 to 100-fold higher, as concentrations down to 1 pM was still detectable on the dendrimer coated slides.[84] A graphical representation of the mentioned immobilisation strategies is shown in Figure 3.1.

3.1.2 *Immobilisation of Proteins*

As for DNA, the immobilisation of proteins is useful for the construction of biosensors. Antibodies are widely used in immuno-assays, and proteins and peptides can be bound to create protein/peptide arrays. The simplest strategy for immobilising proteins is by non-specific adsorption onto a plastic or poly-lysine coated glass substrate, however, this process may cause denaturing of the proteins, rendering them non-functional.[85] Proteins may also be covalently attached through chemically activated surfaces, such as amine or epoxy activated glass.[85, 86] This should be less denaturing to the proteins compared to non-specific adsorption, however, the orientation of the protein is random, and binding sites/active sites that is needed in the assay may be shielded by the surface or surrounding proteins.[85] The amine group on the N-terminus of antibodies may be used to covalently attach the molecules through

epoxide or carboxyl groups. As with DNA, proteins may also be functionalised with a biotin, and avidin coated substrates can be used for binding.[85] Immobilising antibodies in a way that directs the binding sites away from the surface may be accomplished by using intermediate proteins, such as protein A or G, or an Fc-binding antibody. In this way freedom of the binding site may be ensured.[85] This method may reduce the surface density of the immobilised antibodies as two immobilisation steps are required, also it is limited by the stability of the protein-protein interaction, which is typically weaker compared to a covalent bond. Another option for the direct immobilisation of proteins is through the use of a poly-His tag. This tag can be introduced in recombinant proteins during synthesis and binds selectively to Nitrilotriacetic acid (NTA) in the presence of a chelating ion.[87, 88] Examples using this method involves the grafting of glass using a bi-functional PEG linker with poly-l-lysine and NTA functional groups.[88] Comparing the different methods of protein immobilisation is less straight forward compared to DNA, as the utility of the protein on the surface differ in the many applications, whereas DNA is most often used to form a hybrid on the surface with a complementary strand.

3.2 Materials and Methods

In the following sections, the materials and methods used in the immobilisation of biomolecules in this study is presented, and data comparing the different methods is shown.

3.2.1 *Materials*

For the immobilisation of biomolecules on glass substrates, the following reagents were used: For cleaning the glass substrates, acetone, isopropanol and ethanol was used. 96% ethanol was used to dilute the silanes. (3-Aminopropyl)triethoxysilane (amino silane), (3-Glycidyloxypropyl)trimethoxysilane (epoxy silane), N-Hydroxysuccinimide (NHS), N-(3-Dimethyl-aminopropyl)-N-ethyl-carbodiimide hydrochloride (EDC), copper(II) acetate, 4th generation PAMAM dendrimers 10% in methanol, p-Phenylene diisothiocyanate (PDITC), glutar aldehyde, and 50 mM biotin in solution were purchased from Sigma Aldrich. Deglycosylated Avidin (NeutrAvidin™, Invitrogen™(NAv)) was purchased from Thermo Fischer Scientific. Heterobifunctional amine-poly(ethylene glycol)-carboxyl, HCl salt, average poly(ethylene glycol) molar weight 2,000 g/mol ($NH_2-PEG_{2000}-COOH$) was purchased from Jenkem Technology. Nitrile-triacetic acid-functional poly-L-lysine-g-poly(ethylene glycol) (PLL-g-PEG-NTA) was purchased from Surface Solutions. Silane and NHS functional PEG linker was purchased from Nanocs Inc. Dichloromethane, pyridine, and acetone was dried using molecular sieves for the immobilisation of PAMAM dendrimers.

3.2.2 *Immobilisation Using Amino Silane*

Glass functionalised with amino silane was used in conjunction with glutar aldehyde to bind primary amines. First, the glass substrate was cleaned in acetone, isopropanol and ethanol in a sequential matter using an ultrasonic bath. They were cleaned for

10 minutes in each solvent. After a final rinse in ethanol, the slides were submerged in a 1% solution of amino silane in 96% ethanol and left to react for one hour. Next, the slides were rinsed in ethanol and cured in a convection oven at 80 °C for three hours. In order to activate the surface, glutar aldehyde was diluted in MilliQ water to a 10% solution and the glass slides were submerged for one hour. Lastly, the slides were rinsed in MilliQ water, dried, and immediately used to bind amine functional molecules.

3.2.3 *Immobilisation Using Epoxy Silane*

Similarly to the functionalisation with amino silane, the glass slides were first cleaned as described above. Next, the slides were submerged in a 1% solution of epoxy silane in 96% ethanol and reacted for 30 minutes. The glass slides were rinsed in ethanol and cured in a convection oven at 110 °C for 30 minutes. After curing, the epoxy functionalised slides were ready to bind amine functional molecules.

3.2.4 *Carboxyl Groups and Carbodiimide Crosslinkers*

Carboxyl groups were introduced on the glass substrate by binding a bifunctional PEG linker, carrying an amine functional group and a carboxyl functional group. Using either an activated amine functionalised slide, or an epoxy functionalised slide, a 1.0 g L^{-1} solution of $NH_2-PEG_{2000}-COOH$ in phosphate buffered saline (PBS) buffer was prepared, and the slides submerged in the solution. The slides were then incubated for two hours at 40 °C and rinsed in MilliQ water. The carboxyl group was then used to bind amine functional molecules through the use of a carbodiimide crosslinker, here it was used to bind antibodies. NHS and EDC were prepared as separate 50 mg mL^{-1} solutions in 2-(N-morpholino)ethanesulfonic acid (MES) buffer (pH 5.0). The two solutions were mixed in equal volumes and incubated on the slides for 15 minutes. After rinsing with MES buffer, the slide was used to bind an amine functional molecule. The long PEG chain was used as a spacing linker, and it was theorised that the PEG molecule would reduce the non specific binding of the detection enzyme used in many of the applications presented in this study.[89]

3.2.5 *Immobilisation Using PAMAM Dendrimers*

Immobilisation of amine functional DNA probes were attempted using PAMAM dendrimers, following the protocols described by Benters et al.[90] Two methods were explored, one relying on a bi-functional PEG linker for the immobilisation of the dendrimers, and another relying on amine functionalised slides using PDITC as a cross-linker.

Bi-functional PEG linker

A bi-functional PEG linker having a silane group in one end and an NHS group in the other. The silane group reacts directly with the silanol groups present on the surface of clean glass, and the NHS group is capable of binding amine groups on the dendrimers. To functionalise the glass surfaces with the PEG linker, a 20 mg mL^{-1}

solution of silane-PEG-NHS in 95% ethanol was prepared and incubated on the glass for two hours, covalently binding the silane groups to the glass. Slides were then washed with ethanol and milliQ water to remove excess PEG linker, and then quickly dried to minimise exposure to moisture. Next, a 10% w/v solution of the PAMAM dendrimer in methanol was incubated on the slide over night. Slides were eashed with ethanol and acetone and dried using a nitrogen stream to remove unbound dendrimers. In order to activate the amine binding sites on the dendrimers, the PDITC cross-linker was used. For this process, freshly cleaned, dried glass ware had to be used, and reactions were performed in inert atmosphere, here argon was used. In separate glass boxes, a 10 mM solution of PDITC in dichloromethane containing 1% pyridine, dry dichloromethane, and dry acetone was prepared. The slides were first submerged in the PDITC solution for two hours under argon, and then rinsed first in dichloromethane and then in acetone. Amine functional DNA probes or proteins was directly immobilised on the activated dendrimeric surface, by incubating a 10 μM solution of the molecule over night at 4 °C. To block remaining free binding sites, slides were submerged in a solution containing 6-aminohexanol (150 mM) and N,N-diisopropylethylamine (50 mM) in water.

PDITC activated amine modified glass

As an alternative, PAMAM dendrimers were bound on amine modified slides using PDITC as cross-linker. MDA slides were modified using amino silane as described above, and then submerged in a 10 mM solution of PDITC in dichloromethane containing 1% pyridine as when cross linking the dendrimers as described above. After this activation step, the protocol continued with dendrimer immobilisation as just described.

3.2.6 *Immobilisation Using Biotin*

Biotinylated DNA was immobilised on avidin coated glass substrates. The amine groups in the amino acids, particularly in the Lysine, were used to bind the avidin molecules onto the surface of glass slides functionalised with epoxy or by using the carboxyl group on the bifunctional PEG linker as described above. To bind avidin on the surface, a 0.1 mg mL^{-1} solution of NeutrAvidin™was prepared in a PBS buffer (or MES buffer when using the carboxyl PEG linker) containing 1.0 M ammoniumsulphate ($(NH_4)_2SO_4$). The ammonium sulphate was added to aid in the precipitation of the protein onto the surface.[91] The NeutrAvidin™solution was incubated for 30 minutes on the slide and then washed in PBS buffer, and the slide was ready to bind biotinylated molecules.

3.2.7 *Immobilisation Using Nitrilotriacetic Acid for Poly-histidine Tagged Proteins*

In one application, poly-His tagged proteins were expressed on the droplet arrays and were bound onto the surface using a bifunctional PEG linker with an NTA end group. The poly-L-lysine-PEG-NTA molecules were bound onto the clean glass substrates by submerging the slides in a 1 mg mL^{-1} solution of poly-L-lysine-PEG-NTA in HEPES buffer (pH 5.5) for 30 minutes. The poly-L-lysine will form hydrogen bonds

with the glass slides at these conditions. After a rinse in HEPES buffer, the slides were incubated with a 0.01 M solution of copper(II) acetate in HEPES buffer for 10 minutes. The copper ions act a chelating agent for the NTA groups, activating the binding of the poly-His tag.[87] After rinsing, the slides were ready to bind His-tagged recombinant proteins.

3.3 Results

An attempt to compare the different surface chemistries for DNA immobilisation was made by binding an amine or biotin functional oligonucleotide probe and hybridising a fluorescently labelled probe at high concentration. The fluorescent label used was CY3, which fluoresce red when exposed to green light. The following surface chemistry combinations were tested: Neutravidin on both (I) amine and (II) epoxy functionalised glass, the carboxyl PEG linker on both (III) epoxy and (IV) amine functionalised glass, and direct binding on (V) amine and (VI) epoxy functionalised glass. The oligonucleotide probe was manually spotted onto the unstructured glass slide using a pipette and left in a humid chamber to bind. The fluorescence intensity of the spots was evaluated after hybridisation of the fluorescent complement. Fluorescence micrographs of the fluorescent spots are seen in Figure 3.2. From this test it was apparent that the DNA probes immobilised using NeutrAvidin showed the highest signal intensity, and thus this surface chemistry was preferred to bind DNA oligonucleotides. It is possible that the increased signal intensity seen on the NeutrAvidin coated glass is due to effective shielding of the negative charges on the glass substrate, thus making hybridisation easier.

It was also attempted to use the PAMAM dendrimers as a linker to bind aminated oligonucleotides. This was done on a structured glass slide carrying a patterned perfluorodecyltrichlorosilane (FDTS) monolayer as described in Chapter 8. This was, however, unsuccessful as the repeated harsh chemical treatments required in the reactions caused destruction of the FDTS monolayer. A bright field micrograph example of this can be seen in Figure 3.3.

3.4 Discussion and Conclusion

Both DNA oligonucleotides and proteins were successfully immobilised on the patterned glass surfaces by different means. Antibodies were immobilised using a bifunctional PEG linker. The linker was immobilised by a reaction between surface epoxy groups and a primary amine presented on one end of the linker. The other end of the linker could bind to amine groups on the antibodies through the reaction of a carboxyl group and a carbodiimide crosslinker. The PEG-linker provide flexibility and mobility of the surface bound molecules, it lifts the reactions away from the negatively charged glass surface, which might interfere with the interaction between the capture antibody and its antigen, and was also expected to provide protection against nonspecific binding of reporter enzymes in assays.[16] A poly-His NTA interaction was also used to successfully bind proteins.

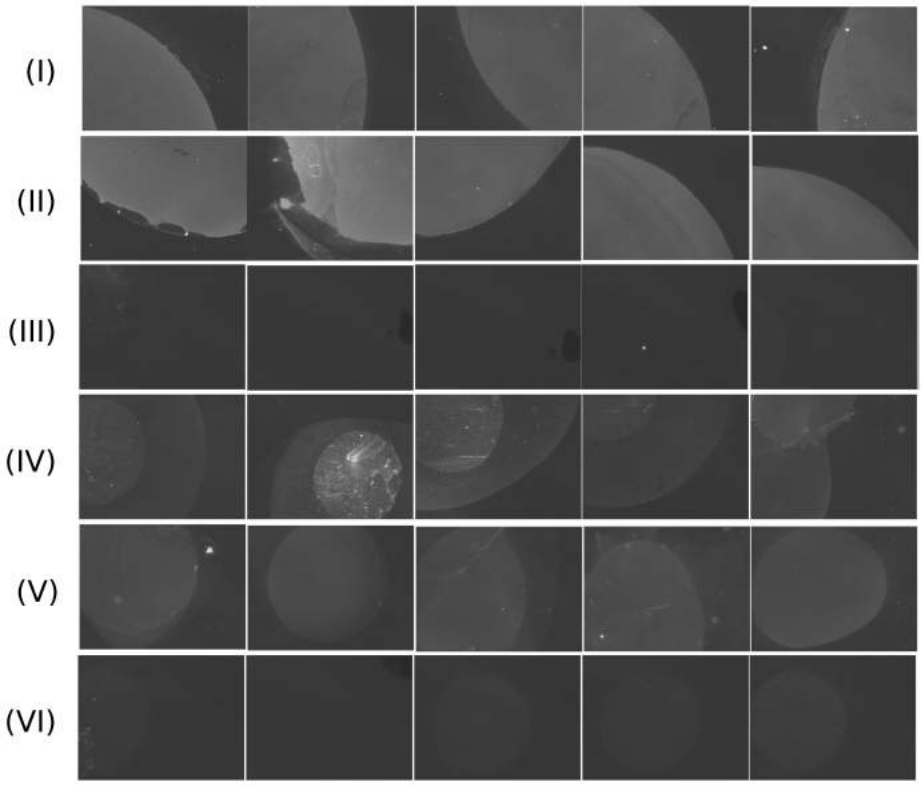

Figure 3.2: Fluorescence micrographs of CY3 labeled DNA oligonucleotide probes hybridised onto capture probes immobilised by six different surface chemistries. (I) Neutravidin on amine functionalised glass using the carboxyl PEG linker, (II) Neutravidin on epoxy functionalised glass, (III) the carboxyl PEG linker on epoxy and (IV) amine functionalised glass, and direct binding on (V) amine and (VI) epoxy functionalised glass. Each row shows fluorescence micrographs from five different spots.

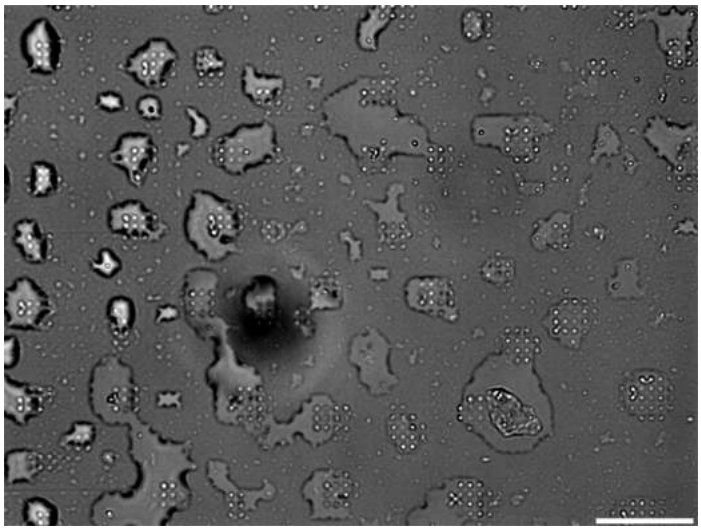

Figure 3.3: Brightfield micrograph showing the destruction of the FDTS monolayer after the immobilisation of dendrimers. The scale bar is 100 μm.

Different methods for immobilising DNA oligonucleotides were compared by hybridising a fluorescently labelled target to the immobilised probes. This indicated that binding streptavidin and utilising the biotin-streptavidin interaction gave the best hybridisation conditions. The immobilised streptavidin acts as a spacer and shields charges from the negatively charged glass, which is believed to reduce the repulsion of the DNA target, hence increasing the hybridisation efficiency.

A dendrimeric functionalisation was attempted, as these branching structures have been shown to greatly increase the density of binding sites. However, the rahter harsh crosslinking chemistries involved with this protocol disrupted the surface patterning of the MDAs, and droplets were no longer supported after surface functionalisation.

4 | Optical Detection Set-up

As a part of the fluidic control and detection scheme surrounding the MDA chip, an optical detection set up was built and programmed. It involved building a miniaturised fluorescence microscope with the possibility of automating chip imaging and fluid supply to the chip. The platform consisted of three parts: (i) The optics, which were used for the actual imaging of the chip, (ii) the motion control, which enabled a sequential tiled imaging of the entire chip, and (iii) fluid control for actuating liquids through the microfluidic channels. These parts were combined to have a platform where an assay could be run in it's entirety. In the following sections, the hardware and software will be described in greater detail, and the results from the characterisation of the set up is presented and discussed.

4.1 Fluorescence Microscopy

In order to understand how an optical detection platform should be put together, a logical place to begin is by explaining the basis of fluorescence and fluorescence microscopy.

4.1.1 *Fluorescence*

Optical detection requires contrast for us to distinguish the features of a sample. One way of achieving good contrast in optical detection is by using a fluorescent dye to stain the sample. As an example, when imaging cells, individual components such as the nucleus and cytoplasm can be specifically stained with dyes of different colour in order to locate and evaluate the state of the cell. Fluorescence is also used as a contrasting agent in a myriad of different applications. Fluorescence is a kind of photoluminescence, which is light of a certain wavelength emitted by chemical substances in response to being illuminated by light of a different wavelength.[92] It is only some molecules that are capable of fluorescence and they are called fluorochromes. When a fluorochrome absorbs light (a photon), the addition of energy lifts an electron from the electronic ground state into an excited state. This can be depicted in a Jablonski diagram as shown in Figure 4.1. S denotes the electronic states and v denotes the vibrational states. The electronic absorption of the photon happens so fast (within femtoseconds) that nuclear displacement (x-axis) is negligible in this time frame. For this reason, the transitions are depicted as vertical lines with respect to internuclear distance. This assumption is termed the Franck-Condon principle. Since the electronic excited state is typically geometrically different from the ground state, and since electronic excitation is assumed to happen without change in internuclear separation, the excited electron will arrive in the first vibrational state of S_1 that overlap with the ground state.[93] From the excited vibrational state, the molecule relaxes into the ground vibrational state in the electronic excited state. This transition

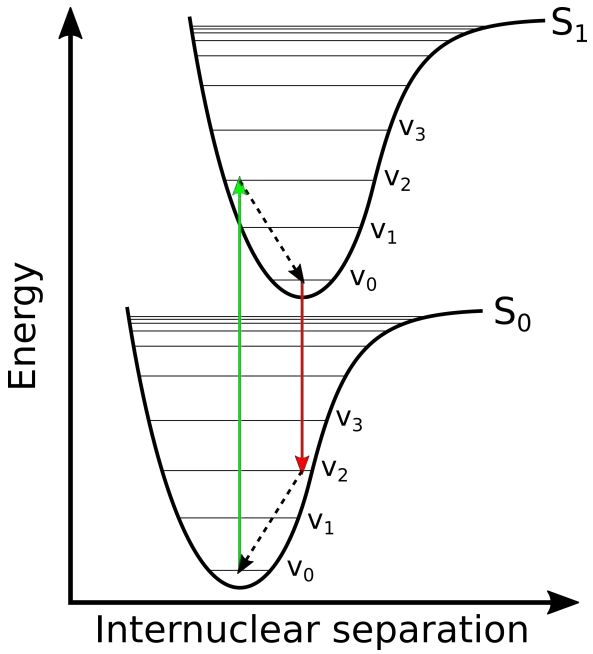

Figure 4.1: Jablonski diagram showing the transition of an electron from the ground state, S_0 to the first excited state, S_1 upon the absorption of a photon. A photon with a lower energy is emitted during the relaxation from the excited state to the ground state.

happens without emission of light, and the energy dissipates as heat or by interaction with other molecules in the solution. Since the molecule is still in the electronic excited state, eventually the electron will relax back to the ground state. This transition is also much faster compared to the nuclear motion, and the electron will relax to the lowest possible vibrational state in the ground state without causing a change in internuclear displacement. The energy released from this transition may be emitted as a photon, however, some energy has already been lost, and therefore, the emitted photon will have a lower energy than the photon that originally excited the molecule, and a red-shift in wavelength is observed. This is called the Stokes shift.[94] Other molecular interactions can also occur, such as internal conversions or intersystem crossings, which lead to other types of molecular relaxation. This means that some of the transitions from the excited state will happen without emission of a photon. For a specific fluorochrome, quantum yield is defined as the ratio of the number of photons emitted to the number of photons absorbed, and as such describes the efficiency of the fluorochrome.[93] Fluorochromes also have a life time. Even though fluorescence is a cyclic process, after being exposed to the excitation light for some time, the fluorochrome will deteriorate, and lose the ability to fluoresce in the process called photobleaching.

4.1.2 *The Fluorescence Microscope*

As just described above, fluorescence involves the conversion of light from one wavelength to another by internal conversion in an absorbing molecule. Detecting the emitted light from the fluorescent molecules provide a selective way of determining their presence. However, the light emitted through the process of fluorescence is not directed, making their photons much more difficult to detect.

A fluorescence microscope provide the required light filtration to observe this weak, scattered signal on top of the excitation light. Essential to the microscope is the microscope objective, which provides both magnification of the specimen but also works as a condenser providing illumination onto the sample.[95] By illuminating the sample through the objective rather than through a condenser above the sample, only a small amount of the excitation light is reflected from the sample and needs to be blocked. In order to separate the excitation and emission light, a filter cube is placed in the light path. The filter cube contains three filters: a band pass filter, which ensures that the wavelength of the excitation light is well defined, a second band pass filter which ensures that only light corresponding to the emission wavelength is transported onto the photo-detector. In the heart of the filter cube is a dichroic beamsplitter mirror, which is capable of transmitting light above a certain cutoff wavelength while reflecting light of lower wavelength. This is schematically represented in Figure 4.2.

In order to generate an image, a light source is required. traditional fluorescence microscopes incorporate arc lamps, such as a mercury or xenon arc lamp. These are expensive and require special lamp housings, as a damaged lamp may produce harmful substances.[95] In recent years the development of light emitting diodes (LEDs) has led to inexpensive light sources with sufficient light intensity to replace the arc lamps, as it is seen in for example the Zeiss Axio Observer.

In order to deliver the excitation light and collect the emission light, the microscope objective is a central component of the microscope. For fluorescence microscopy, a high numerical aperture objective is important. The numerical aperture is a parameter that describe the the range of angles from which the light can enter and exit the objective. Accepting light from a broad angle increase the number of photons captured from the fluorescence. A high numerical aperture also increase the resolution of the objective.[95]

Lastly, the photo-detector is what transforms the captured photons from the fluorescence into a digital image which can be manipulated and analysed on a computer and transformed into data. the quality of the detector in the microscope camera also impact the quality and resolution of the microscopy. The photo-detector collects photons in a grid of pixels during the exposure and converts them into electrons. The number of photons colliding with the pixel is translated into a brightness value of the corresponding pixel in the digital image on the computer. Hence, the pixel size is the limiting factor on the spatial resolution of the detector. Different types of detectors exist and are good for different applications, however, the difference will not be covered here.

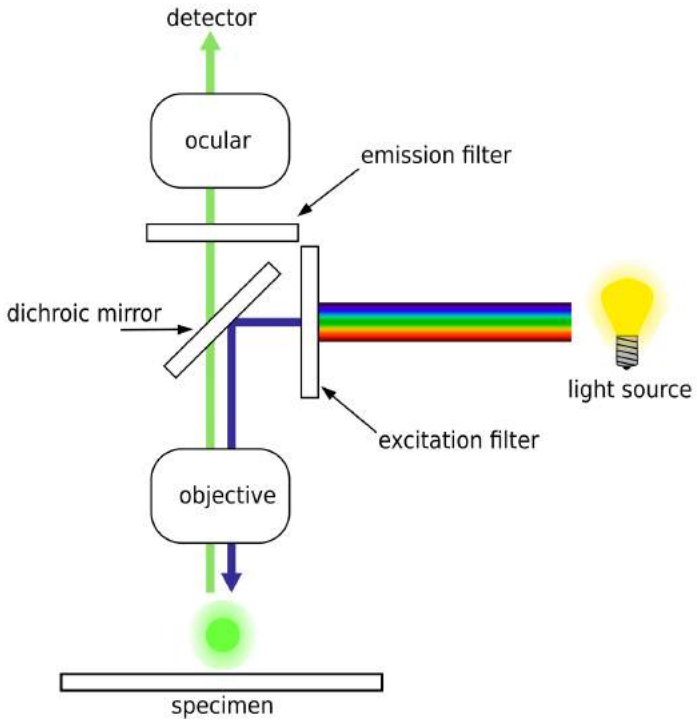

Figure 4.2: Schematic representation of the light filtration in a fluorescence microscope. From [1].

4.2 The optical Detection Platform

To image the MDAs, a microscope-like optical set up was constructed. The platform was built upon the principles of the fluorescence microscope as just described. Two different configurations were built; One based on a microscope objective, and later another which was based on a bi-telecentric lens system (see Figure 4.3 A and B). In the next parts, the differences and benefits of both set ups will be discussed.

4.2.1 *Microscope Objective-based Set Up*

The first set up that was built, used a microscope objective to collect the fluorescence given off from the sample. Photons emitted by fluorescent samples are randomly directed, and hence a lens that collects as much light is wanted in order to detect the signal with ease. Microscope objectives are excellent for fluorescence imaging, therefore this was chosen. Following the optical path from sample to sensor as seen in Figure 4.3 A, each component has the following function:

- Microscope objective: works as condenser for the excitation light, and collects the photons given off by the fluorescent sample.
- Filter cube: Splits and filters the light so that only light of the right wavelength is transmitted on to the sensor.

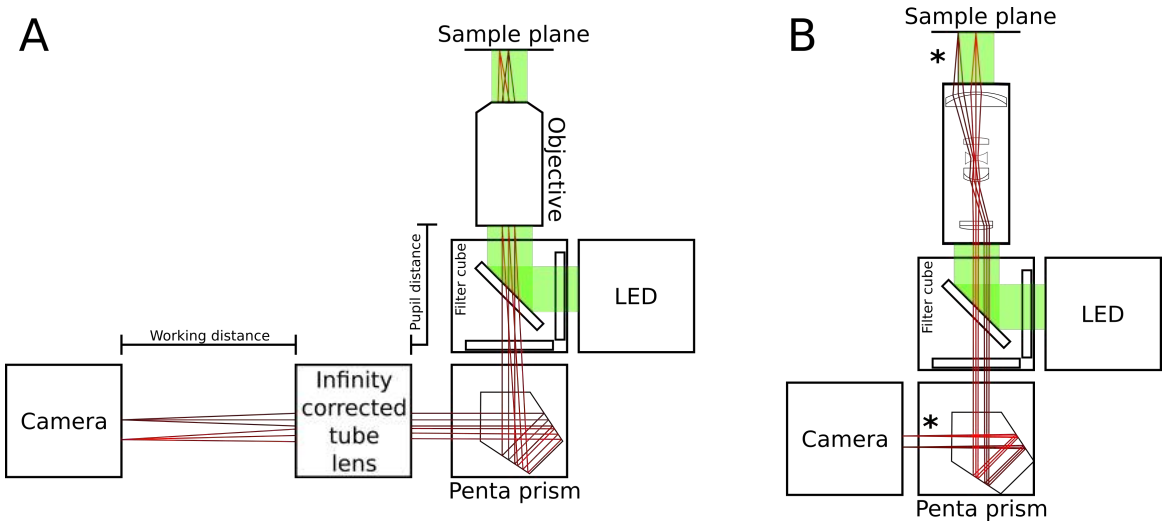

Figure 4.3: A) Optical set up based around a microscope objective for focusing the light from the fluorescing target onto the sensor. B) Optical set up based around a telecentric lens for a larger depth of focus.

- LED: Provide excitation light of the correct wavelength.
- Penta prism: The penta prism reflects a beam of light with a constant 90 ° angle. The beam is reflected twice inside the prism allowing the transmission of an image without inverting it.
- Infinity corrected tube lens: Focuses the parallel beams from the objective onto the detector.
- Camera: Transforms the photons into a digital image.

All the optical components were connected using lens tubes and embedded in lens cages as this reduced the amount of stray light able to enter the system, in turn reducing the noise in the image.

4.2.2 *Telecentric Lens-based Set Up*

Similar to the microscope objective based set up, a set up using a bi-telecentric lens was built. The telecentric lens offers constant magnification over the depth of field, which is much wider than that of a microscope objective. This phenomenon occurs because the lens and aperture configuration ensures that the central rays are parallel to the optical axis in both the object and the image plane. The aim of using a bi-telecentric lens was to avoid refocusing on the sample, as the sample was scanned by utilising the large depth of field. The components of this set up was mostly the same with the telecentric lens replacing the microscope objective and the infinity corrected tube lens, as seen in Figure 4.3 B.

4.2.3 *Image Tile Scanning*

In order to image the entire MDA, a set of mechanical stages could move the optics in the x and y directions, creating a tile scan of the chip. One image frame could

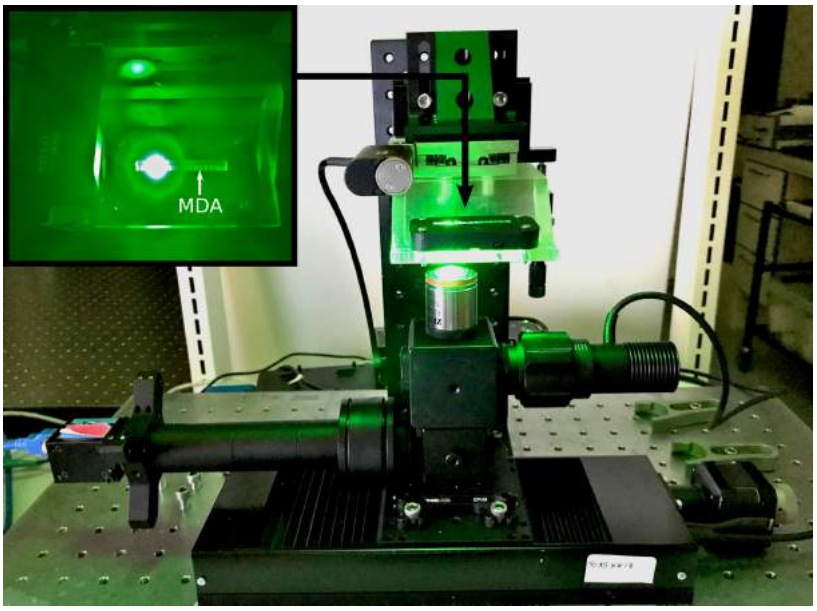

Figure 4.4: Photograph of the optical detection set up mounted on translation stages for image tile scanning. The insert shows the position of the MDA in the microfluidic interface.

capture almost the entire width of the channel, and hence the MDA was imaged by scanning each channel in the y-direction and moving between channels in the x-direction. A stepper motor based mechanical stage with a 10 cm track was installed beneath the chip and carried the entire optical set up. This was used to move the image in the x-direction. A smaller stepper motor based stage with a 2.5 cm track was installed and used to hold the microfluidic interface, allowing the scanning in the y-direction. The stepper motor and microfluidic interface was in turn mounted on a manual translation stage, which eased focusing on the sensor surface. A photograph of the set up mounted with the microscope objective can be seen in Figure 4.4 with the insert showing the position of the MDA chip in the microfluidic interface.

Besides the optics and translational system, a peristaltic pump was fabricated, which could actuate liquid through all 16 microfluidic channels simultaneously. The miniaturised pump was easily integrated in the set up on a small platform in front of the microfluidic interface above the optics where it was free of the moving parts, though not shown in Figure 4.4. The pump was driven by a stepper motor rotating the driving shaft. On the driving shaft was mounted two rollers with pump houses holding eight tubings each. When the rollers were rotated by the stepper motor, the pressure on the tubings would actuate liquid through the tubings. A photograph of the pump is shown in Figure 4.5. The pump housing was micromilled in house and consisted of aluminium end walls, a Poly(methyl methacrylate) (PMMA) top, and tubing connectors in polytetrafluoroetylen (PTFE). The rollers consisted of two PTFE end pieces connecting eight steel pins. The steel pins could easily rotate in the PTFE end pieces.

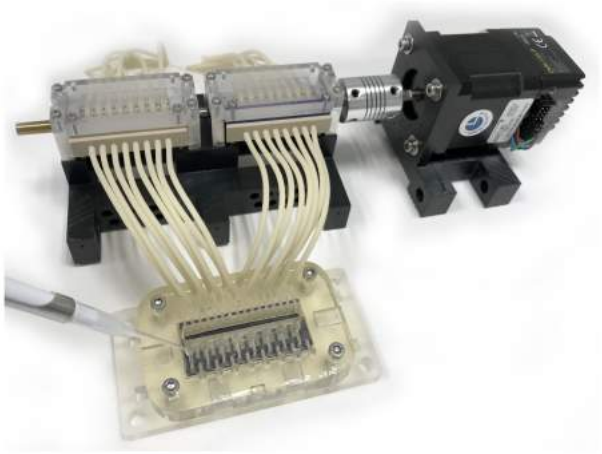

Figure 4.5: Photograph of the 16 line peristaltic pump connected to a microfluidic interface.

4.3 Software Programming for Imaging, Motion- and Fluid Control

To simultaneously control the imaging, motion and liquid actuation, a custom LabView script was made, which integrated the communication to all the devices on the set up. The stepper motor stages and the stepper motor controlling the peristaltic pump as well as the camera came with plug-ins to use in LabView directly, and the LED was controlled using a digital to analogue converter.

4.3.1 *LabView*

LabView from National Instruments is a graphical programming language, which is designed with systems engineering in mind. It features easy communication to many different pieces of hardware through plug-ins, making integrated systems easier to combine. In order to ease the understanding of the following explanations, a few definitions will be given here. LabView operates via a front panel and a block diagram. The block diagram is the equivalent of the programming code and the front panel is the UI. The combination of a block diagram and it's front panel is referred to as a VI (virtual instrument file). In the next sections, a description of the construction of the LabView system and user interface will be given.

The entire LabView script was tied together by references to the main user interface (UI), also referred to as the graphical user interface (GUI), through the use of a GUI cluster. This cluster passed event and data queues, values, and properties between the different parts of the script. Besides this, the UI also handled user inputs and passed these on to the other parts of the program. The program was built as a modified master/slave (or producer/consumer) architecture, and an overview of the hierarchy is sketched in Figure 4.6 A, and the main VI linking together the components of the script is shown in panel B. In the following sections, each part of the main VI is

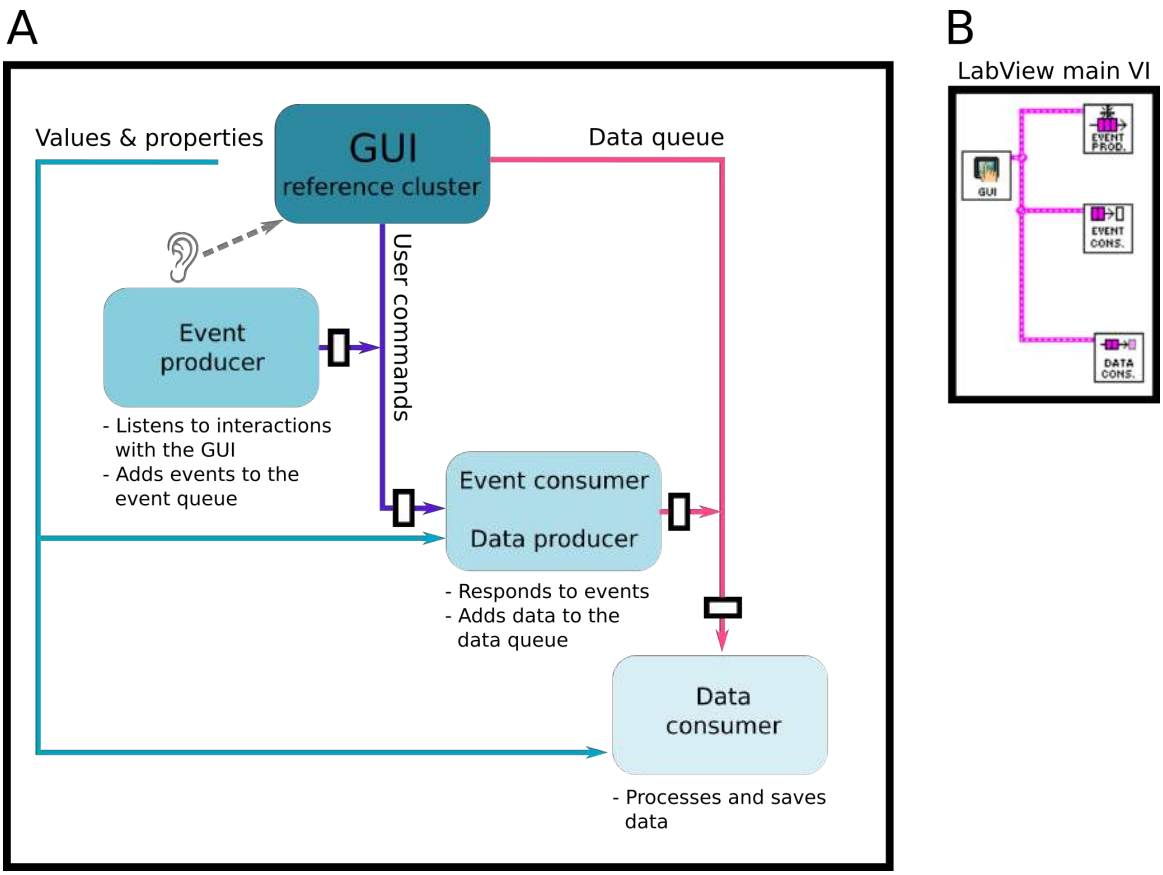

Figure 4.6: A) Sketch of the hierarchy of the Master/slave architecture of the LabView script controlling the optomechanical detection platform. B) The main VI which ties together the event producer, event consumer, and data consumer with the GUI.

explained in more detail.

4.3.2 *User Interface*

From the user interface, the user has control over both of the translational stages, the pump, camera properties, the LED, and the data analysis properties and has access to the live view from the camera. Figure 4.7 shows the user interface with the live view in the middle and controls on the right. The parameters for the image analysis is found in the bottom. Each button, indicator and control is combined to form the GUI reference cluster in the GUI block diagram, and this cluster is passed between the other parts of the programme using a VI server reference. This allows all parts of the programme to access the values, properties and events handled by the programme simultaneously. The GUI block diagram can be seen in Figure B.1 in Appendix B and shows how all the units of the user interface is bundled together.

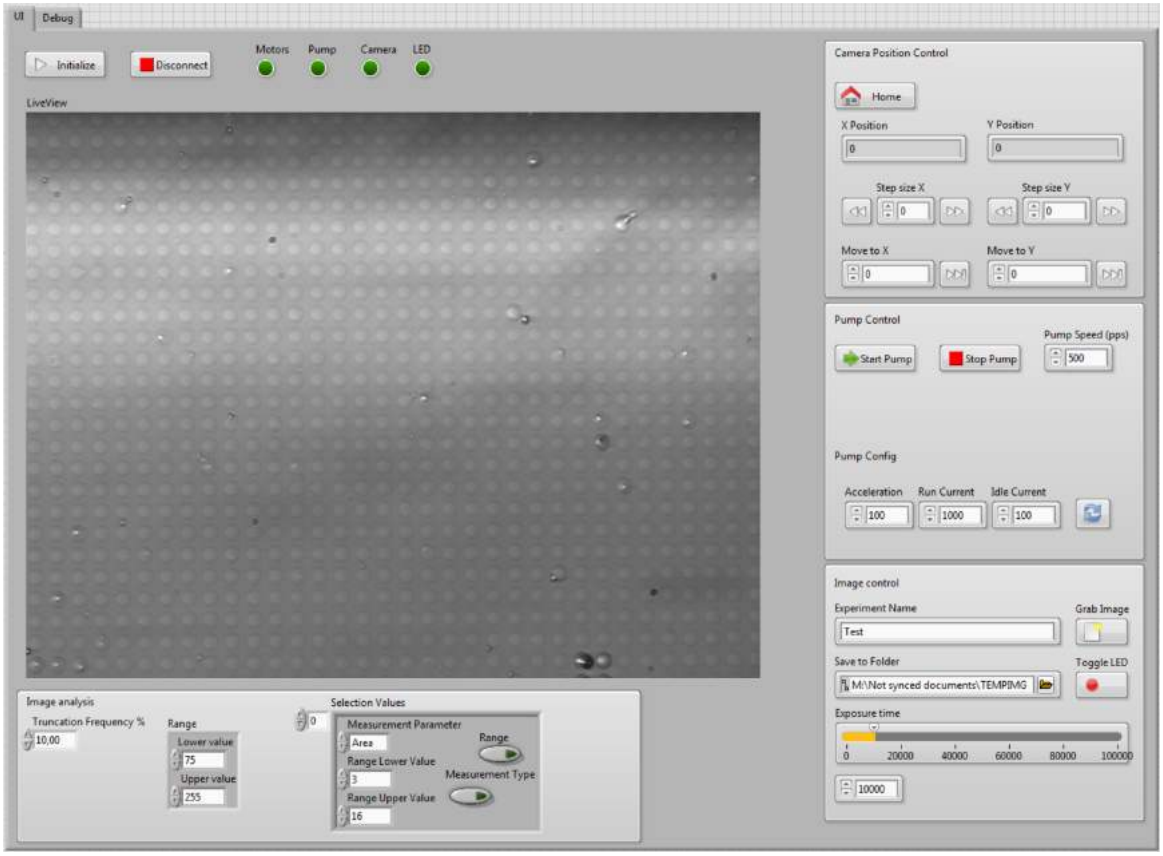

Figure 4.7: The LabView user interface for the platform control software.

4.3.3 *The Event Producer*

The event producer is the master or controller of the programme. This part of the programme listens to user commands from the UI and queues them as events in an event queue. A more detailed description is most easily given by following the visual code, which can be seen in Figure 4.8. First the GUI reference cluster is passed into the programme loop (1). From the GUI reference cluster, the event queue is unbundled, and the button references are registered to listen for events from the GUI (2). An event structure (3) handles the queuing of the events registered from the GUI, in such a way that the events are handled in the same order as they were registered (first in, first out queue). The sequence structure (4) is used to pass a GUI update command after registering each GUI event such that every other element in the queue will ensure that the GUI is updated with new values etc. Lastly, when the programme is terminated, the event queue is released and the event registration stopped (5). The events registered to the event queue through the GUI reference cluster by the event producer is now ready to be handled by the event consumer.

4.3.4 *The Event Consumer - Data Producer*

The event consumer is both a slave to the event producer, and a master to the data consumer in the master/slave architecture. The primary function of the event

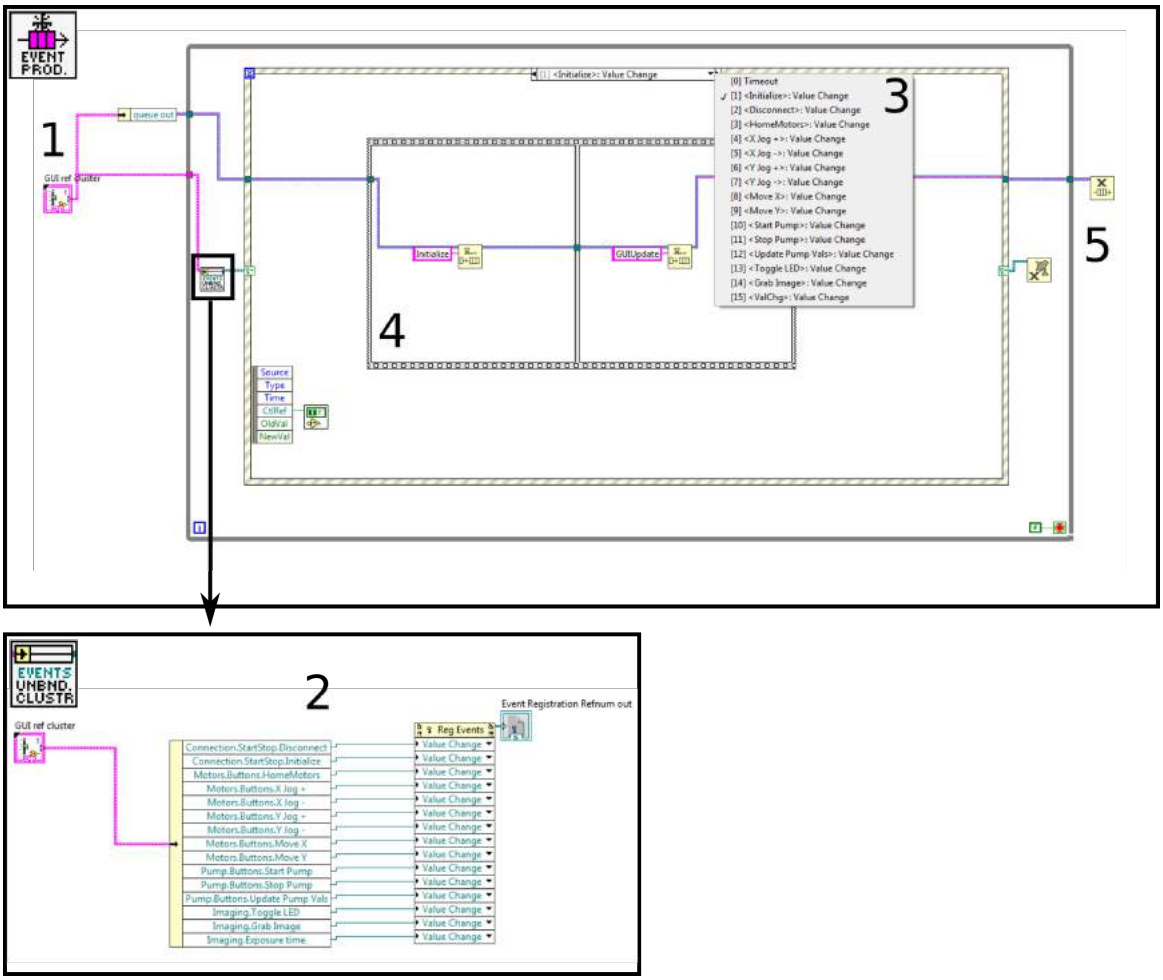

Figure 4.8: The event producer block diagram.

consumer is to respond to the user commands registered by the event producer. Some of these events will result in the generation of data, which in turn is enqueued and passed on to the data consumer. The event consumer block diagram is shown in Figure 4.9. As in the event producer, the GUI reference cluster is passed into the programme loop (1), where the event and data queue is unbundled. Elements from the queue is passed to a case structure (2), which contains the actions matching the GUI events. In the example shown here ("Start Pump" command), the pump speed value is unbundled from the GUI reference cluster and passed to the pump control plug-in via a property node (3). The plug-in to control the pump stepper motor sends and receives commands to and from the stepper motor. In this case, the desired pump speed is sent to the stepper motor controller followed by the command to start jogging in the motors negative direction (J-). Similar actions exist for every possible event handled by the program. Lastly, the queues are released when the programme is terminated (4). The data (images) enqueued by the event consumer is now passed to the data consumer via the data queue through the GUI reference cluster.

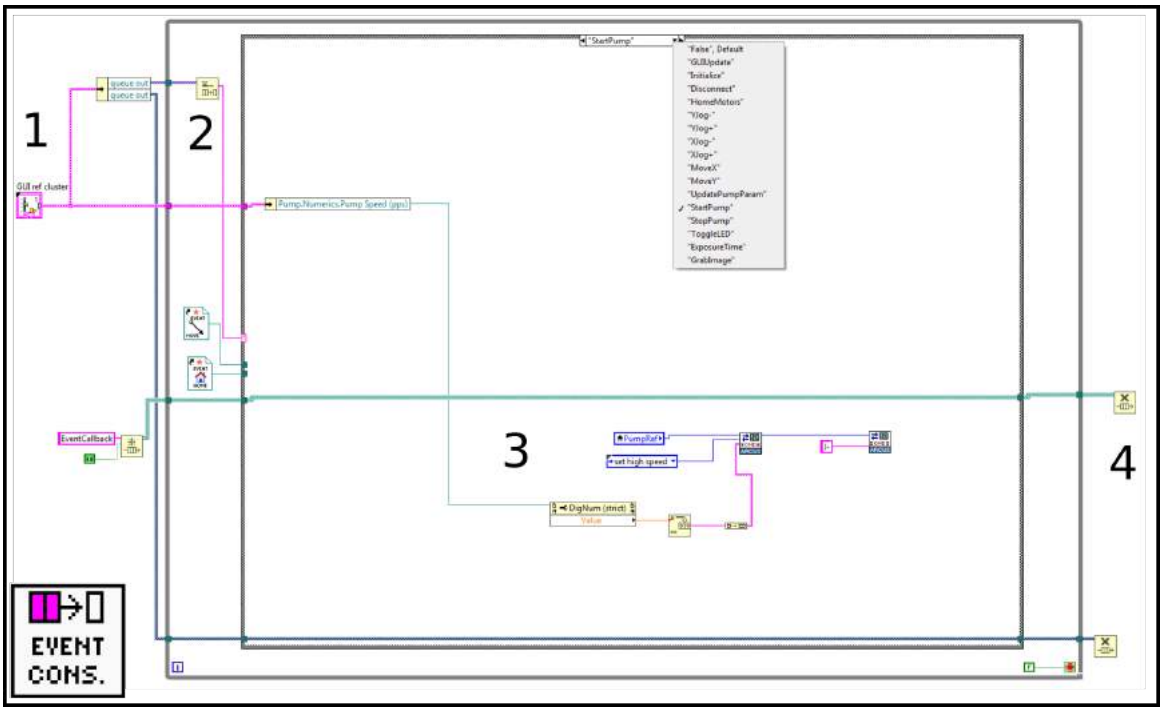

Figure 4.9: The event consumer - data producer block diagram.

4.3.5 *The Data Consumer*

The data consumer is tasked with the data analysis. In this case, the aim is to count fluorescent spots and to save the images taken during the assay. Figure 4.10 shows the data consumer block diagram and the image analysis sub-VI. As with the other parts of the script, the GUI reference cluster is passed onto the programme loop (1), where the data queue is unbundled. Inside the loop, the events are taken one by one from the queue (2) and handled. The values provided by the user setting the parameters for the image analysis is unbundled (3) and passed to the image analysis sub-VI (4). In the image analysis, the colour image is converted to gray scale by extracting one of the colour planes (5). Next, the background noise is reduced by applying a high pass, fast Fourier transform filter (6). The noise reduced gray scale image is then converted to a binary image by applying an intensity threshold (7). All pixels above the threshold is assigned the value 1 and those below is assigned the value 0. In the binary image, clusters of positive pixels are considered particles, and the first operation on the binary image filters the particles by size (8). The size of each spot or droplet is well defined by the photolithographic fabrication process, and thus particles much smaller or larger than the droplet size is not considered a specific signal. Lastly, the image analysis programme counts the remaining number of particles (9).

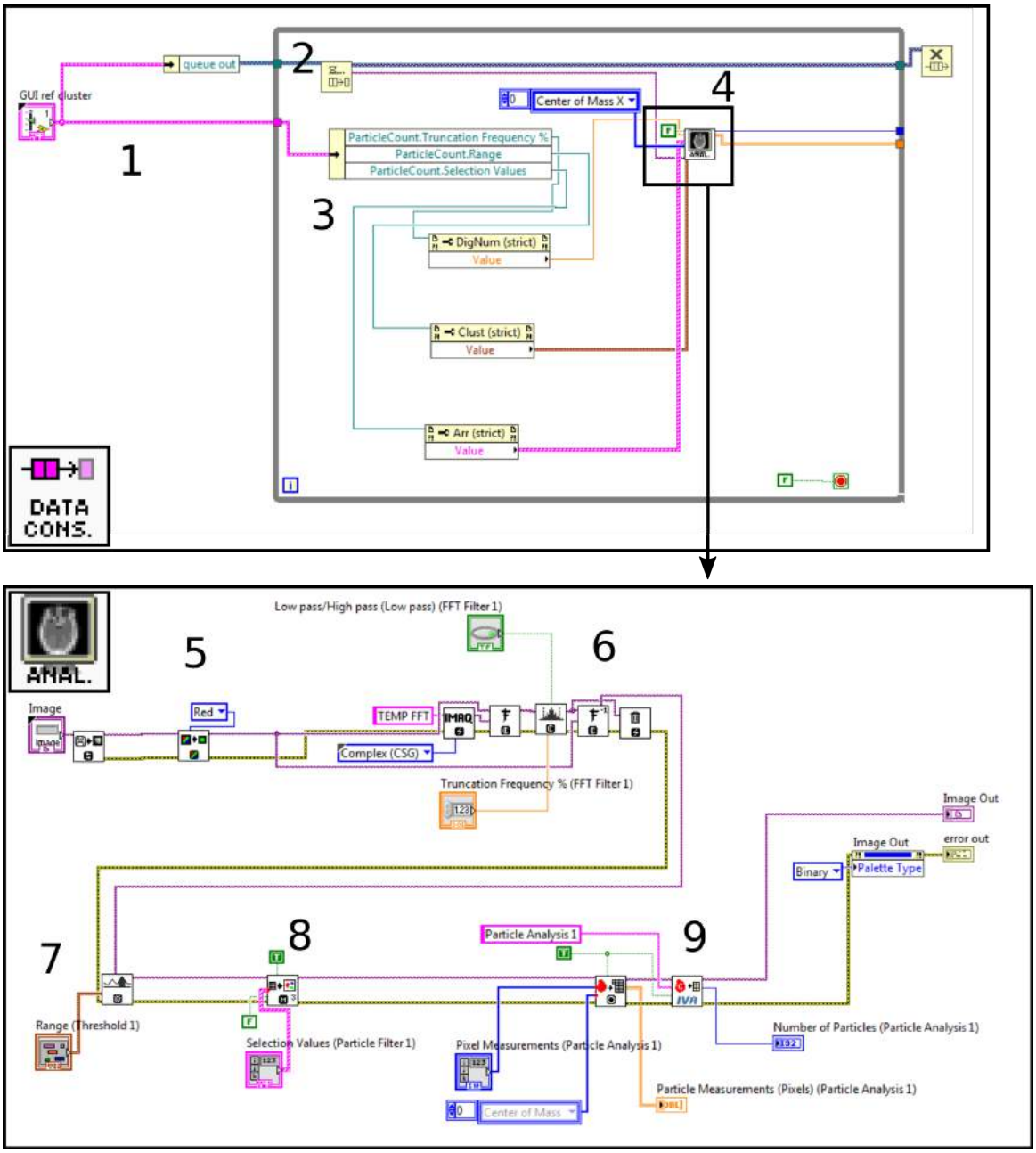

Figure 4.10: The data consumer block diagram, including the image analysis VI.

4.4 Imaging of MDAs Using the Optical Detection Set up

The set up described above was used to image the MDAs in parallel to using an inverted fluorescence microscope. By using the ambient light above the set up, bright field pictures could be obtained, and to obtain good fluorescence images, the ambient light was turned off, and a frame with dark panels was added around the set up to reduce stray light.

Imaging the MDA using the objective based set up turned out very nicely. Images were comparable in quality to those taken with a commercial fluorescence microscope, albeit the fluorescence appeared slightly weaker. Bright field and fluorescence micrographs taken using the objective based set up can be seen in Figure 4.11 A and B respectively.

Using the alternative set up based on the telecentric lens turned out more challenging. Due to the large depth of field, covering the MDAs with the fluidic interface introduced alot of noise in the images. A nice pattern was obtained when imaging a fluor acryl based MDA without the microfluidics, as seen in Figure 4.12 A, but as shown in panel B, the image became very noisy when adding the microfluidics on top of the MDA. Due to noise from the lid, it was not possible to obtain fluorescence images where the droplets were clearly seen.

Using the microscope objective based set up seemed like the best working solution so far, even though it is a bit more labour intensive, as it requires constant manual refocusing. This also limits the automatability of the system, as it was originally designed towards handling the tile scanning autonomously. It is postulated that the telecentric lens system may function better if a non-transparent microfluidic lid is used, which absorbs more of the stray light during fluorescence imaging. This, however, limits the use of the system for bright field imaging. another thing to keep in mind for the telecentric lens based set up is to reduce the spontaneous formation of puddles in the lid. It has been observed that liquid retained on the surface of the lid may be a source of substantial fluorescence background due to nonspecific binding of the HRP in the lid, and particularly with the large depth of field of the telecentric lense, this would impair the ability to distinguish the small, fluorescent droplets.

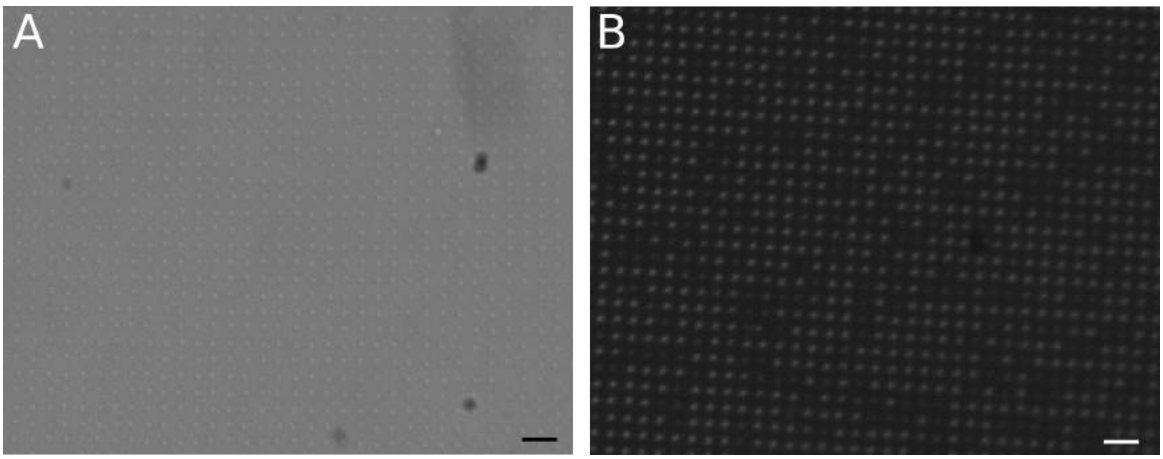

Figure 4.11: Micrographs taken using the microscope onjective based set up. A) Bright field micrograph of an FDTS based MDA chip containing a solution of HRP and its fluorescent substrate. B) Fluorescence micrograph showing fluorescent droplets from the conversion of a fluorogenic substrate by HRP. Scale bar is 20 μm.

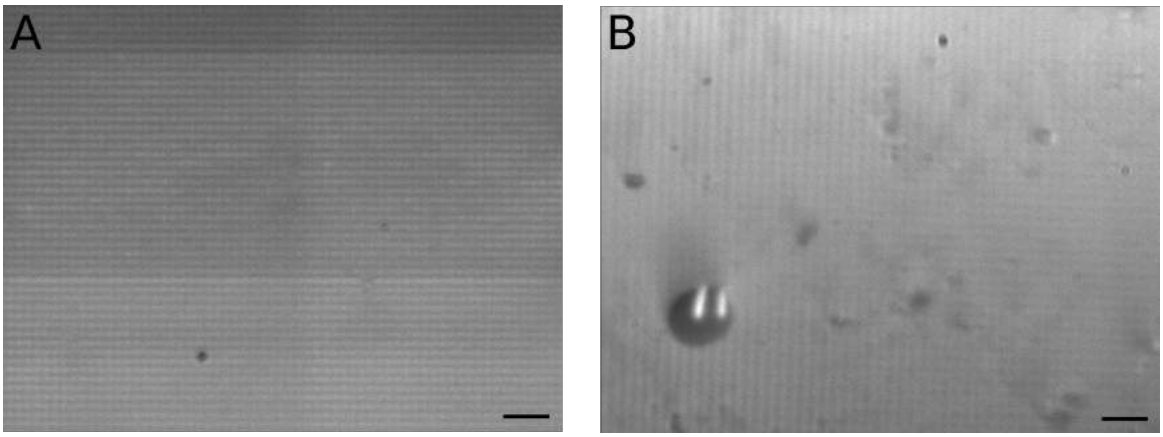

Figure 4.12: Micrographs taken using the telecentric lens based set up. A) Bright field micrograph of a bare, fluor acryl based MDA chip without the microfluidic lid. B) Bright field micrograph of an FDTS based MDA embedded in the microfluidic interface. Droplets are generated using a solution of HRP and its fluorescent substrate. Scale bar is 50 μm.

4.5 Conclusion

To summarise the chapter, an optomechanical detection platform was built, which integrated tile scan fluorescence imaging and liquid actuation. All the components were controlled from an integrated LabView script based on a master/slave architecture to execute the commands given by the user through the user interface. Two optical configurations were built. One based on a microscope objective, and one based on a bi-telecentric lens system, which was supposed to alleviate the need to refocus on the sample due to the large depth of field compared to the microscope objective. Fluorescence and bright field images taken using the objective based set up, and image quality was approaching that obtained using a standard fluorescence microscope. However, when imaging microfluidics integrated MDAs using the bi-telecentric lens based platform, the droplet pattern was obscured by microscopic features and optical effect coming from the transparent lid. It was suggested that fabricating a non-transparent lid and ensuring that liquid was not retained in puddles on the lid to interfere with the fluorescence imaging may solve these issues.

5 | Design and Fabrication of the Microfluidic Interface

5.1 The Design and Fabrication of Microfluidic Chips

A large part of performing bio assays involve fluid handling. In traditional assays such as ELISA performed in microtitre plates, the fluid handling involves pipetting the reagents into the wells. However with the development of microfluidics and lab-on-a-chip technologies, many different methods for controlling the fluid handling can be achieved. Microfluidic channels can be used to deliver liquids in a very controlled manner to well defined places. In this study, microfluidics were used to transport the reagents required to perform a certain assay onto the microdroplet arrays. Using microfluidic channels in this case aid in decreasing the required reagent volume, decrease the diffusion distance of the reagents onto the surface of the MDA, and allows for rapid and controlled droplet formation.

Microfluidic chips can be fabricated in a myriad of ways. Common fabrication methods in the academic world include PDMS casting, micromilling and photolithography. Common to these fabrication methods is that the turn over time between design iterations is very short, however, upscaling is very limited. All of the above mentioned methods primarily result in planar structures, which limits the spatial degrees of freedom of the designs of such devices. In recent years, 3D printed microfluidic systems have emerged as the technology develops. Increasing resolution now allow for microscopic structures to be realised.[96] The 3D printing method gives total spatial freedom of the design. This may allow whole systems to be printed as one part eliminating the need for bonding the structures to form closed systems. Using both traditional PDMS casting (soft lithography), micromilling and photolithography, bonding is required to form a closed channel system. When thinking about commercialisation of the microfluidic systems, scalable fabrication methods are typically desired. Popular fabrication methods for up-scaling include injection moulding and hot embossing. 3D printing may also be considered, as the technology evolves, and 3D printing factories become available.

The choice of material is also of great importance for microfluidic systems, and may vary depending on the application at hand. Particularly systems that are designed to interact with mammalian cells or bacteria has to consider the bio-compatibility of all parts that contact the fluids transported in the system to avoid toxicity. PDMS is a popular choice of material due to it's biocompatibility, optical transparency and low cost.[97] However, PDMS fabrication is difficult to scale, and now other materials to replace PDMS is being investigated. One example is off-stoichiometry thiol-enes, which share many of the desireable properties of PDMS.[98] Bridging the gap between proto-

typing and commercial fabrication is the main challenge of microfluidics. Commercial devices are typically made from thermoplastic materials such as PMMA, polystyrene, or COC, which are easily mass produced using injection moulding. However, using thermoplastics in prototyping is impractical, since the fabrication of the tools for injection moulding or hot embossing is more expensive and time consuming.[98]

In this study, several design iterations utilising different fabrication methods was performed to optimise the microfluidic interface. Initially, injection moulded microfluidic channels were used, however, when further development of the microfluidic design was required, PDMS casting and 3D printing was applied for fast prototyping. In the following sections, the different designs and their fabrication is reviewed.

5.2 Micromilled Fluidic Interface

The first design of the microfluidic interface was a combination of an injection moulded lid which was tape bonded directly onto the MDA. The assembly was then placed in a micromilled clamp which worked as pump interface and input reservoirs. This assembly was used in conjunction with the microscope slide sized MDAs (26 x 75 mm).

5.2.1 *Lid*

The lid was fabricated in COC using injection moulding. COC is optically clear as glass and have high transmission of UV light, as well as having a low moisture absorption rate, which is beneficial for microfluidic purposes. The lid itself comprised 16 low aspect ratio channels used to direct liquids across the surface of the MDA. 16 separate channels allowed for 16 individual samples to be tested simultaneously. The COC lid was 1.3 mm thick with channels 2.7 mm wide and 100 μm high. The distance from inlet to outlet was 21 mm. The lid design is seen in Figure 5.1 A. The inlet and outlet holes were drilled in a computer numerical control (CNC) machine using a 1.5 mm drill bit. The lids were then engraved with an identification number using a CO_2 laser. Next, the COC lid was bonded onto the MDA substrate using a 142 μm thick pressure sensitive adhesive (PSA). When placed between the lid and the MDA substrate in a bonding press, the PSA would compress and flow to fill out the cavity between the channels in the lid resulting in a final channel height of 100 μm as defined by the fetures on the lid. The final, bonded chip is seen in Figure 5.1 B.

5.2.2 *Clamp*

To interface with the bonded MDA chip, a clamp or microfluidic interface was fabricated. It comprised of two layers of PMMA bonded together, containing the inlet reservoirs, channels, and outlet pump connections. Two strips of PDMS gaskets were used to form a seal between the clamp and the MDA chip, which was secured using a micromilled aluminium brace which applied the necessary force on the seal. Sketches of the two parts comprising the clamp and the PDMS gasket are seen in Figure 5.2 A, and a photograph of the whole assembly is shown in Figure 5.2 B. The top part

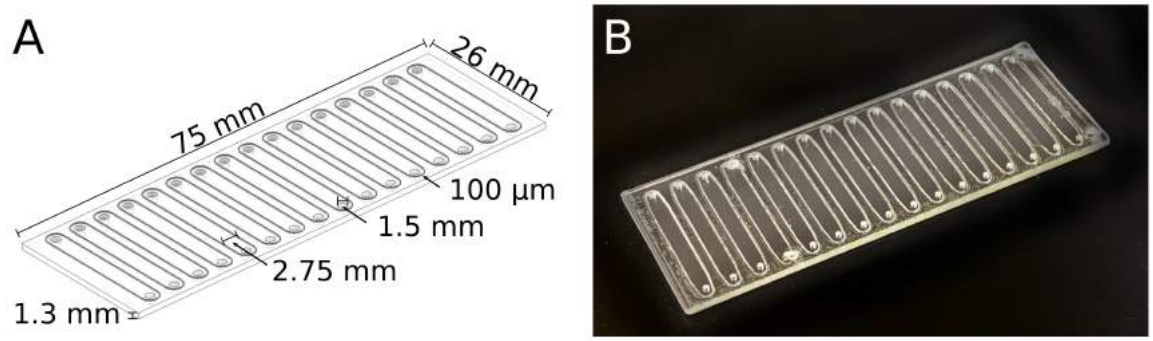

Figure 5.1: A) 3D sketch of the injection moulded COC lid with dimensions. B) Photograph of the assembled MDA chip. The MDA glass substrate and the injectionmoulded COC lid is bonded together using a pressure sensitive adhesive.

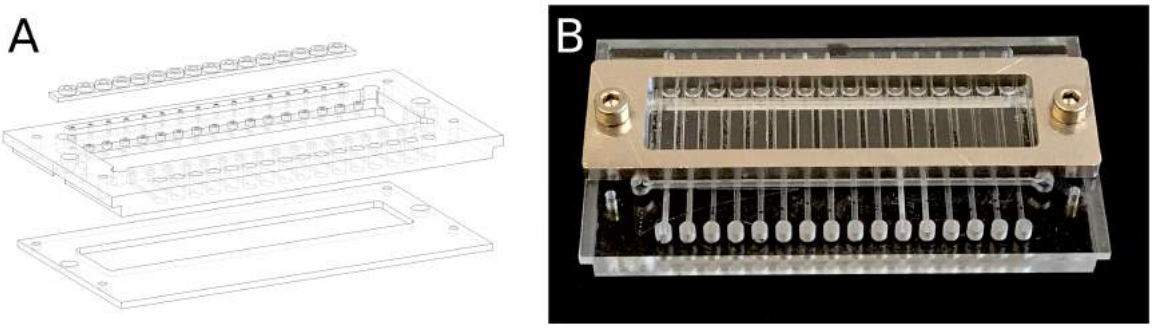

Figure 5.2: A) Sketch of the components comprising the micromilled PMMA microfluidic interface and the PDMS gaskets used to seal the interface between the MDA chip and the microfluidic interface. B) Photograph of the MDA chip assembled in the microfluidic interface.

of the clamp contained the fluidic channels as well as the inlet and outlet interfaces. This part was fabricated by micromilling both sides of a PMMA substrate using steel pins for alignment of the two sides. The simpler bottom part was also micromilled. To bond the two PMMA parts together, the bonding surfaces were wiped with isopropanol and UV irradiated for 120 seconds. Immediately following the UV exposure, the two parts were brought into contact, using steel pins for alignment. The assembly was then placed in a bonding press for 1 hour at 90 °C and 10 kN of pressure. To fabricate the PDMS gaskets, a three part, micromilled PMMA mould was assembled using bolts. PDMS elastomer (Sylgard 184, Dow Corning) was mixed with the curing agent in a 10:1 ratio and injected into the mould using a syringe. The PDMS was then cured at 80 °C over night.

5.3 3D Printed Fluidic Interface

In order to reduce the turn over time between design iterations while optimising the microfluidic interface to fit the smaller MDA chip, a 3D printed clamp was designed, which could be used in conjuction with a PDMS or 3D printed lid. A Formlabs stere-

olithography printer was used to fabricate the clamp. One down side of using a UV cured polymer as the clamp was that the photoactive compounds gave rise to autofluorescence, resulting in an increased background signal when detecting fluorescence on the MDAs. This was reduced greatly by using a black resin rather than a clear resin, as this had increased absorption of the generated autofluorescence photons. This did, however, limit the use of bright field microscopy which was typically used to focus on the surface of the MDA. A small viewing window was introduced which allowed focusing on the chip surface using bright field microscopy.

In the following, the fabrication of the lid and clamp is desribed in greater detail.

5.3.1 *PDMS Lid*

Initially, a PDMS lid was used in conjuction with the 3D printed clamp. The soft PDMS allowed quick, reversible sealing of the microfluidic channels when pressed lightly against the MDA chip, making the lid reusable. The PDMS lid was fabricated by moulding, and a fully three dimensional mould was made in PMMA using micromilling. The three parts of the mould was tightly clamped using bolts, and the inlet and outlet holes were created by inserting blunt syringe needles into dedicated slots in the mould. Figure 5.3 shows a sketch with the dimensions of the PDMS lid (A), a photograph of the mould (B) and the final lid (C). As seen in Figure 5.3 A, small gaskets (red arrows) protrude from the sealing surfaces. The gaskets were 200 μm tall and 500 μm thick, limited by the size of the tools used to make the mould. Thin PDMS structures are very soft and require less pressure to form a seal compared to a flat PDMS surface.

The size of the PDMS slab was 45 mm by 19.5 mm to fit the smaller MDA substrate, and 6.25 mm thick. The channels in the PDMS lid were 1 mm wide and 15 mm long. The height of the channel depended on the amount of compression of the gaskets, with a maximum height of 200 μm when the gaskets were uncompressed. The surface of the PDMS could be rendered more hydrohpobic by activating the surface with oxygen plasma and applying a hydrophobic, fluorinated silane compund (Aquapel®). This also worked to reduce the background fluorescence as less liquid was trapped in the lid.

The assembly and disassembly of the mould was highly time consuming, and post-proccing of the lid was required due to PDMS leaking between the needles used to form the inlets and outlets. For this reason a 3D printed lid was designed to reduce the manual processing time, while also increasing the flexibility of the design.

5.3.2 *3D Printed Lid*

The 3D printed lid consisted of a rigid clear part, which defined the channels, inlets, and outlets, and two gaskets made in the Formlabs flexible resin. The three parts were press fit together. To use the 3D printed lid with bright field microscopy, some post processing of the part was required. Due to surface structures arising from the printing process, the clear parts did not come out optically clear from the print, however, applying thin layers of clear resin and curing the parts in a UV oven would

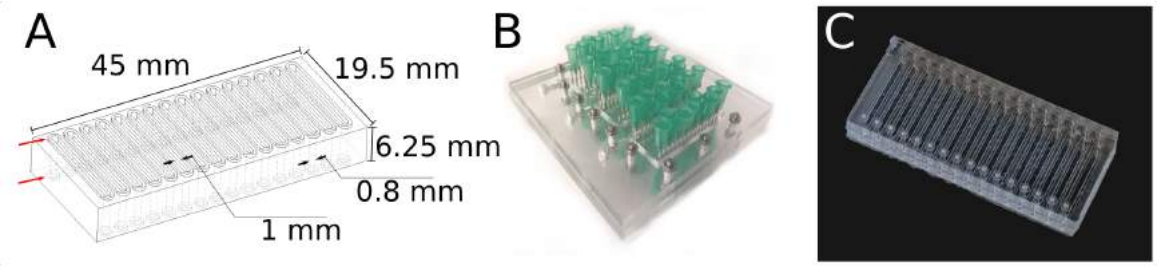

Figure 5.3: A) Sketch of the PDMS lid with dimensions. The two red arrows indicate the thin gaskets used to form seals between the PDMS and the MDA substrate, and the PDMS and the microlfuidic interface. B) Photograph of the assembled PDMS mould. C) Photograph of the finished PDMS lid.

Figure 5.4: A) Sketch of the 3D printed lid. A rigid, clear core is sandwiched between two flexible gaskets. The outer dimensions are 45 mm by 19.5 mm by 6 mm. B) Photograph of the clear part before (bottom) and after (top) applying a coating of clear resin to increase the optical tranparency of the part. C) Photographs of the 3D printed lid and the assembly in the microfluidic interface.

even out the surface, rendering the part optically clear. This method has even been used to fabricate optical lenses.[99] Figure 5.4 shows a sketch of the 3D printed lid (A), the clear part of the lid before and after applying the thin coat of clear resin (B), and a photograph of the chip assembled with the 3D printed lid (C). The 3D printed lid had the same dimensions as the PDMS lid, however, the channel height was now defined by the height of the protrusions on the clear part, as well as the thickness of the channel gasket, however, this was also subject to change due to compression of the gasket. The maximum height was aswell 200 μm.

5.3.3 *Clamp*

Two versions of the 3D printed clamp was made. In the first version, the clamp used strong earth magnets to seal the chip, each magnet applying 740 grams of force (strength N45). The magnets were 6 mm in diameter and 2 mm tall. The magnets applied sufficient force to seal the PDMS lid, however, the flexible resin from Formlabs is stiffer than PDMS, and more force was required to seal the system. In the second version of the 3D printed clamp, four holes were added to clamp the chip with bolts

Figure 5.5: A) Sketch of the 3D printed clamp with the MDA glass substrate and PDMS lid. B) 3D printed, magnetically clamped microfluidic interface. C) Magnetically clamped microfluidic interface including four bolts for added compression.

in addition to the magnets. Figure 5.5 shows a sketch of the 3D printed clamp with the MDA glass substrate and the PDMS lid (A), a photograph of the magnetically clamped 3D printed fluidic interface (B), and a photograph of the fluidic interface with the addition of four bolts for tighter clamping (C). The outer dimensions of the microlfuidic interface is 8.5 cm by 5 cm. The bottom of the clamp was designed to interface with a holder on the optical detection platform, and four millimeter screws could be used to adjust the level of the clamp.

5.4 Discussion and Conclusion

Three different microfluidic interfaces for the MDAs were fabricated. In the first version, a reusable clamp was fabricated in PMMA by micromilling, and the disposable lid was fabricated in COC using injection moulding. In a manufacture setting, an injection moulded disposable part is practical, as this is one of the most widely used fabrication methods in industry. However, in a research setting, injection moulding is very inflexible, as the fabrication of new moulds is very time consuming and labour intensive. This was the main reason why the second and third versions were invented. The second version relied on the moulding of reusable PDMS lids. PDMS casting is a method preferred in research, as it is cheap, and PDMS has many desirable properties. The flexibility of the PDMS allows it to form a reversible seal with glass by applying light pressure, which was utilised here. The third version was also reusable, and relied on 3D printing, as this was the least labour intensive fabrication method.

The fabrication and bonding of the injection moulded lids had a very high success rate, where leaking was seldom a problem. This also provided the most well defined channel dimensions. Using the PDMS lid and 3D printed lid, some leakage was observed, which should be expected from reversible seals at low pressures. Although the leakage was sometimes observed, it was not always impairing the use of the device, however the robustness of this configuration was worse than that using the injection moulded lid. The benefits of using the PDMS or 3D printed lid was the high degree of design freedom.

6 | Summary of Part I

This chapter will summarise Part I of this thesis. The motivation for the development of a versatile MDA platform was based on the relevant case of monitoring residual disease and mutations in chronic myeloid leukaemia. To add versatility to the platform, target immobilisation directly in the MDA spots and avoiding the use of an oil phase to displace the aqueous phase was suggested. As previous single molecule assays has mainly utilised target capture on beads, numerical simulations were used to confirm the feasibility of capturing the targets on a planar surface, where the reaction rate is highly diffusion limited. Using experimentally determined parameters for the diffusivity and kinetic constants, these simulations showed that indeed a detectable number of molecules were caught on the planar capture surface, even at low target concentrations. The impact of the model parameters were investigated, and it was observed that the volume of sample screened had the highest impact on the number of molecules caught. This was concluded by increasing the flow rate with which the sample was passed over the sensor. This revealed that increasing the flow rate also increased the number of molecules caught, thus establishing the minimal influence of diffusion on the number of molecules caught. Finally, a theoretical detection limit was determined, ignoring the non specific binding of reporter molecules. This investigation suggested a detection limit of 100 zM, which resulted in the binding of 130 molecules. In typical single molecule experiments using enzymatic signal amplification by horseradish peroxidase, the non specific binding of the reporter enzyme is around 0.5%. Taking this into account, a detection limit around 2 aM could be assumed, when the array consisted of 300.000 spots. The numerical simulations indicated that the surface bound assay could reach detection limits similar to those reported using bead based capture, thus answering the first problem statement presented in Chapter 1.5.

The reminder of Part I described the methods and technologies involved in the use of the MDAs, but were more general to the use of the MDAs than the applications described in the remaining two parts. First, some of the immobilisation strategies employed to bind proteins and DNA on glass substrates were reviewed. The surface chemistry protocols employed in this study were presented, and a comparison of a few different methods of immobilising DNA oligonucleotides was conducted based on the hybridisation of a fluorescently labelled target strand. This investigation established that the strongest signals were seen on surfaces modified with streptavidin. The explanation is likely that the proteins shield the negatively charged glass surface, decreasing the repulsion of the negatively charged DNA oligonucleotides. The surface functionalisation was an important part of developing specific assays on the MDA, as was the aim of the fourth problem statement presented in Chapter 1.5.

Secondly, the assembly of an optical platform capable of fluorescence imaging of the

MDA was presented along with custom made LabVIEW software for the simultaneous control of motion, imaging, and liquid actuation. The parallel combination of scanning stages, imaging and liquid control appealed to the prospect of automation, though this was not achieved here. The main component of the imaing system is the lens collecting the emitted fluorescence. Two types of objectives were tested on the set up; a traditional, high numerical aperture microscope objective and a bi-telecontric lens. The objective based set up produced clear images comparable in quality to imaging on a standard fluorescence microscope. The telecentric lens has a very deep depth of focus, and due to the parallel optical paths through the lens system, the magnification is constant all through the depth of field. This was utilised in the set up to alleviate refocusing during tile scanning, however, due to the large depth of field, the microfluidic lid interferred with fluorescence detection.

Lastly, the design and fabrication of the microfludics interfacing with the MDA was described. Three iterations of designs were made to overcome different issues. The first microfluidic interface consisted of a single use injection moulded lid which was irreversibly bonded to the MDA. The consumable chip was interfaced to reservoirs and a pump by clamping in a micromilled interface. The injection moulded lid provided very robust microfluidics, however, making adjustments to the design was very troublesome. For this reason, a reusable lid in PDMS was conceived combined with a 3D printed clamp. Because of the flexibility of PDMS, a reversible seal could be formed by small gaskets by applying light pressure. As the moulding of the PDMS is also rather time consuming, a third design based entirely on 3D printed parts was presented. The seal was formed similarly to the PDMS lid, by 3D printing gaskets in a flexible polymer. Methods have been developed for the production of transparent 3D printed parts, and this was utilised to allow bright field microscopy using the 3D printed lid.

With the infrastructure surrounding the MDAs in place, next, the fabrication and applications of the MDAs will be presented.

Part II

FDTS-based Microdroplet Arrays

7 | Introduction

7.1 Hydrophillic in Hydrophobic Pattern Using Perfluorodecyltrichlorosilane

The first MDA fabricated for this study relied on photo-lithographic patterning of a photoresist followed by deposition of a self-assembled monolayer of the hydrophobic compound FDTS. FDTS coatings on planar surfaces reach water contact angles of around 110-115°,[100] which creates a stark contrast in surface energy to the hydrophilic nature of borosilicate glass (40°). The contrast in surface energy between the bare glass and the FDTS coating was used to allow the spontaneous formation of droplets on the bare glass patches when contacted by a liquid.

Another advantage of the Teflon-like FDTS coating is that it is chemically inert, as the carbon-fluoride bond is one of the strongest covalent bonds in organic chemistry.[101] Glass, however, can be chemically functionalised to effectively bind biomolecules such as proteins and nucleic acids as described in Chapter 3. This difference in surface properties was utilised to build the different assays on the chip surface. Several methods for reducing the surface energy of glass can be imagined, and the FDTS was initially chosen, since it has been widely used as an anti-stiction coating in e.g. nano imprint lithography.[100] As such, the deposition process was well defined and thoroughly tested.

Part II of this thesis is begun by describing the fabrication process of FDTS based MDAs. This fabrication process was developed as a part of the NADINE project. Following the description of the fabrication process, a brief characterisation of the MDA was conducted, and finally two applications of the FDTS based MDA was demonstrated. The first application demonstrated in this study was digital ELISA for the sensitive detection of Alzheimer's related biomarkers. This application was chosen as several reports on digital ELISA exists, and it allowed us to determine whether this platform could perform on the same level as the bead based assays. The second application demonstrated the transcription and translation of DNA into proteins on the MDA. By binding the synthesised proteins onto the MDA surface using a poly-His tag, we were capable of detecting the proteins by antibody recognition. This assay required two separate compartmentalisation steps as opposed to the digital ELISA assay, which only require compartmentalisation during the detection step. This demonstrated a higher degree of flexibility of this platform as no beads or oil covers were required.

8 | Fabrication

In this chapter, the fabrication process of FDTS based microdroplet arrays is presented along with a short characterisation and then briefly discussed.

8.1 Fabrication of FDTS Microdroplet Arrays

The FDTS MDA chip was fabricated from a 4" borosilicate wafer, 500 μm thick. For the first design of the FDTS MDA chip, two miscroscope slide sized chips (75 mm by 26 mm) were fabricated per wafer. Each chip contained 16 separate droplet arrays each hosting 448.000 individual droplets just 5 μm in diameter with a center to center distance of 10 μm. This MDA chip was used in conjunction with the injection moulded lid and micromachined chip interface previously described. A second iteration using the same fabrication process produced 4 slides 19.5 mm by 45 mm per wafer, also comprising 16 separate arrays, each hosting 415.000 droplets just 4 μm in diameter with a center to center distance of 6 μm. These were used in conjunction with the PDMS lid and the 3D printed lids, and the 3D printed interface also previously described. The second version of the FDTS MDA was also fabricated with droplet diameters of 7 μm, 10 μm, 15 μm, and 25 μm. Figure 8.1 A and B shows the two mask designs for the FDTS MDA chips. A third mask design was tested as well, which produced spots on the entire wafer, eliminating the need to align the channels and arrays. This is depicted in Figure 8.1 C.

To fabricate the FDTS MDA, two rounds of lithography was performed. The first lithography step had the aim of producing chromium guides on the wafer. These served as a dicing guide as well as a processing side indicator on the transparent substrate. The second round of lithography created the patterned hydrophobic coating. The photoresist used to create the pattern masks was AZ 5214E (Microchemicals GmbH), for which robust, automated spin coating recipes existed at our clean room facilities.

Figure 8.2 shows the following 14 steps involved in the fabrication process:

1. The wafer was primed with hexamethyldisilazane (HMDS) to promote adhesion of the photoresist.
2. The wafer was spin coated with a 1.5 μm thick layer of AZ 5214E photoresist and soft baked for 90 seconds at 90 °C on a hotplate.
3. The photoresist was exposed to UV light (i-line, 365 nm) through a chromium mask in hard contact with the wafer for 5 seconds at 7 mJ cm^{-2}.
4. The wafer was then heated to 110 °C for 120 seconds on a hotplate to reverse the pattern. After baking, the wafer was left to cool down for 10 minutes.
5. The photoresist was then flooded with UV light for 20 seconds at 7 mJ cm^{-2} to solubilise the resist which had not been exposed in the masked exposure.

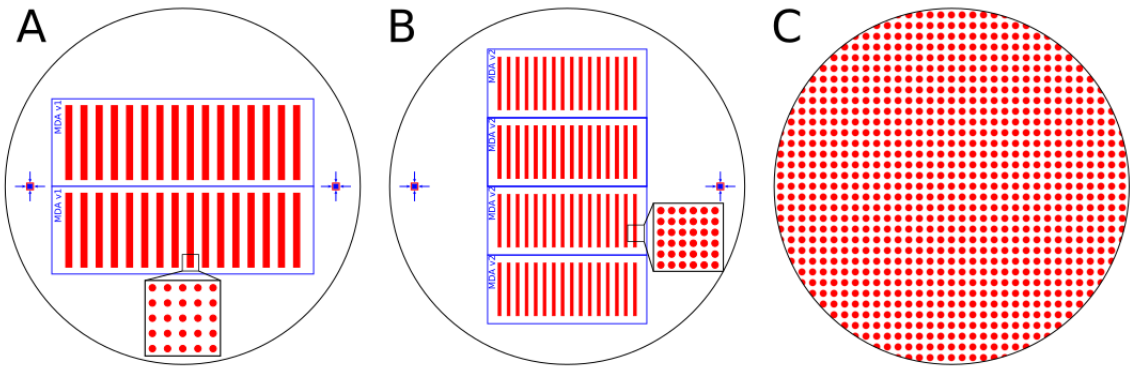

Figure 8.1: Sketches of the mask designs for three iterations of the MDA chip. A) First design iteration used for FDTS MDAs. One wafer makes two chips (75 mm by 26 mm) with 16 arrays each, each array containing 448.000 droplets. The blue features show the chromium pattern, while the red features show the inverse FDTS pattern. B) Second design iteration used for FDTS MDAs. One wafer makes four chips (45 mm by 19.5 mm) with 16 arrays each, each array containing 415.000 droplets. The blue features show the chromium pattern, while the red features show the inverse FDTS pattern. C) Third design iteration used for FluorAcryl MDAs. The entire wafer is patterned with spots 10 μm in diameter with a pitch of 15 μm, which alleviated the need for two masks, and two rounds of lithography.

6. The solubilised photoresist was developed for 60 seconds on a puddle developer containing a developer with tetramethyl-ammonium hydroxide (TMAH, AZ 726 MIF Developer, Micro-chemicals GmbH).
7. The wafer was then coated with a 200 Å thick chromium layer using an e-beam evaporation system at a rate of 1 Å per second.
8. Lift-off of the photoresist was carried out by sonicating the wafer for 10 minutes in acetone and lastly the wafer was rinsed in deionised (DI) water.
9. For the second round of lithography, the wafer was again primed with HMDS.
10. Another 1.5 μm thick layer of AZ 5214E photoresist was spin coated on the wafer and soft baked for 90 seconds at 90 °C.
11. The wafer was exposed to UV light through a second chromium mask which is aligned to marks in the chromium pattern on the wafer. The wafer was exposed for 8.5 seconds at 7 mJ cm^{-2}.
12. The photoresist was then developed for 60 seconds in AZ 726 MIF Developer.
13. The wafer was coated with a self-assembled monolayer of FDTS using molecular vapour deposition (MVD). An automated system (Applied Microstructures Inc. MVD 100 Molecular Vapor Deposition System) was used, which first exposed the wafer to a mild oxygen plasma to prepare the surface for silanisation. Next FDTS and water vapour was heated and the wafers were carefully exposed to the vapour phases in a vacuum chamber.
14. The remaining photoresist was removed by sonicating the wafer in acetone for

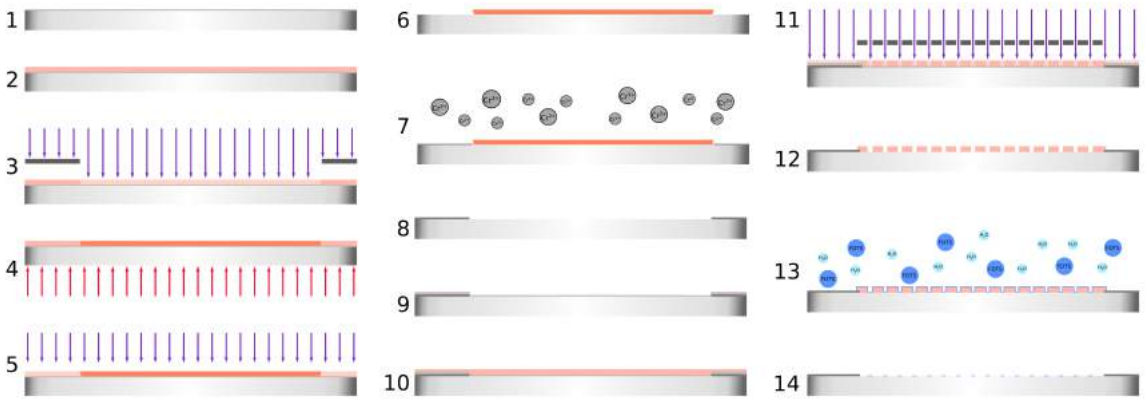

Figure 8.2: Overview of the fabrication process of the FDTS MDA chip. The substrate is a 500 μm thick 4" borosilicate wafer.

10 minutes followed by a rinse in DI water.

Before using the chips for any application, the wafer was diced and cleaned by submerging the slides in acetone, 2-propanol, and ethanol in a sequential manner for five minutes each in an ultrasonic bath. This prepared the slides for further surface functionalisation.

8.2 Characterisation of the FDTS Microdroplet Array

The FDTS based MDA was characterised by measuring the contact angle, determining the stability of the aqueous droplets in the microfluidic channels and looking at the stability of the droplet formation process by showing nine consecutive rounds of droplet generation.

8.2.1 *Contact Angle Measurements*

The contact angle with water was simply determined by imaging a 2 μL droplet automatically deposited on the surface by the drop shape analyser (Krüss Drop Shape Analyzer DSA100). After FDTS coating using molecular vapour deposition and removing the left over resist by sonication in acetone, the wafer was placed in the drop shape analyser and a droplet was deposited on a part of the wafer away from the array, where the FDTS supposedly form a uniform monolayer coating. The droplet shape was automatically analysed by the software controlling the drop shape analyser. Using this method, contact angles on FDTS of 115° were routinely measured. Angles below 100° were seldom, indicating the robust deposition of FDTS.

8.2.2 *Droplet Stability*

The life time of droplets in the microfluidic channels was investigated, as this would put a limit to the length of incubations in droplets possible in an assay. Droplets were generated on an MDA bonded to the injection moulded COC lid, and then the

microfluidic interface was reversibly sealed by filling the inlet reservoirs with water and applying one layer of scotch tape over the inlets and outlets. Nine channels were filled in total, three with pure MilliQ water, three with PBS, and three with PBS containing 10 g L^{-1} PEG. Bright field images were recorded and the diameter of 100 droplets per sample was measured using ImageJ. The diameter is plotted as a function of time in Figure 8.3 A, and bright field images of the droplets taken right after droplet formation (0 h), 1 hour, 3 hours, 5 hours, and 72 hours after droplet formation is seen in Figure 8.3 B. It was observed that even though the MilliQ droplets were smaller from the beginning, the average the diameter of the droplets had reduced by 12.5% over 72 h independent of the buffer. This reduction corresponds to a reduction in volume of approximately 33% assuming that droplets are the shape of a half-sphere. After 5 hours, the diameter was minimum 95% of the initial diameter, which corresponds to a 85% of the original volume. The reduction in volume may have an impact at longer incubations, as in many bioassays the salt concentration has a profound impact on e.g. enzyme function, and as the water evaporates, the salts in the droplets are concentrated.

The quantitative measurement in this case is not very precise, however it is apparent that the evaporation from the droplets is very slow. The measured diameter of the droplets depends highly on the position of the focal plane, and using a large (40x) magnification, a very small change in the height above the objective results in a big change in the appearance of the image. Care was taken to achieve the same focus on each sample.

8.2.3 *Robustness of Droplet Formation*

To evaluate the robustness of droplet formation, nine consecutive droplet formations were carried out and the MDA was imaged after each step. Each time the buffer was changed, cycling between PBS, resorufin in PBS, and ATTO 488 labelled oligonucleotides (1 μM) in PBS. Figure 8.4 shows bright field and fluorescence micrographs in the green (ATTO 488) and red (Resorufin) channel for each round of buffer exchange. By bright field microscopy, it was observed that the quality of the droplets has decreased slightly. It was also observed that the fluorescence could be washed away by the exchange of the buffer. This is very helpful in multi-step assays where the surface bound molecules are interrogated several times.

In general the success rate of droplet formation was very high. From the data obtained in the consecutive rounds of droplet formation just described, the number of defect droplets was evaluated. Droplets were considered defect if the shape was highly irregular, or if several droplets were conjoined. at least 10.000 droplets were evaluated for defects for each sample and time point. On average, each sample lane contained between 0.3% and 0.9% defect droplets. A one-way ANOVA analysis was applied to test if the number of defects were equal across the nine rounds of droplet formation. No significant difference was found between the means ($p > 0.4$), thus it could not be concluded that more defects were found in the later rounds of droplet formation. In general, a low amount of defects will not affect the ability to run an assay on the MDA.

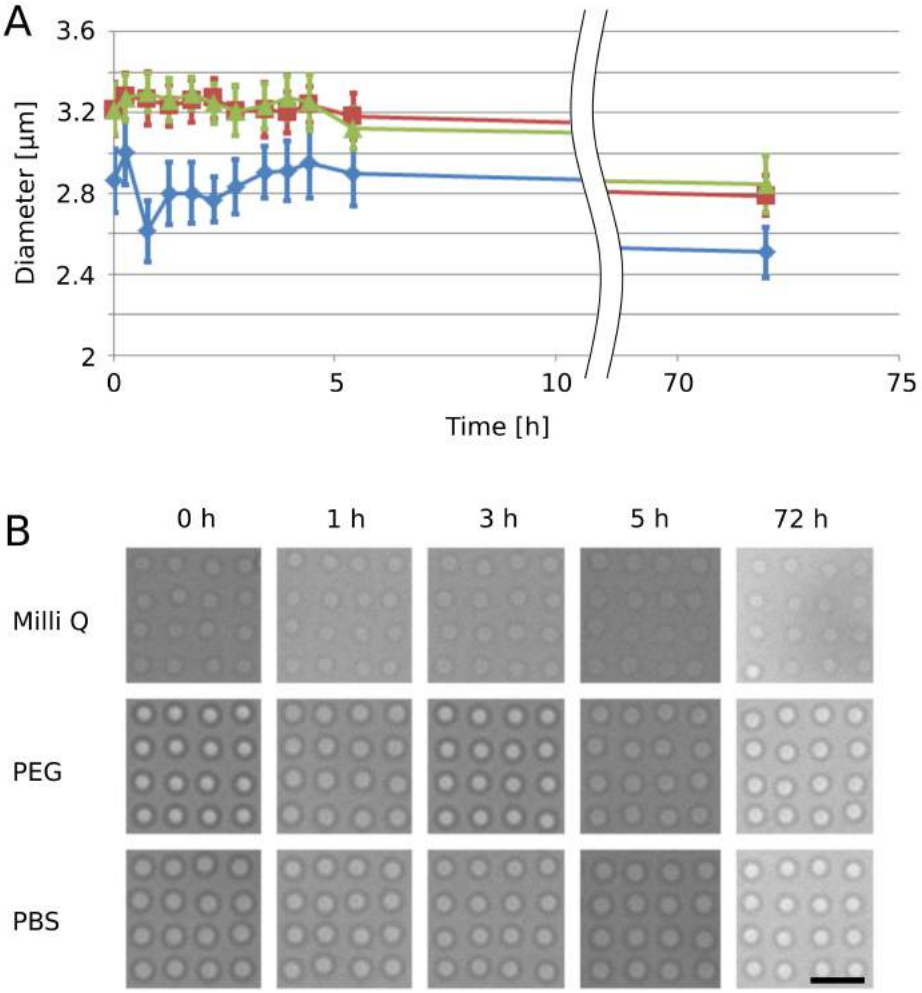

Figure 8.3: A) The diameter of droplets as a function of time. Error bars represent the standard deviation (n=100). B) Representative bright field images of droplets on the MDA taken at 0 h, 1h, 3h, 5h, and 72 h after droplet formation. The scalebar is 15 μm. This data is also presented in [32].

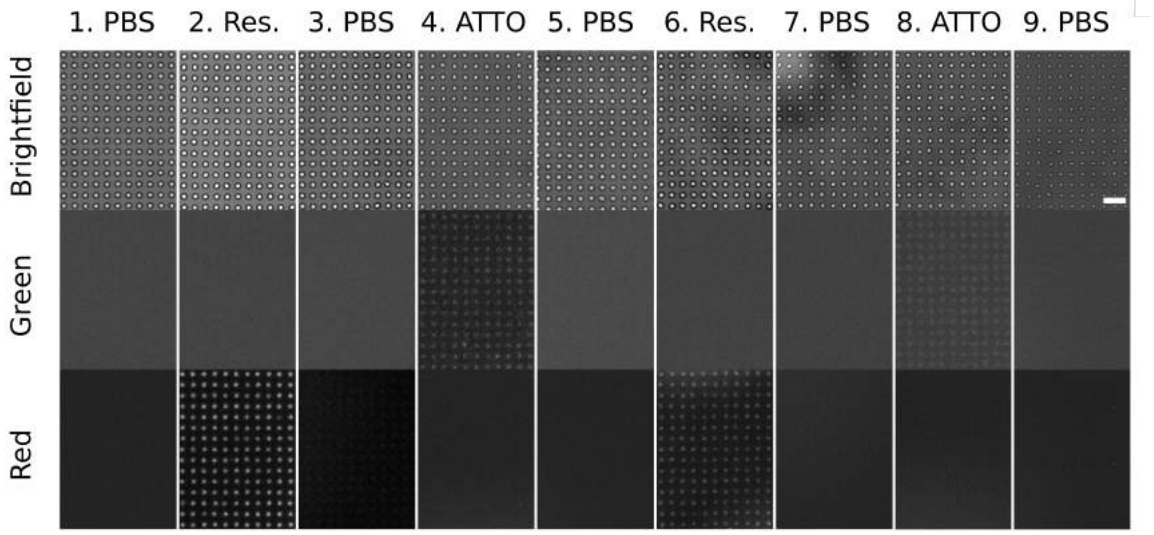

Figure 8.4: Representative micrographs from the test of the robustness of droplet formation by nine consecutive rounds of buffer exchange. The rows show bright field images (top) and fluorescence micrographs from the green (middle) and red (bottom) channel respectively. Each column represent one round of droplet formation. This data is also presented in [32]

During image analysis, defect parts of the array are removed, and the only implication this has on the analysis is a reduction in the total number of compartments analysed.

We also observed a good batch to batch reproducibility to begin with, however, suddenly we began observing defect batches of MDAs. The only change to the process was the relocation of the MVD system inside the clean room facilities. Ultimately, no droplet formation was seen in more than 50% of batches, and incomplete arrays were observed in almost every batch. Initially, the lift-off process was investigated to see if incomplete removal of the photoresist could be observed. As this did not seem to remedy the issues, the purity of the glass substrate prior to FDTS deposition was investigated. First, a harsher oxygen plasma treatment of the wafers before deposition of FDTS was tested, and secondly, the wafers were developed for up to 180 seconds after the second round of lithography to ensure the complete removal of photoresist from the areas where FDTS should be bound, both to no avail. Towards the end of this study, by chance, we observed that droplet formation was regained in small test batches of only two wafers. In a typical batch, six wafers were processed simultaneously in the MVD system. The explanation could be that too little FDTS was added to the chamber to create complete monolayers on six wafers, but was enough for the complete coating of two wafers simultaneously. Henceforth, only two wafers were processed at a time in the MVD system, however, much time had been wasted on the troubleshooting of the process.

8.2.4 *Concluding Remarks*

In summary, the characterisation of the FDTS based MDAs showed a very high degree of droplet stability, where droplets retained 85% of their volume over 5 hours, and were easily observed after 72 hours with a volume reduction of 33%. This lead us to conclude that longer incubations in droplets should be straightforward without any big interference in the concentrations within the droplets. We also demonstrated that repeated droplet formation on the same array was uncomplicated, and the rate of defects observed in the arrays were low. It turned out that the fabrication process was very sensitive to changes in the FDTS deposition, which was observed as suddenly whole batches of wafers were unable to support droplets. This was attributed to an unknown change in the FDTS deposition, which meant that the amount of FDTS in the reaction was insufficient to cover a whole batch of wafers. As this conclusion took a very long time to reach, another way of fabricating the MDAs was conceived and developed in parallel with the troubleshooting of the FDTS process. The alternative fabrication process was based on the patterning of a hydrophobic, fluorinated polymer and will be described in Part III.

9 | Digital ELISA

9.1 Introduction

In order to understand how the digital ELISA on MDAs work, a brief introduction to immunoassays and enzymatic signal amplification is mandatory.

9.1.1 *Enzyme-linked Immunosorbent Assay*

The ELISA assay was invented in the 1970's, and has had great success in many different areas of applications, including clinical diagnostics.[102] ELISA is used for the detection of antibodies or antigens (typically proteins or peptides), which play an important role in the human immune system. Antibodies are generated by the immune system in response to an antigen, and as such, the presence of antibodies against a known disease target is evidence of that disease in the patient. Proteins are also generated in the human body, and the expression of some specific proteins can be directly linked to or be bystanders in disease in humans, and are termed disease biomarkers. Other proteins or peptides, such as membrane proteins, can be used to detect and identify infections e.g. from bacteria or viruses.[102] Since proteins are such a fundamental building block in most organisms, the extent of applications is too monumental to review here, though a summary can be found in [102].

ELISA can be carried out in a few different ways: direct-, indirect-, sandwich-, double sandwich-, and competitive ELISA (see Figure 9.1). The indirect and the double sandwich method can be used to detect antibodies from the patient samples, whereas direct, sandwich, double sandwich and competitive ELISA can be used to detect antigens in the patient sample. In general, the antigen or an antibody is immobilised in the bottom of a microtitre plate well, and immunocomplexes are formed with the target and detection antibodies. The detection antibody is conjugated to an enzyme, which catalyses a substrate, resulting in the formation of a product which leads to a colourimetric change, or a fluorescent or luminescent signal. The amount of product is related to the concentration of the target in the sample. The simplest assay is the direct ELISA, where the target is attached in the well and directly detected by the detection antibody. However it requires a purified sample, as other proteins might interact with the well and introduce error in the assay. Compared to direct ELISA, the more complex double sandwich and competitive ELISA are more lengthy and expensive, however the specificity is significantly improved. The sandwich ELISA is in-between. It requires an extra incubation and washing step compared to direct ELISA, but has a higher specificity.[102] The standard ELISA assay is capable of detecting protein concentrations down to around 1 pM.[4] Applying fluorescence detection using quantum dots, the limit of detection can be decreased to 500 fM.[103] Another sensitive alternative to digital ELISA is immuno-PCR.[103]

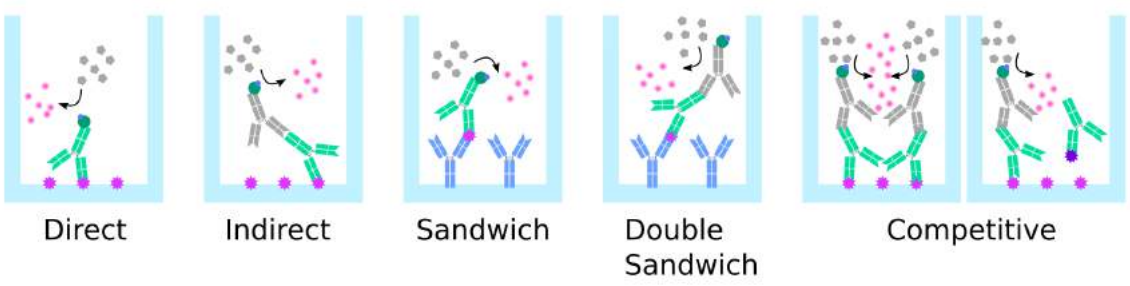

Figure 9.1: Five different ELISA methods are used to detect antigens or antibodies in patient samples.

Digital ELISA

The digital ELISA method was developed to improve the detection limit of standard ELISA. In many clinical cases, including cancer, infectious diseases, and neurological disorders, the clinically relevant level of protein target falls below 1 pM, and is hence undetectable by standard ELISA.[4] Enabled by the ability to capture and measure single enzymes in micro-wells[12, 15], a single-molecule bead based ELISA assay was developed, which was capable of detecting serum proteins in concentrations down to and below 1 fM.[24] Digital ELISA is based on the same principle as a standard ELISA assay, however, the binding of the target is carried out on microscopic beads functionalised with the capture antibody (see figure 9.2 A). After the target is bound, the beads are collected and washed, and an enzyme labelled detection antibody is bound on the captured targets. The beads are washed and distributed in femtolitre sized wells with the enzyme substrate, which is converted to a fluorescent product in the wells containing beads with the bound target (see figure 9.2 B). The number of wells that fluoresce is directly related to the concentration of analyte in the sample.[24]

9.1.2 *Fluorescence Signal Amplification*

The most common fluorescence signal amplification used in droplet microfluidics is the combination of either horseradish peroxidase (HRP) or β-galactosidase (β-gal) and their fluorescent substrate.[12, 20] This is because the conversion of the substrate is fast and generates a detectable signal in a few minutes. Horseradish peroxidase is a 44 kDa protein, which catalyses the oxidation of many organic compounds in the presence of hydrogen peroxide. β-Galactosidase is a larger, 465 kDa protein[1] (four subunits of 116.3 kDa each), which catalyses the breakage of glycosidic bonds. A substrate which is catalysed into a fluorescent compound is commercially available for both enzymes. One argument for choosing HRP over β-gal is the size. β-Gal is a big protein compared to HRP, which in turn makes the diffusion slower as well. In this study, HRP was chosen as the signal amplification system. Figure 9.3 shows the 3D structure of HRP (A) and the reaction with the substrate, Ampliflu Red™(AFR)(B). When the HRP and the substrate exists in the presence of hydrogen peroxide, the

[1]From Sigma Aldrich company website, β-Galactosidase from *Escherichia coli* https://www.sigmaaldrich.com/catalog/product/sigma/g3153.

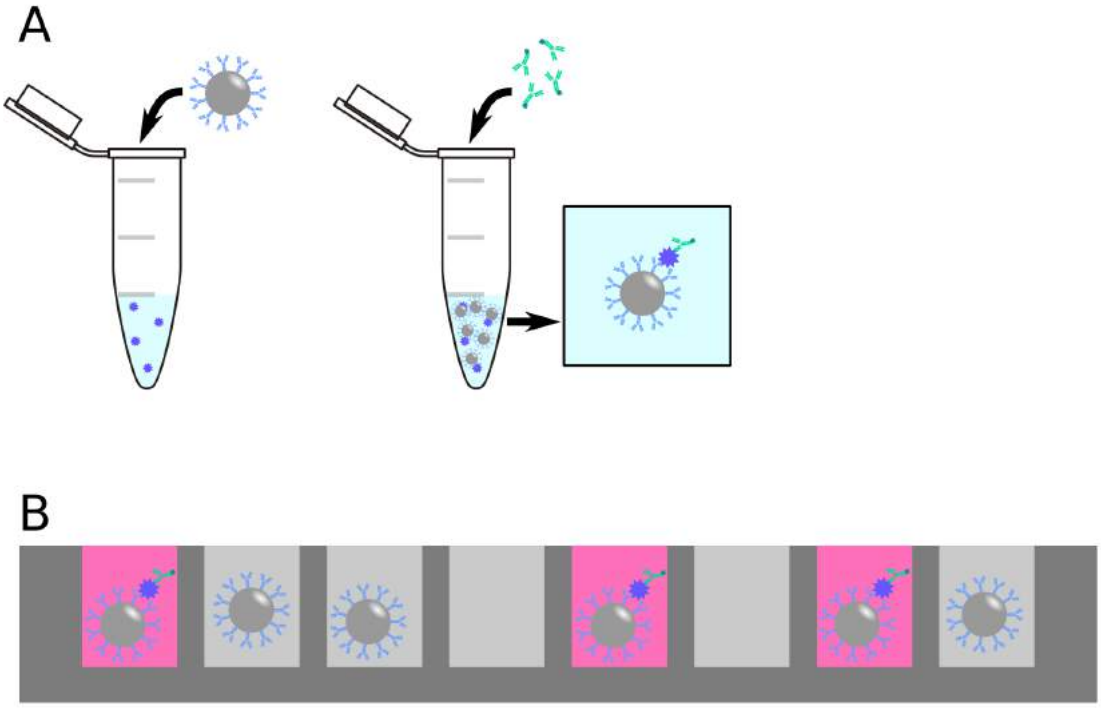

Figure 9.2: Bead based digital ELISA. A) Microscopic beads carrying antibodies are mixed with the sample containing the target analyte. After extracting and washing the beads, a detection antibody is added forming immunocomplexes on the beads. B) Beads with and without immunocomplexes are distributed in femtolitre microwells with a fluorogenic enzyme substrate. Wells containing beads with immunocomplexes fluoresce and can be counted in an automated fashion by image analysis.

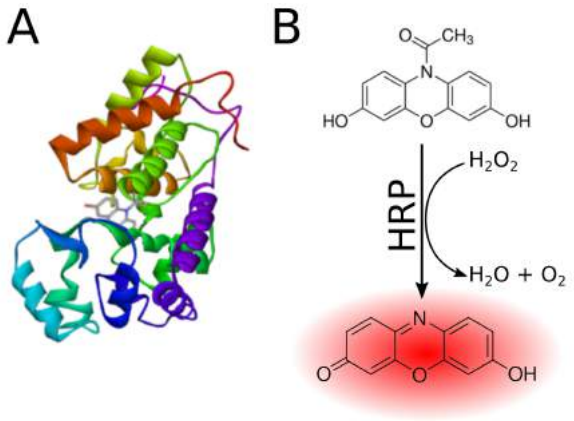

Figure 9.3: A) 3D structure of HRP (PBD ID: 1H5A [104]). B) The oxidation of Ampliflu Red™to the fluorescent compound resorufin.

HRP enzyme catalyses the redox reaction of hydrogen peroxide and the substrate. In the case of Ampliflu Red™(also sold as Amplex Red), the resulting compound, resorufin fluoresce red (λ_{em} =586 nm) when exposed to green/yellow light (λ_{ab} =573 nm).

9.2 Methods

9.2.1 *Surface Functionalisation*

MDAs for digital ELISA was functionalised with an amino- and carboxyl modified PEG-linker, as PEG is known to reduce the nonspecific binding of proteins onto the glass substrate, as discussed in Chapter 3. The full chemical surface functionalisation is depicted in Figure 9.4, and described here in detail:

1. The functionalisation with epoxy silane and the bi-functional PEG linker was carried out as described in Section 3.2.3 and 3.2.4 in Chapter 3.
2. Next, the channels were rinsed with the MES buffer and a 0.1 mg mL^{-1} solution of the capture antibody (mouse monoclonal anti-Amyloid β_{42} (Aβ_{42}), cell line 295F2, Synaptic Systems, Germany) in 100 mM MES buffer was loaded onto the chip and allowed to react for 30 minutes followed by thorough rinsing with 50 mM Tris buffer (pH 8.0).
3. The final product containing the epoxy-linked amino-PEG-carboxyl molecule and bound antibody.

The MDAs were used for digital ELISA directly after binding the capture antibodies.

9.2.2 *Digital ELISA Assay*

Here, the protein Aβ_{42}, which is a known biomarker of Alzheimer's disease,[105, 106] was detected by digital ELISA in cerebrospinal fluid (CSF) patient samples. The digital ELISA assay is sketched in Figure 9.5. A detailed description of the assay is given here:

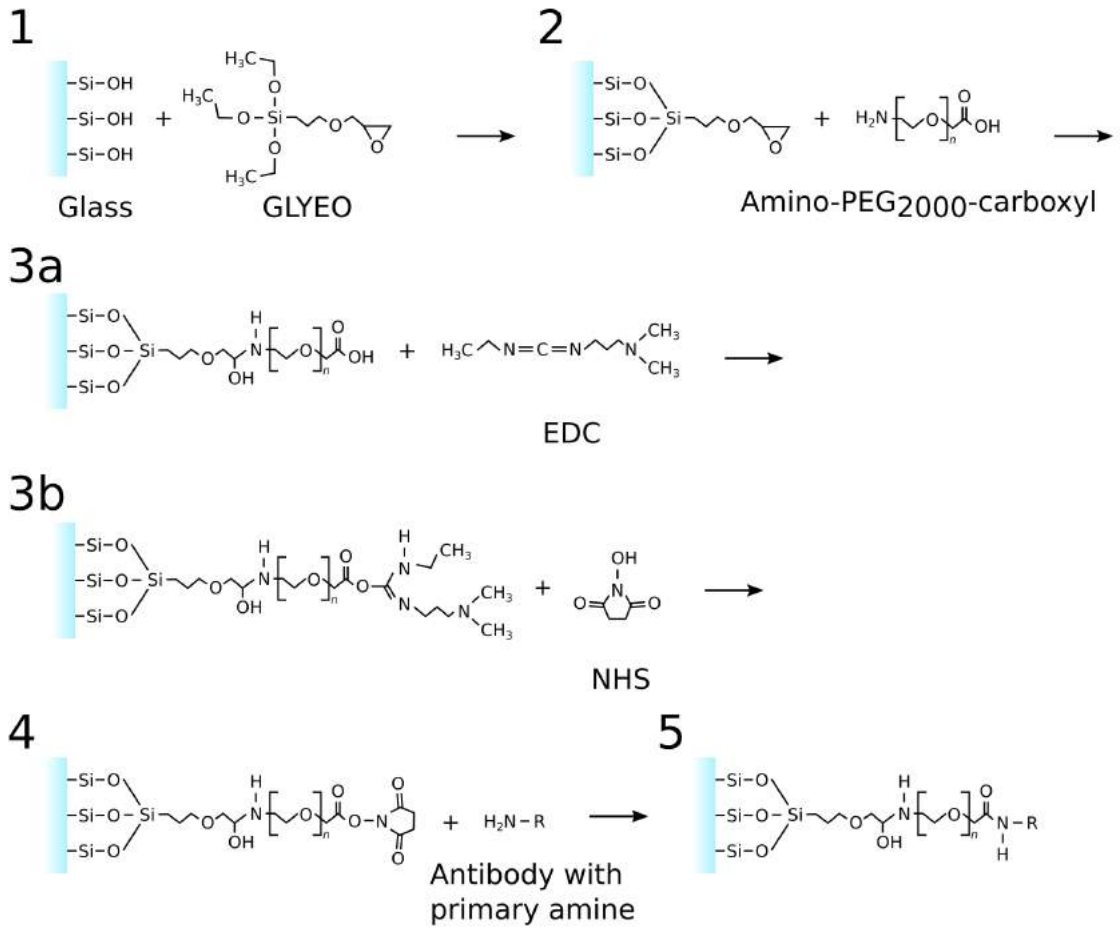

Figure 9.4: The immobilisation of antibodies on a glass substrate using epoxy silane, PEG linker and a carbodiimide crosslinker. The chain, R (frame 4 and 5), represents the capture antibody.

1. An MDA with the capture antibody (mouse monoclonal anti-$A\beta_{42}$, cell line 295F2, Synaptic Systems, Germany) was prepared for digital ELISA.
2. Patient samples (CSF) were diluted 10-fold in sample buffer containing 0.05% (v/v) Triton X-100, and 1.0 g L^{-1} bovine serum albumin (BSA) in 10 mM PBS. 100 μL sample was slowly perfused through the microfluidic channel on the MDA at a flowrate of 3.3 μL min^{-1}, corresponding to a total incubation time of 30 minutes.
3. The MDA was rinsed by flushing the channels with 10 mM PBS containing 10 g L^{-1} PEG_{20000}, and a 100 pM solution of HRP-conjugated detection antibodies (HRP conjugated Anti-Human Aβ (N) (82E1) Mouse IgG monoclonal antibody from *Amyloid-beta (1-40) High Sensitive ELISA kit*, IBL international, Switzerland) in labelling buffer containing 0.1% (v/v) Triton X-100, 10.0 g L^{-1} BSA, and 10 g L^{-1} PEG_{20000} in 10 mM PBS was incubated on the chip in bulk for 30 minutes, forming surface bound immunocomplexes.
4. The MDA was again rinsed with 10 mM PBS containing 10 g L^{-1} PEG_{20000}, removing unbound detection antibodies. Finally, detection buffer was prepared containing 200 μM Ampliflu Red, 1.0 mM H_2O_2, and 10 g L^{-1} PEG_{20000} in 10 mM PBS, and a 5 μL aliquot was drawn through the channels, leaving droplets on the array.

After the final step, the chip was imaged in a fluorescence microscope. The droplets containing a surface bound immunocomplex would fluoresce due to the conversion of Ampliflu Red into resorufin (λ_{ab} = 573 nm, λ_{em} = 586 nm), catalysed by the HRP, as previously described.

A similar protocol for the detection of the protein ApoE3 (another biomarker for Alzheimer's Disease) was developed in the NADINE project, however this was not used in this study. The two protocols were used by Andreas Hjarne Kunding to create standard curves describing the relation between positive droplets and target concentration within the project, but was not directly associated with this study. The results obtained can be seen in Figure C.1 in Appendix C. A detection limit of 10 fM for the detection of Aβ is deducted from these results.

Patient Sample Handling

20 samples of patient CSF (9 male, 11 female, median age: 66 years) were evaluated for the level of $A\beta_{42}$ by digital ELISA. 40 samples shipped from Germany on dry ice were kept at -21 °C upon arrival until used. The samples comprised two groups; one group with samples from patients diagnosed with Alzheimer's disease (n=10) and one control group (n=10), as described in [32]. The control group patients were diagnosed with the following: tension headache (n=3), normal pressure hydrocephalus (n=3), exclusion of an inflammatory process (n=1), traumatic subarachnoidal bleeding (n=1), septic encephalopathy (n=1), migraine (n=1), and myasthenia gravis (n=1).

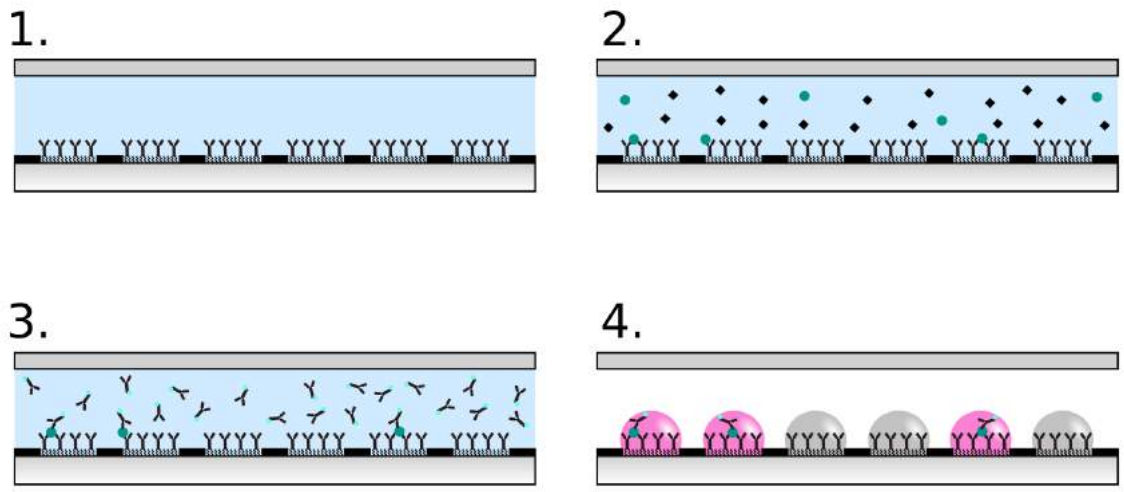

Figure 9.5: Sketch of the digital ELISA assay. 1. The capture antibody is bound on the surface. 2. The target is captured by the antibodies. 3. An HRP-conjugated detection antibody is bound to the captured targets. 4. The HRP substrate is converted to a fluorescent compound in the droplets containing a target.

9.2.3 *Image Analysis*

The fluorescence microscope was used to make a tile scan of each array. The resulting images contained information from approximately 300.000 droplets. Image analysis was conducted in Vision Assistant 2013 (National Instruments, Austin, TX). First, background noise was reduced by applying a Fast Fourier transformation (FFT) filter. The image was truncated, and a high-pass filter (5%) was applied. This reduced background noise and removed larger areas with high background fluorescence. Secondly, a pixel value threshold was applied to transform the gray scale image into a binary image. The threshold value chosen was 75. Thirdly, any remaining signal which lay outside the array area was removed by filtering by x- and y-coordinates, leaving only signal from within the array area in the image. Lastly, the signals were filtered by size depending on the magnification used for imaging, and subsequently counted. The area of the image was used to determine how many spots had been analysed in total, excluding areas with a lot of noise or other obstructions. The image processing did not affect the result of the analysis, as generally only a small fraction of the imaged array had to be removed from the analysis.

9.3 Results and Discussion

Patient CSF samples from two patient groups were analysed for the content of Aβ_{42} by digital ELISA in a blinded fashion. The number of fluorescent spots were used an indication of the concentration of Aβ_{42} in the sample. Figure 9.6 A) shows the number of fluorescent spots in an array of 300.000 spots for the 20 samples. After the primary analysis, the data were divided into the correct patient groups (see Figure 9.6

B), to evaluate any misdiagnosed individuals. Figure 9.6 C-E shows representative fluorescence micrographs of a control group sample (C), an AD group sample (D), and a negative control (E). In general, the occupation of the array was low (maximum 1%), which indicate a bad capture efficiency. In the boxplots shown in panel B, it is observed that the low quantile in one group overlapped with the upper quantile in the other. Despite this, in the ten samples with the lowest count, only one individual belonged to the control group, and vice versa with the ten highest counts. The two groups were significantly different by Welch's t-test ($p<0.001$), however a large variation between the individual observations was observed, particularly in the control group (see Figure 9.6 B, patient group 1). The counts from the AD patient group was only just distinguishable from the background binding, mean background + 3σ (mean $\pm$ sd: 384 ± 22.67).

The aim of performing the digital ELISA assay on our MDA platform, was to demonstrate that a very common application on other MDA platforms was feasible, as it has been questioned weather such an assay was practical on a planar sensor.[75] Even though the limit of detection obtained (approximately 10 fM) is somewhat lower (10-100 fold) than that obtained for example in the study by Rissin et al.[24], we demonstrate that two patient groups can be identified based on the capture of Aβ_{42}, which is an accepted biomarker for Alzheimer's disease. As Aβ_{42} is involved in the formation of amyloid plaques, a decrease in CSF Aβ_{42} is observed, which is in agreement with previous reports.[105, 106] The level of CSF Aβ_{42} for AD patients were close to the detection limit of the system, and in general the capture efficiency of the specific antibody-pair seemed poor. It is suggested that further optimisation of the anti-body pair could lead to a more sensitive assay. With the digital ELISA presented here, one false positive result was obtained (Patient ID: 13/284), and four samples were indecisive (Patient ID: 13/285, 13/294, 4/1145, and 4/1191), meaning that 15 out of 20 patients were grouped correctly. However, in a clinical diagnostic setting, the level of a single molecular marker is not going to form the basis of a diagnosis. Combining this biomarker with other molecular biomarkers and an evaluation of the general state of the patient is more likely to form the basis of the diagnosis. For early detection of Alzheimer's, where clinical symptoms are still repressed, a multiplexed assay with several Alzheimer's related biomarkers could serve as a good indication for the development of Alzheimer's disease in the patient. Other biomarkers related to Alzheimer's and other neurodegenerative diseases are reviewed in [107].

9.4 Conclusion

In conclusion, we have shown that a simple bioassay is feasible on the planar MDA, and have established a good detection protocol using horseradish peroxidase, which can be used in several other bioassays. The Aβ_{42} signal from the CSF samples were low but distinguishable compared to the background signal of the HRP arising from nonspecific binding, which may be a result of an inefficient antibody pair. Future work on the digital ELISA platform could advantageously focus on optimising the antibody-pair and determine the detection limits and sensitivity/specificity of the

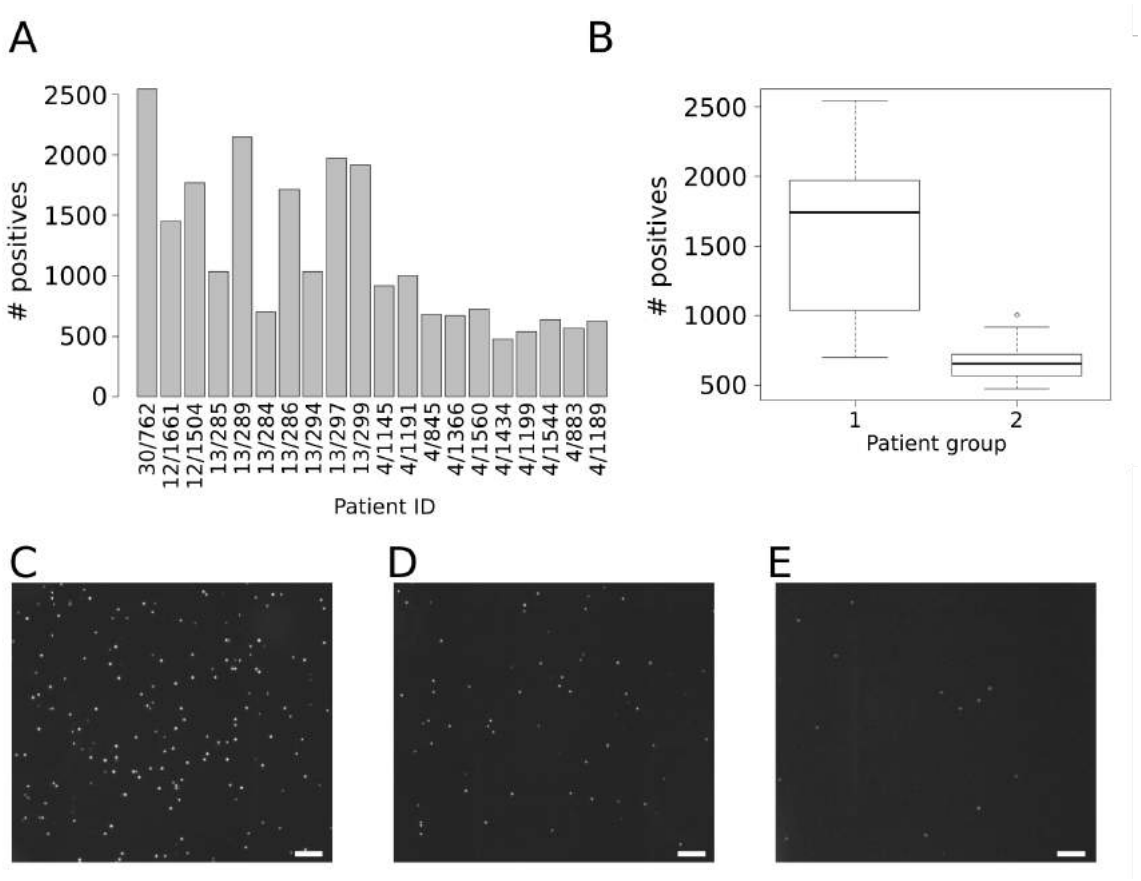

Figure 9.6: A) Bar graph showing the number of spots containing the Aβ_{42} target on an array consisting of 300.000 spots for the 20 patient samples. B) Boxplots with the data from the divided patient groups. C-E) Fluorescence micrograph from: C) a sample from the control group, D) a sample from the Alheimer's group, and E) a negative control. The scale bar is 50 μm. This data is also presented in [32].

system using known concentrations of a synthetic Aβ_{42} peptide.

10 | Cell-free Protein Expression

The second application of the MDA which was explored in this study in the fulfilment of the third research question, was the expression of proteins or peptides inside the droplets. This application was interesting to show, as it require two separate steps carried out in isolated partitions. The most common applications of MDAs has only demonstrated one step carried out in the isolated partitions, such as the example of digital ELISA. In the following, an introduction to peptide and protein expression is given as well as the materials and methods used in the experimental work. Next, the results of the protein expression in droplets are presented and discussed.

10.1 Introduction

Cell-free protein expression is a method for synthesising functional, recombinant proteins without the use of bacterial systems or mammalian cells. Compared to protein synthesis by bacteria, cell-free protein expression is less likely to degradate eukaryotic proteins, and the cumbersome DNA cloning and gene identification procedures can be replaced by a plasmid, PCR generated linear templates, or even linear double stranded synthetic oligonucleotides.[108, 109] An extract or cell lysate from *E. Coli* is used to supply the enzymes required for transcription and translation, as well as the co-factors involved in the process. In a reaction buffer, Amino acids, rNTPs, salts, and energy sources are added to the mix. When supplyed with a suitable DNA template, protein synthesis can proceed. Figure 10.1 show the cell-free protein expression in microdroplet arrays and the process of protein synthesis from the DNA template (insert).

By directly immobilising the expressed proteins on the surface of the MDA, a direct way of creating protein arrays from DNA libraries has been enabled. A similar method has been applied in a microtitre plate in order to increase the throughput of protein synthesis for protein arrays compared to standard proceedures.[108]

10.2 Materials and Methods

10.2.1 *Reagents*

Poly(ethylene glycol) (average molecular weight: 20.000 g mol^{-1}, PEG_{20000}, Cat. No.: 81300-1KG), and Ampliflu Red™(AFR, Cat. No.: 90101-5MG-F) were purchased from Sigma Aldrich. The cell-free expression kit (Expressway™Mini Cell-Free Expression System) and HRP-conjugated detection antibody (HA Tag Monoclonal Antibody, 2–2.2.14-HRP) were purchased from Thermo Fischer Scientific (Cat. No.: K990100 and 26183-HRP, respectively). Annealed, complimentary ssDNA oligonucleotides were used as the template for the peptide expression. Two different pairs of ssDNA

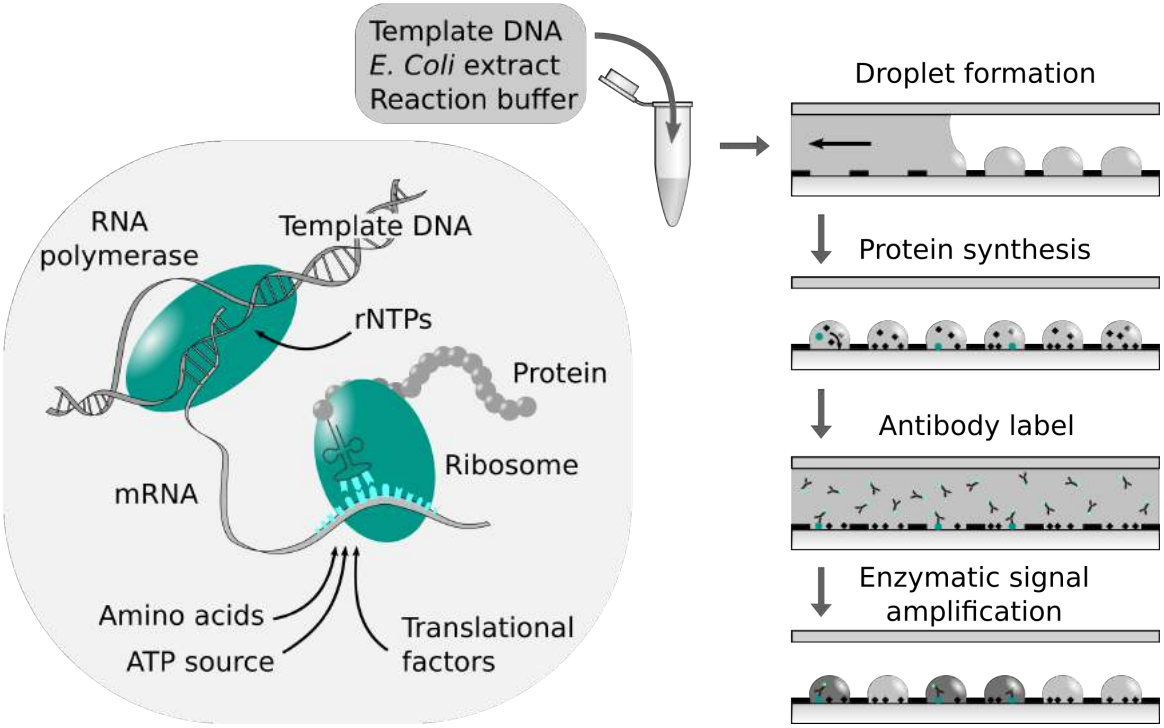

Figure 10.1: A sketch of the cell-free expression of proteins in droplets with subsequent detection by antibody labeling. The insert shows the steps in protein synthesis. Part of this figure is presented in [32].

oligonucleotides were purchased from TAG copenhagen (see Table 10.1), and contained the **T7 promoter**, *Ribosomal binding site* (Shine-Dalgarno sequence), ***His(6)***, and the sequences of interest, here hemagglutinin (*HA*) and SRY box-2 (*SOX2*).

10.2.2 *Surface Functionalisation of the MDA*

The MDAs were functionalised according to the protocol described in Section 3.2.7 in Chapter 3, and the MDA was used immediately for cell-free protein expression.

10.2.3 *Protein Expression in Droplets*

The aim of this application was to mimic the expression of a peptide library in the droplets and look for rare targets using a detection antibody. This was simulated by mixing two DNA templates together present in different concentrations. In this case, the *HA* tag peptide was used as the rare target, and was prepared in two concentrations corresponding to an average of 0.01 and 1 copy per droplet (0.3 pM, and 33 pM respectively). The *SOX2* DNA template was used as background, and was present in a concentration corresponding to 10 copies per droplet (330 pM). A solution containing only SOX2 template was used as a negative control experiment.

The templates were bought as ssDNA oligonucleotides, and to anneal the two complimentary strands, the solution was heated to 95 °C in a PCR thermocycler and allowed to cool to room temperature at a rate of 0.1 °C per second. The cell-free protein ex-

Table 10.1: The sequences of the DNA templates used for peptide expression in droplets.

Name	Sequence
T7-RBS-His(6)-HA	5'-CGA AAT **TAA TAC GAC TCA CTA TAG** GTT GTT TAA CTT TAA G*AG GAG* GAC AGC TAT G***CA CCA CCA CCA CCA CCA*** ***C***AT GTA CCC ATA CGA TGT TCC AGA TTA CGC TTA AGC GAT TCG AAC TTC T-3'
T7-RBS-His(6)-SOX2	5'-CGA AAT **TAA TAC GAC TCA CTA TAG** GTT GTT TAA CTT TAA G*AG GAG* GAC AGC TAT G***CA CCA CCA CCA CCA CCA*** ***C***AT GAT AAT AAC AAT CAT CGG CGG CGT AAG CGA TTC GAA CTT CT-3'

pression kit was thawed according to manufacturers instructions and aliquoted. The *E. Coli* extract was diluted three fold in the reaction buffer to prevent surface fouling due to high protein content. Next,the components of the kit was mixed according to manufacturers instructions together with the DNA templates, and 15 μL of the mix was introduced in the channels covering the MDA. To prevent excessive evaporation of the reaction mixture, scotch tape was used to seal the inlets and outlets of the system. The MDA and microfluidic interface assembly was then placed in an incubater at 37 °C for two hours to let the protein expression occur. During the expression of the proteins, these would bind on the surface due to the His(6)-tag. Next, the chip was rinsed with a 10 g L^{-1} solution of PEG_{20000} in phosphate buffered saline (PBS, pH 7.4) (PEG-PBS buffer). In order to block any remaining free NTA groups, the chip was incubated with an unrelated antibody (in this case an anti-amyloid beta antibody) in a solution containing 1 g L^{-1} bovine serum albumin (BSA), 10 g L^{-1} PEG_{20000} and 0.1% Triton X-100 in PBS. The blocking solution was incubated for 30 minutes, and was supposed to prevent the capture antibodies from binding nonspecifically to the MDA surface. The chip was then rinsed in the PEG-PBS buffer, and a 0.2 μg mL^{-1} solution of anti-HA antibody conjugated to HRP containing 1 g L^{-1} BSA, 10 g L^{-1} PEG_{20000} and 0.1% Triton X-100 in PBS was incubated on the chip for 30 minutes. To remove any unbound antibodies, the chip was rinsed for 15 minutes in PEG-PBS buffer before finally introducing the HRP substrate, AFR, which was infused on the chip at a final concentration of 0.2 mM. Droplets were spontaneously formed when passing the plug of liquid containing the substrate across the surface of the MDA. In the droplets, the conversion of the substrate occurs rapidly, and the chip could be immaged on a fluorescence microscopei immediately after introducing the substrate.

10.3 Results and Discussion

Expressing and detecting peptides in the MDA resulted in fluorescent droplets, where an increase in DNA template concentration related to an increase in the number

of fluorescent spots (see Figure 10.2). The nonspecific adsorption of the detection antibody-HRP conjugate (Figure 10.2 A) resulted in 1% of the droplets fluorescing. This level of background binding is comparable to the reported background binding of digital ELISA in the literature of around 0.3%[20] to 1% [24]. With the background level subtracted, 1% (0.3 pM, Figure 10.2 B), and 30% (33 pM, 10.2 C) of droplets fluoresced for the two concentrations of DNA template, 0.3 pM and 33 pM respectively. Bright field microscopy confirmed that droplets were still successfully generated on the MDA after the assay (Figure 10.2 D), with only around 1% of the array showing irregularities. This suggests that the three fold dilution of the *E. Coli* extract was sufficient to prevent fouling of the surface, but still contained a sufficient amount of reagents to translate the proteins.

The theoretical number of fluorescent droplets can be estimated, as the DNA template will be randomly distributed in the droplets following the Poisson statistics, where λ is the average number of DNA molecules per droplet. A concentration of 0.3 pM in 50 fL droplets corresponds to $\lambda = 0.01$. This Poisson distribution dictates that 0.99% of all droplets will contain just one molecule, 99% of all droplets will be empty, and 0.1% of all droplets will contain two or more molecules. This correlate very well with the obtained value of 1%. A concentration of 33 pM in 50 fL droplets corresponds to $\lambda = 1$. Theoretically, this means that 37% of all droplets will be empty, and hence 63% of all droplets will contain one or more DNA molecule, resulting in fluorescence. This deviates substatially from the obtained 30%. A likely reason can be that the coupling efficiency of the annealing does not result in 100% double stranded templates, thus reducing the effective concentration in solution. By showing that a protein expressed in a droplet from a single DNA template can be successfully detected, the path towards generation of full protein arrays from DNA libraries have been paved. The MDA platform offers advantages over microtitre plates in terms of reduced reagent consumprion, shorter reaction times due to the small volumes, and easy access through the microfluidic systems. With some further development of the platform, high throughput screening of proteins may become feasible, if a method for retrieving the positive hits is developed.

10.4 Conclusion

In summary, successful transcription and translation of DNA into proteins has been demonstrated on the droplet array. This assay required two compartmentalised reaction steps compared to digital ELISA, which require only one. This was possible due to the flexibility of the water/air interface in which droplets remain stable for several hours due to the small microfluidic chamber, and which allow repeated switching between reacting in bulk and in droplets. Proteins were bound through a poly-His NTA interaction and detected by complementary HRP conjugated antibodies. The capture antibody HRP conjugate nonspecifically bound in 1% of the droplets, still allowing us to detect protein expression from a 0.3 pM solution of target DNA. This opens up for the rapid and direct generation of protein arrays from single strands of DNA template for high throughput screening.

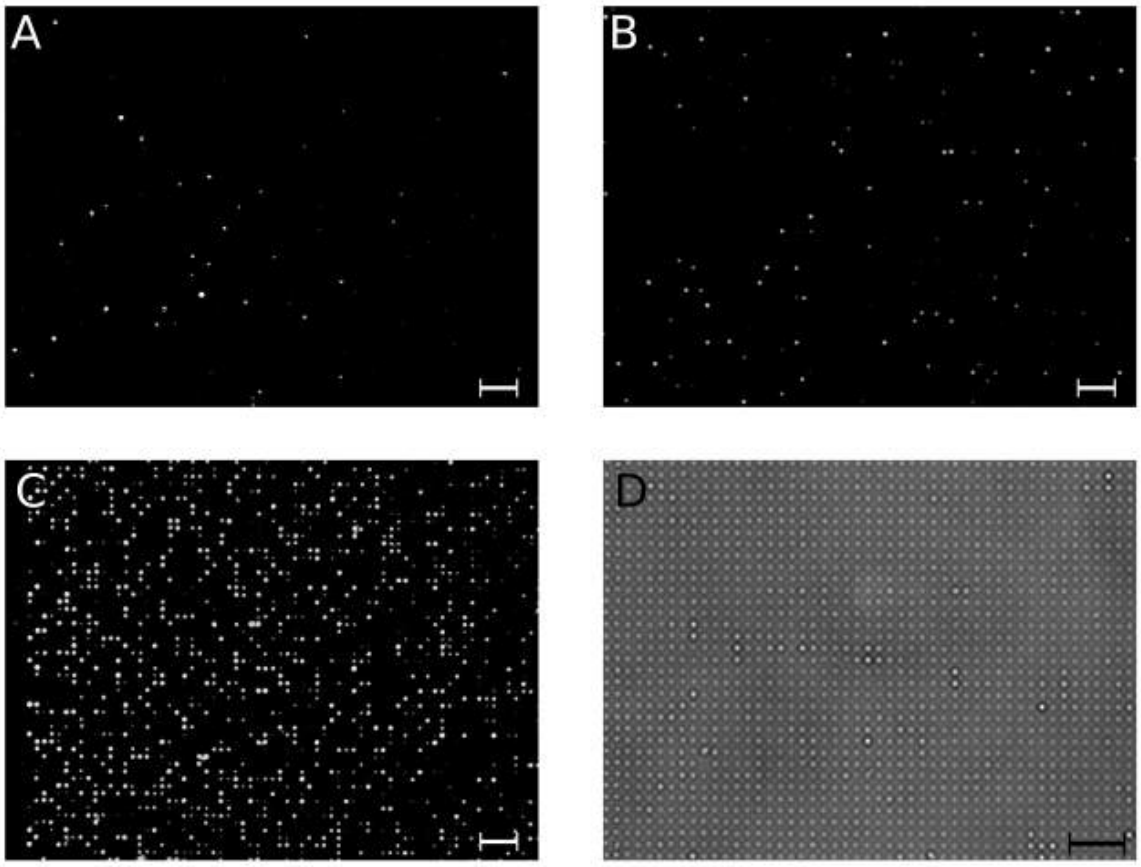

Figure 10.2: Fluorescence and bright field micrographs of MDA after cell-free protein expression. A) Fluorescence micrograph from the negative control, containing no target DNA template. The fluorescence arise from nonspecific binding of the detection antibody-HRP conjugate. B) Fluorescence micrograph from MDA with 0.3 pM concentration of the target template. C) Fluorescence micrograph from MDA with 33 pM concentration of the target template. D) Bright field micrograph of the MDA after the protein expression assay showing stable droplet formation. The scale bar is 50 μm. This data is also presented in [32].

11 | Summary of Part II

This chapter will summarise Part II of this thesis. In this part, the fabrication of an FDTS based MDA was described. The fabrication process used two consecutive rounds of photo-lithography to create (I) a chromium pattern which served as a dicing guide and processing side indication, and (II) the hydrophillic in hydrophobic pattern. The glass was rendered hydrophobic by coating it with a self assembled monolayer of FDTS. The FDTS based MDA was characterised in terms of contact angle, droplet stability and the reproducibility of the droplet formation process. It was shown that droplets were stable for more than 72 hours, and that the reduction in volume was slow, indicating the feasibility of incubations several hours long before the concentration of the reagents in the droplets become significant.

It was also shown that the amount of defect droplets in each array was low (less than 1%) and would not affect the analysis of assays on the MDA. The fabrication process also seemed robust, until unknown changes in the FDTS coating process resulted in batches where droplets were not supported on the arrays. Coating smaller batches of wafers produced working MDAs, and hence it was believed that an insufficient amount of FDTS was added to the reaction to be able to completely cover the six wafer batches, however, this was discovered very late in the project.

With the working batches of MDAs, digital ELISA was demonstrated for the detection of the Alzheimer's biomarker, $A\beta_{1-41}$. The limit of detection was around 10 fM, which is somewhat lower than those reported previously in literature. This could be attributed to an inefficient antibody pair. Despite this, detection of $A\beta_{1-41}$ in patient CSF samples were capable of dividing the samples into two group, namely patients diagnosed with AD and a control group.

Lastly, cell-free protein expression and subsequent detection was demonstrated on the MDA. This assay required compartmentalisation in two steps, as opposed to digital ELISA, which only required compartmentalisation in the detection step. Two DNA templates encoding for His-tagged *HA* tag and His-tagged *SOX2* were added to the celf-free expression assay, and expressed in the droplets. The His-tag bound to NTA groups on the MDA surface, which allowed the subsequent detection of *HA* tag by antibody recognition. Varying the amount of *HA* tag template resulted in varying amount of positive signals. The demonstration of this assay suggests the feasibility of the expression of DNA libraries on large arrays for example for the fabrication of protein arrays. It also promised the feasibility of more complex assays, which would be required for example for multiple interrogations of the same molecule.

Part III

Fluor Acryl-based Microdroplet Arrays

12 | Introduction

12.1 Hydrophilic in Hydrophobic Pattern Using Fluor Acryl 3298

The fabrication process of the FDTS MDA chips was rather complex, and one batch of 6 wafers would typically take two working days to complete. However, the main issue was that it also turned out that parts of the process were very sensitive to the state of the equipment, and failed batches of chips slowed down the development of assays. As the issues regarding the fabrication of FDTS MDAs proved troublesome to resolve, an MDA fabricated by patterning a fluorinated acrylate polymer was developed as an alternative.

12.1.1 *Fluor Acryl 3298*

Fluor Acryl 3298 is a fluorinated acrylate polymer, which can be UV cross-linked by the addition of a photoinitiator, in this case a mixture of Trimethylbenzoyldiphenyl-phosphineoxide-α-hydroxyketones and Benzophenone derivatives. The acrylate polymer is used as an anti-fouling conformal coating. As a fluorinated polymer, it should have good chemical resistance and should be both hydrophobic and oleophobic. These properties are essential for this application, as it suggests that the glass surface can be functionalised without destroying the polymer layer. Aswell, running samples with high protein content might be feasible, as the surface should be resistant to fouling. Fluoropolymers are widely used in other medical applications due to the low surface energy and biocompatibility of many fluoropolymers.[110]

12.1.2 *Existing MDA Platforms Using Hydrophobic Polymers*

A hydrophillic-in-hydrophobic platform relying on the patterning of a hydrophobic polymer has been described by Kim et al.[20] In their reports, the hydrophobic polymer, CYTOP, is spin coated on glass substrates and patterned by masked reactive ion etching. CYTOP is an amorphous perfluoropolymer, which in addition to exhibiting the common perfluoropolymer characteristics of low surface energy also has excellent optical properties (low refractive index, low colouring and high transmittance[1]) due to the amorphous morphology. CYTOP can be spin coated to extremely thin films, just a few nanometers thick.[18] The fabrication process is slightly complexed as the polymer is not inherently patternable. One challenge in this process is the spin coating on a low surface energy and low friction substrate, which require a high viscosity photoresist.[19] However, the major drawback of the use of CYTOP is the price, as CYTOP costs 2000 EUR per 100 grams. In comparison, 100 grams of Fluor Acryl 3298 costs 50 USD (43 EUR). However, the strength of this process is the ability to

[1] From the company website of AGC Chemicals Europe

ensure complete removal of the polymer from the spots, as the etching rate of glass by oxygen reactive ion etching is much slower than the etching rate of polymers[2], which allow some degree of over etching. Ensuring the exposure of a pure glass substrate is important for the successful functionalisation of the glass exposed on the bottom in applications where capture molecules are immobilised directly in the spots.

In the following sections, the fabrication of MDAs based on the patterning of Fluor Acryl and the characterisation of the devices is presented, followed by a short demonstration of the detection of a nucleic acid duplex immobilised on the MDA spots.

[2]Data from DTU Danchip local resources.

13 | Fabrication and Characterisation of Fluor Acryl MDAs

The contents of this chapter is omitted for confidentiality reasons.

14 | Nucleic Acid Detection

The contents of this chapter is omitted for confidentiality reasons.

15 | Summary of Part III

This chapter will summarise the third and final part of this thesis. In this part, the fabrication of an MDA based on the photopatterning of a hydrophobic acrylate polymer was presented. No previous records on the use of this polymer was found in the scientific literature, hence a broad characterisation of the fabrication process had to be conducted. Using a drop shape analyser, the contact angle with water on the Fluor Acryl was determined to be between 100° and 110°, hence comparable to the contact angle achieved on FDTS coated glass.

As the manufacturer of Fluor Acryl 3298 claims that the polymer is highly resistant to chemicals, the cured samples were exposed to a range of organic solvents, acids and bases, and the film was inspected for damage. None of the treatments had an apparent impact on the integrity of the Fluor Acryl film. The chemical inertness of the polymer was important in the further funtionalisation of the MDA, as its function relies on the selective funtionalisation of the glass in the spots. The Fluor Acryl MDA was exposed to the silanisation protocol described in Chapter 3, and a fluorescently labelled streptavidin was immobilised. The fluorescence from the protein was seen only in the areas where glass was exposed, and hence it could be assumed that no reaction had occurred with the polymer.

The patterning of the Fluor Acryl was characterised next. First the response to UV light was examined by performing a dose response test. This test revealed that partial cross-linking occurred even at very low doses, which complicated the fabrication process and hampered the use of traditional masked exposure. Patterning of the Fluor Acryl was most successful on a maskless alignment system, where reflection of the UV light was less profound. The pattern was investigated by stylus profilometry and SEM, and these results were used to generate curves which linked the film thickness to the concentration of Fluor Acryl and the spin speed. The SEM images also displayed the sloped edges of the pattern, which was due to the very gradual dose response. Lastly, droplet formation was confirmed on triangular, hexagonal and octagonal spots. Even very dense arrays were capable of supporting droplets.

Lastly, the preliminary findings of nucleic acid detection on the MDA was presented. Streptavidin coated beads were immobilised in the spots and used to bind a biotinylated oligonucleotide probe. The complementary probe was allowed to form a hybrid, and the duplex was detected by the binding of streptavidin conjugated HRP. The fluorescence was solely generated in spots where beads were present, and a negative control sample not containing the complementary strand produced a few fluorescent spots, which was due to non-specific binding, as also seen on the FDTS MDA.

16 | Discussion and Conclusion

16.1 Discussion

In this study, the fundamental steps in the development of a highly versatile microdroplet array platform were demonstrated. These involved the numerical analysis of nucleic acid hybridisation of dilute targets on planar surfaces, the construction of an optical detection platform, two different fabrication methods for the generation of hydrophillic-in-hydrophobic droplet arrays and their characterisation, as well as the demonstration of three different applications on the MDAs. Developing a platform which does not rely on displacement of the aqueous phase by oil and the use of beads for target capture opens up for a large range of more complex assays to be conducted on the MDA. Several areas within diagnostics, drug development, and high-throughput screening could greatly benefit from the effect of miniaturisation, such as cost reduction, lower reagent consumption, increased reaction kinetics and increasing sensitivity and specificity.

In terms of sensitivity, droplet digital PCR is the biggest competitor to nucleic acid detection on MDAs. Recent studies report that DNA quantification on MDAs have a detection in the 1-10 fM range,[16, 22] whereas droplet digital PCR in theory is capable of detecting 5 molecules in 20-50 μL sample[1] (Poisson limited), corresponding to a concentration around 0.1-1 aM. It is probably for this reason that reports on DNA and RNA quantification using MDAs has been limited. PCR reactions are primarily limited in the sample size, as the presence of a single copy of DNA should result in a detecable signal due to the exponential growth of DNA copies. Droplet PCR is limited by the number of partitions generated and analysed, and this is the limiting factor of the sample size which can be screened. In conventional qPCR, the sample size is typically limited due to the increased presence of inhibitors if the amount of DNA added to the reaction is increased, despite purification of the template DNA aims to remove these inhibitors. Because droplet PCR is Poisson limited (the average number of copies per sample result in the low probability of taking a sample containing no targets), in theory droplet PCR can reach an infinitely low detection limit by indefinitely increasing the amount of partitions screened, and hence the sample size. MDAs are primarily limited by the non-specific binding of the reporter enzyme, as shown in the digital ELISA and in the cell-free protein expression assays conducted in this study, and in numerous reports on MDAs using HRP or β-Galactosidase as signal amplification systems.[20, 24] Previous reports on the detection of nucleic acids on MDAs[16, 22] has been limited both in sample size and in non-specific binding. In the first report by Li et al.,[16] the nucleic acid detection was performed in wells formed by

[1] From the company websites of Bio-Rad (QX200 Droplet Digital PCR) and RainDance Technologies (RainDrop Digital PCR System)

etching the end of bundles of optical fibres. These wells were sealed from one another by pressing down a silicone gasket on the end of the fibre bundle. As the array was not integrated in a microfluidic system, static hybridisation to the array was required. This was done in 50 μL of PBS containing the DNA target. Increasing the sample size in the case of static incubations is not likely to improve the number of surface bound molecules substantially, as the process is diffusion limited, and increasing the sample size would also mean increasing the diffusion distance. In the other report by Cohen et al., [22] the nucleic acids, here miRNAs, were bound on beads. For the efficient target capture, 50.000 beads per μL were added to the samples. In this particular study, the sample containing capture beads were shaken during incubation, which increase the mobility of the beads and prevent them from sedimenting. Diluting the beads in a larger sample would increase the average distance between beads, and thus also the diffusion distance of the target, hence in order to increase the sample size, the amount of beads used should be increased proportionally. In this study, the Simoa HD-I analyser was used, which typically interrogate between 25.000 and 50.000 beads in one array containing 216,000 wells.[21] This means that as 100 μL of sample was incubated with beads, just one in every hundred beads are actually analysed. In the report, the number of active beads in negative control samples is not reported, so assuming 0.5% as stated in other reports,[25, 16] a minimum of 250 molecules should be captured on 50.000 beads. In 100 μL, containing 5 million beads, a minimum of 25.000 molecules should be captured, which corresponds to 0.4 fM. So, in the set-up as described in this study, 0.4 fM is the theoretical limit of detection. In order to increase the detection limit, the number of beads analysed could be increased, which would require the use of a larger array, or a larger sample could be screened, which would require either more beads (and an even bigger array), or longer incubation time. In contrast to the two mentioned reports on nucleic acid detection on MDAs, our platform is in theory not limited by sample size. As the numerical analysis in Chapter 2 indicated, the process is highly diffusion limited, and the greatest increase in number of molecules caught was achieved by increasing the size of the sample. As our MDA is embedded in a microfluidic channel and capture the targets directly on the MDA surface, the slow perfusion of the sample is possible. Theoretically, running the sample across the MDA at 6.7 μL min^{-1} would allow us to screen a full 10 mL sample in 24 hours. Despite the slightly larger diffusion distance in the microfluidic channel (100 μm) compared to the bead based assay (average bead to bead distance of 27-58 μm[22, 75]), and the absence of active mixing, the numerical model predicted a limit of detection of around 2 aM, assuming 0.5% non-specific binding. This is a 1000-fold decrease in limit of detection compared to the previous reports. It is possible, that the addition of a passive mixing structure in the lid of the microfluidic channel could drastically increase the number of molecules caught on the planar MDA. During the numerical analysis it was observed that the targets were very quickly depleted from the boundary layer close to the absorbing surface, and the transport by diffusion into the boundary layer happened too slowly to have an impact on the number of molecules caught. One example of a passive chaotic mixer for microfluidic channels was described by Stroock in 2002.[114] This structure relies on a series of herringbone

groves which result in the formation of vortices in the cross section of the channel. Such structures could be realised in for example PDMS lids or injection moulded lids. If this should increase the number of molecules caught as expected, the detection limit of nucleic acids on the MDA platform presented here would approach or improve that of droplet digital PCR (0.1 aM, assuming five molecules in 50 μL).

The next question to raise is then in which cases detecting these low concentrations is of clinical relevance. Since droplet PCR is capable of detecting nucleic acids at these levels, the clinical relevance of rare nucleic acid biomarkers is more well described than the equivalent protein biomarkers, which have been more difficult to detect and quantify at low concentrations by traditional assays, such as ELISA. For the detection of nucleic acids, the monitoring of residual disease in cancer treatment has already been discussed. Other applications could be for the detection of cell-free DNA.[115] Since droplet PCR already has the ability to quantify nucleic acids at very low concentrations, the major impact of nucleic acid detection on MDAs is expected to be very limited. It might be useful as an integrated platform for acquiring several pieces of information from the same nucleic acid molecule, for example the quantity and the level of mutations including compound mutations. In protein detection, the digitalisation of the ELISA assay has already increased the limit of detection by three orders of magnitude or more compared to the traditional ELISA assay. Another area where the MDA might be able to have a greater impact, is in high-throughput screening.

Both emulsion droplets and MDAs are powerful tools in HTS, however they cater different applications. The exchange of reagents in emulsion droplets are near impossible, which limit their applications to homogeneous assays (mix, encapsulate, detect). This is not entirely true, as the addition of reagents can be achieved using controlled droplet fusion or by picoinjection. On MDAs relying on the surface capture of the molecules, heterogeneous assays are easily performed. As shown in this study, droplets can be formed repeatedly with different buffers by passing a new liquid plug across the MDA. This enables the sequential addition and removal of reagents, allowing more complex assays to be performed. It was also shown that proteins could be directly synthesised from single strands of DNA and immobilised in 5 μm spots, which enables a range of high-throughput assays, for example epitope mapping, protein biomarker discovery, protein expression profiling, or the screening of protein-protein interactions. Where droplet microfluidics really comes to its full power, is in applications, where the target of the analysis is the product of a reaction or the excreted molecules from a process, for example within a cell.[116]

16.2 Future Work

The fundamental investigations of water in air microdroplet arrays on a hydrophillic in hydrophobic surface presented here demonstrate the promising characteristics which should enable more complex assays to be performed. Here it has been shown that since the targets are immobilised directly in the spots rather than on beads, several reactions with the target can be made, and the flexibility of the displacement of water

using air rather than oil allow the consecutive formation of droplets and the complete exchange of buffer in the droplets.

Building on these characteristics and other ideas briefly explored but not realised during this study, the further development of the platform could follow these suggestions:

16.2.1 *The Development of a Combined Platform for the Simultaneous Quantification and Mutational Analysis in Residual Disease CML*

The power to interrogate single molecules multiple times could be used to develop a platform for the simultaneous quantification and detection of known single-nucleotide substitution mutations. To realise this, first a robust nucleic acid quantification assay should be developed. From the results obtained in this thesis on the immobilisation of oligonucleotides, the next step would be to optimise the hybridisation conditions, and to show proportionality between the concentration of target and number of positive spots using synthetic oligonucleotides. If the streptavidin conjugated HRP signal amplification system is used, the buffer and concentration of the HRP should be optimised to reduce the non-specific binding, as this is the limiting factor on the detection limit. Subsequently, the assay should be run with the real RNA target. The cell line K562 is positive for the bcr-abl fusion gene, and can be used in place of patient samples.[117] When the detection can be run robustly, the mutational analysis can be developed. In place of the detection probe (as described in Chapter 14), a polymerase primer should be annealed to the target, and followed by a single base extension using biotinylated ddNTPs with a cleavable linker between the biotin and the nucleotide, and following the same method as used in pyrosequencing. To exemplify the procedure after hybridisation of the primer, first a PCR-like buffer mixture containing polymerase and biotinylated ddATP should be incubated on the MDA. This step can be carried out in bulk. Next, streptavidin conjugated HRP should be incubated on the MDA in a similar fashion as when quantifying the nucleic acids. Lastly, droplets are formed containing the HRP substrate, the chip is imaged, and the amount and position of positive signals are recorded. To start the next reaction, the biotin is cleaved from the incorporated nucleotides, and the process is repeated for the remaining three nucleotides. To detect several mutations, a strategy to remove the primer should be conceived. One option is to take inspiration from DNA nanomachines. In one example, a molecular tweezers is designed. This involves repeated annealing and removal of a complementary stand by utilising a dangling strand.[118] The same principle could be applied here. The 5' end of the primer is extended by for example three bases which are non-complementary to the target sequence. Upon the addition of a fully complement primer strand, the lower energy of the primer duplex should facilitate the removal of the primer from the target.

This type of assay would be very long and involve many different reagent additions and imaging steps. To be practical in reality, automated imaging and liquid handling would be required. This could be done by extending the detection platform described in this study with the means to deliver different reagents to the MDA, for example by the use of a cartridge or rotation valve. An extension of the software to handle

automated activation of liquid actuation and imaging would also be required, but could be built upon the existing software.

16.2.2 *The Development of Novel Signal Amplification Systems with Low Non-specific Binding*

As non-specific binding of HRP greatly limits the detection limit in the single molecule studies on MDAs, developing alternative reporter systems where non-specific binding occur less frequently could be of great advantage. Such systems could be multicomponent systems, because the non-specific binding of each component individually will not result in the generation of a positive signal, and the probability of both components binding non-specifically in a way that enables signal generation should be very low.

One such systems could be the amplification of DNA using a T7 polymerase and an intercalating dye or molecular beacons. For nucleic acid quantification, the detection probe could consist of a target specific sequence, and a double stranded non-target sequence to be amplified using the T7 polymerase. As the T7 polymerases copy the target, an increase in signal in the droplets is generated. This amplification scheme is much slower than the enzymatic conversion of Ampliflu red by HRP, however if the non-specific binding virtually become non-existing, the added reaction time might be acceptable.

Another such reporter system could rely on the cleavage of RNA modified molecular beacons by DNAzymes. DNAzymes are a specific DNA sequence which enable the cleavage of RNA at specific sites. The DNAzyme bind to a target sequence, and upon activation by the target DNA, the DNAzyme will stay constantly active. A method similar to that described by Tian and Mao[119] could be applied in the droplets. For nucleic acid quantification, the detection probe would consist of a target specific sequence and the DNAzyme target sequence. The DNAzyme would only by activated in the droplets where a detection probe had been bound on the target, and fluorescence would accumulate as the RNA modified molecular beacons were cleaved by the DNAzyme, allowing the separation of the fluorophore and the quencher.

The main concern regarding these methods is whether the accumulation of fluorescence is sufficient for detection by standard fluorescence microscopy. The use of an intercalating dye would allow the incorporation of several fluorescent molecules per synthesised strand, however, using molecular beacons, just one fluorophore is associated with each one molecular beacon. An educated guess on the scale of synthesised molecules would be between 10 and 1000 molecules depending on the incubation time, which would correspond to a concentration between 30 pM and 3 nM in 5 μm droplets. It is possible that the application of more sensitive fluorescence detection techniques would have to be applied, for example confocal fluorescence microscopy.

16.2.3 *Clean-room Free Fabrication of MDAs*

Fabrication in the clean-room is always associated with increased costs. Because of the large number of spots per array, the fabrication is less sensitive to small defects,

as defect areas of the arrays would simply be excluded from the analysis, and thus the fabrication does not strictly require the ultra-clean atmosphere of a clean-room. For less sensitive applications, UV exposure on mask-less alignment systems can be used outside a clean-room facility. The use of masks are more sensitive to the presence of particles, as it affects the distance between the substrate and the mask negatively, and hence masked UV exposure outside the clean room cannot be recommended. Patterning of UV cross-linkable hydrophobic polymers such as Fluor Acryl might be feasible in this manner.

Another method, which is currently being explored in our group, relies on creating bi-phillic surfaces by immobilising a photo-cleavable compound which is hydrophobic until exposed to UV light, as shown by Yamahira et al.[120] The pattern can be created by laser induced patterning or by masked UV exposure.

16.2.4 *Implementation of Passive Mixing Structures in the Microfluidic Channels*

Mixing in microlfuidic channels is an issue due to the laminar flow at low Reynold's number. Microstructures in the channel surfaces have been shown to create vortices, enabling passive mixing between the liquid layers.[114] As it was shown in this study that the capture of targets such as nucleic acids is highly diffusion limited, the addition of passive mixers in the channels might improve the number of molecules caught on the surface, and in turn improve the limit of detection. To realise such structures in the microfluidic channels, a more complex fabrication process would be required for the fabrication of the microfluidic lids. At least two rounds of lithography is required to define the mixing grooves and the microfluidic channels.[114] Such a process could be feasible with the fabrication of moulds for either PDMS casting[114] or injection moulding.

16.2.5 *High-Throughput Screening Applications - Peptides, Bacteria and More*

The versatile MDA platform would also be ideal in several high-throughput applications. Even though emulsion droplets are promising tools for several high-throughput applications, they suffer from the drawback that the droplets are not individually identifiable. This limits their value in applications where the droplets should be observed over longer periods of time. This could be applications where the screening is based on kinetic information (an example of such an assay is given in [121]).

The demonstration of the in-situ expression of functional peptides on the MDA directly enables high-throughput epitope mapping. Epitope mapping is useful in many applications, for example in therapeutic antibody discovery, discovery of cancer-specific epitope markers, in vaccine development,[122] and as a tool in the diagnosis of food allergies.[123] The assays are typically carried out either in microtitre plates or on peptide arrays. Microtitre plates allow the screening of a few hundred epitopes per plate, and volumes in the microlitre range is required per well. On the other hand, peptide arrays require the synthesis of many different peptides, which is both cumbersome and expensive,[123] or complicated synthesis procedures, which only result in short linear epitopes.[124] Creating functional proteins and peptides by synthetic

methods are difficult, hence cell-free protein expression for in-situ synthesis of functional proteins in microtitre plates has been previously described.[108] This method would greatly benefit from the reagent consumption reduction and increased reaction speed achieved on MDAs.

Lastly, bacterial screening should be possible on the MDA. The encapsulation of single bacteria have been shown on MDAs,[19] and the viability and proliferation of bacteria in emulsion droplets have been demonstrated.[125] In a student project undertaken in our group, we also demonstrated the encapsulation of bacteria on the MDA.

The current challenge limiting the use of the presented MDA platform in high-throughput screening applications is the recovery of positive hits. Other reports use micro-pipettes to address single droplets 10 μm in diameter.[19] The practicality of this on a large scale can be questioned, and alternative, less manual methods could be devised.

16.3 Conclsuions

In summary, four fundamental areas important to the fabrication and use of water-in-air microdroplet arrays were developed: (I) A finite element analysis was applied to evaluate the feasibility of surface bound hybridisation of low concentration targets. The model predicted a detection limit of 100 zM for an array 1 mm by 15 mm in the absence of non-specific binding of the reporter enzyme. Taking the non-specific binding into account, a more realistic detection limit was found to be 10 aM. This is comparable to the detection limits reported in literature, hence supporting the claim that beads were unnecessary for the efficient capture of rare targets. (II) A detection platform was presented, which was capable of scanning the MDA and recording fluorescence images while simultaneously controlling the liquid actuation in the microfluidic channel. All the components of the detection platform was controlled from one piece of software written in LabVIEW. This provided a good foundation for the full automation of assays including images, as all components could be integrated with LabVIEW. Furthermore, the price of the platform was one fourth that of a good fluorescence microscope. (III) Two different processes for the fabrication of MDAs was presented. The first process involved the deposition of the hydrophobic compound FDTS on a masked glass substrate. The method produced good MDAs, however it was experienced that an unknown change in the deposition process dramatically changed the outcome of batch processing. Towards the end of the study, it was found out that running smaller batches resulted in functional MDAs. While the batch process of FDTS based MDAs was diagnosed, a second fabrication process was developed. This process was based on the photopatterning of a thin film of hydrophobic polymer. Due to the novelty of using the polymer for photopatterning in this way, the whole fabrication process was characterised. Particularly obtaining a high purity glass surface in the spots proved troublesome. Protecting the spots by patterning a negative photoresist prior to the application of the hydrophobic polymer seemed the most promising solution to this issue. (IV) Two relevant bioassays and preliminary findings on DNA hybridisation on the MDAs were presented. Firstly, digital ELISA for the detection

of Alzheimer's biomarkers was carried out on the MDAs, and despite only achieving a detection limit of 10 fM, which is somewhat higher than other reported findings, it was still possible to distinguish two populations in a collection of patient samples, one group diagnosed with Alzheimer's disease and a control group. Secondly, in-situ protein synthesis and immobilisation followed by detection by antibody recognition was demonstrated. Two different DNA templates were mixed in varying ratios to model the expression of a peptide library in the droplets. As expected, the amount of positive droplets and the starting concentration of target template were related, although the efficiency of the expression was lower than expected. This could be explained by the quality of annealed oligonucleotides as a template. Lastly, the preliminary results of oligonucleotide hybridisation on the MDA was presented. A sample containing a high concentration of target resulted in a saturated array, whereas a control sample containing no target produced very few positive droplets. Due to the challenges in the fabrication process, the assay was not completed for the detection of BCR-ABL.

These findings pave the way for a great number of applications with diagnostics and high throughput screening, both areas which have benefited greatly from miniaturisation associated with an increase in speed and sensitivity and a great reduction in price, and in turn availability of the assay.

Bibliography

[1] Ashleigh B. Theberge, Fabienne Courtois, Yolanda Schaerli, Martin Fischlechner, Chris Abell, Florian Hollfelder, and Wilhelm T.S. Huck. Microdroplets in microfluidics: An evolving platform for discoveries in chemistry and biology. *Angew. Chemie - Int. Ed.*, 49(34):5846–5868, 2010.

[2] B T Kelly, J C Baret, V Taly, and A D Griffiths. Miniaturizing chemistry and biology in microdroplets. *Chem.Commun.*, pages 1773–1788, 2007.

[3] Andrew D. Griffiths and Dan S. Tawfik. Miniaturising the laboratory in emulsion droplets. *Trends Biotechnol.*, 24(9):395–402, 2006.

[4] Limor Cohen and David R. Walt. Single-Molecule Arrays for Protein and Nucleic Acid Analysis. *Annu. Rev. Anal. Chem.*, 10(1):345–363, 2017.

[5] B. Vogelstein and K. W. Kinzler. Digital PCR. *Proc. Natl. Acad. Sci.*, 96(16):9236–9241, aug 1999.

[6] Linas Mazutis, Ali Fallah Araghi, Oliver J. Miller, Jean-Christophe Baret, Lucas Frenz, Agnes Janoshazi, Valérie Taly, Benjamin J. Miller, J. Brian Hutchison, Darren Link, Andrew D. Griffiths, and Michael Ryckelynck. Droplet-based microfluidic systems for high-throughput single DNA molecule isothermal amplification and analysis. *Anal. Chem.*, 81(12):4813–4821, jun 2009.

[7] Jon F. Edd, Dino Di Carlo, Katherine J. Humphry, Sarah Köster, Daniel Irimia, David A. Weitz, and Mehmet Toner. Controlled encapsulation of single-cells into monodisperse picolitre drops. *Lab Chip*, 8(8):1262–1264, aug 2008.

[8] Todd P. Lagus and Jon F. Edd. A review of the theory, methods and recent applications of high-throughput single-cell droplet microfluidics. *J. Phys. D. Appl. Phys.*, 46(11):114005, mar 2013.

[9] N. Reginald Beer, Elizabeth K. Wheeler, Lorenna Lee-Houghton, Nicholas Watkins, Shanavaz Nasarabadi, Nicole Hebert, Patrick Leung, Don W. Arnold, Christopher G. Bailey, and Bill W. Colston. On-chip single-copy real-time reverse-transcription PCR in isolated picoliter droplets. *Anal. Chem.*, 80(6):1854–1858, 2008.

[10] Jean-Christophe Baret, Oliver J. Miller, Valerie Taly, Michaël Ryckelynck, Abdeslam El-Harrak, Lucas Frenz, Christian Rick, Michael L. Samuels, J. Brian Hutchison, Jeremy J. Agresti, Darren R. Link, David A. Weitz, and Andrew D. Griffiths. Fluorescence-activated droplet sorting (FADS): efficient microfluidic cell sorting based on enzymatic activity. *Lab Chip*, 9(13):1850–1858, jul 2009.

[11] Takao Ono, Takanori Ichiki, and Hiroyuki Noji. Digital enzyme assay using attoliter droplet array. *Analyst*, 143(20):4923–4929, 2018.

[12] Yannick Rondelez, Guillaume Tresset, Kazuhito V Tabata, Hideyuki Arata, Hiroyuki Fujita, Shoji Takeuchi, and Hiroyuki Noji. Microfabricated arrays of femtoliter chambers allow single molecule enzymology. *Nat. Biotechnolgy*, 23(3):361–365, 2005.

[13] Tanyu Wang, Mohan Zhang, Dakota D Dreher, and Yong Zeng. Ultrasensitive microfluidic solid-phase ELISA using an actuatable microwell-patterned PDMS chip. *Lab Chip*, 13(21):4190–7, 2013.

[14] Michaela Bowden, Linan Song, and David R. Walt. Development of a Microfluidic Platform with an Optical Imaging Microarray Capable of Attomolar Target DNA Detection. *Anal. Chem.*, 77(17):5583–5588, sep 2005.

[15] David M. Rissin and David R. Walt. Digital concentration readout of single enzyme molecules using femtoliter arrays and poisson statistics. *Nano Lett.*, 6(3):520–523, 2006.

[16] Zhaohui Li, Ryan B Hayman, and David R Walt. Detection of Single-Molecule DNA Hybridization Using Enzymatic Amplification in an Array of Femtoliter-Sized Reaction Vessels Detection of Single-Molecule DNA Hybridization Using Enzymatic Amplification in an Array of Femtoliter-Sized Reaction Vessels. *J. AM. CHEM. SOC.*, pages 12622–12623, 2008.

[17] David R Walt. Fibre optic microarrays. *Chem. Soc. Rev.*, 39(1):38–50, 2010.

[18] Shouichi Sakakihara, Suguru Araki, Ryota Iino, and Hiroyuki Noji. A single-molecule enzymatic assay in a directly accessible femtoliter droplet array. *Lab Chip*, 10:3355–3362, 2010.

[19] Ryota Iino, Kohei Hayama, Hiromi Amezawa, Shouichi Sakakihara, Soo Hyeon Kim, Yoshimi Matsumono, Kunihiko Nishino, Akihito Yamaguchi, and Hiroyuki Noji. A single-cell drug efflux assay in bacteria by using a directly accessible femtoliter droplet array. *Lab Chip*, 12:3923–3929, 2012.

[20] Soo Hyeon Kim, Shino Iwai, Suguru Araki, Shouichi Sakakihara, Ryota Iino, and Hiroyuki Noji. Large-scale femtoliter droplet array for digital counting of single biomolecules. *Lab Chip*, 12(23):4986–4991, 2012.

[21] David H. Wilson, David M. Rissin, Cheuk W. Kan, David R. Fournier, Tomasz Piech, Todd G. Campbell, Raymond E. Meyer, Matthew W. Fishburn, Carlos Cabrera, Purvish P. Patel, Erica Frew, Yao Chen, Lei Chang, Evan P. Ferrell, Volker von Einem, William McGuigan, Marcus Reinhardt, Heiko Sayer, Claus Vielsack, and David C. Duffy. The Simoa HD-1 Analyzer: A Novel Fully Automated Digital Immunoassay Analyzer with Single-Molecule Sensitivity and Multiplexing. *J. Lab. Autom.*, 21(4):533–547, 2016.

[22] Limor Cohen, Mark R. Hartman, Aaron Amardey-Wellington, and David R. Walt. Digital direct detection of microRNAs using single molecule arrays. *Nucleic Acids Res.*, 45(14):e137–e137, aug 2017.

[23] B. Rotman. Measurement of activity of single molecules of beta-D-galactosidase. *Proc. Natl. Acad. Sci. U. S. A.*, 47:1981–1991, 1961.

[24] David M Rissin, Cheuk W Kan, Todd G Campbell, Stuart C Howes, David R Fournier, Linan Song, Tomasz Piech, Purvish P Patel, Lei Chang, Andrew J Rivnak, Evan P Ferrell, Jeffrey D Randall, Gail K Provuncher, David R Walt, and David C Duffy. Single-molecule enzyme-linked immunosorbent assay detects serum proteins at subfemtomolar concentrations. *Nat. Biotechnol.*, 28(6):595–599, 2010.

[25] Soo Hyeon Kim, Shino Iwai, Suguru Araki, Shouichi Sakakihara, Ryota Iino, and Hiroyuki Noji. Large-scale femtoliter droplet array for digital counting of single biomolecules. *Lab Chip*, 12:4986–4991, 2012.

[26] Andrew J. Rivnak, David M. Rissin, Cheuk W. Kan, Linan Song, Matthew W. Fishburn, Tomasz Piech, Todd G. Campbell, Derek R. DuPont, Melissa Gardel, Sean Sullivan, Brian A. Pink, Carlos G. Cabrera, David R. Fournier, and David C. Duffy. A fully-automated, six-plex single molecule immunoassay for measuring cytokines in blood. *J. Immunol. Methods*, 424:20–27, 2015.

[27] Guan Sheng Du, Jian Zhang Pan, Shi Ping Zhao, Ying Zhu, Jaap M. J. Den Toonder, and Qun Fang. Cell-based drug combination screening with a microfluidic droplet array system. *Anal. Chem.*, 85:6740–6747, 2013.

[28] Marcel Margulies, Michael Egholm, William E. Altman, Said Attiya, Joel S. Bader, Lisa A. Bemben, Jan Berka, Michael S. Braverman, Yi Ju Chen, Zhoutao Chen, Scott B. Dewell, Lei Du, Joseph M. Fierro, Xavier V. Gomes, Brian C. Godwin, Wen He, Scott Helgesen, Chun He Ho, Gerard P. Irzyk, Szilveszter C. Jando, Maria L I Alenquer, Thomas P. Jarvie, Kshama B. Jirage, Jong Bum Kim, James R. Knight, Janna R. Lanza, John H. Leamon, Steven M. Lefkowitz, Ming Lei, Jing Li, Kenton L. Lohman, Hong Lu, Vinod B. Makhijani, Keith E. McDade, Michael P. McKenna, Eugene W. Myers, Elizabeth Nickerson, John R. Nobile, Ramona Plant, Bernard P. Puc, Michael T. Ronan, George T. Roth, Gary J. Sarkis, Jan Fredrik Simons, John W. Simpson, Maithreyan Srinivasan, Karrie R. Tartaro, Alexander Tomasz, Kari A. Vogt, Greg A. Volkmer, Shally H. Wang, Yong Wang, Michael P. Weiner, Pengguang Yu, Richard F. Begley, and Jonathan M. Rothberg. Genome sequencing in microfabricated high-density picolitre reactors. *Nature*, 437(7057):376–380, 2005.

[29] Jian Bing Fan, Kevin L. Gunderson, Marina Bibikova, Joanne M. Yeakley, Jing Chen, Eliza Wickham Garcia, Lori L. Lebruska, Marc Laurent, Richard Shen, and David Barker. Illumina Universal Bead Arrays. *Methods Enzymol.*, 410(06):57–73, 2006.

[30] A. Rival, D. Jary, C. Delattre, Y. Fouillet, G. Castellan, A. Bellemin-Comte, and X. Gidrol. An EWOD-based microfluidic chip for single-cell isolation, mRNA purification and subsequent multiplex qPCR. *Lab Chip*, 14:3739–3749, 2014.

[31] Ansgar Huebner, Dan Bratton, Graeme Whyte, Min Yang, Andrew J. DeMello, Chris Abell, and Florian Hollfelder. Static microdroplet arrays: a microfluidic device for droplet trapping, incubation and release for enzymatic and cell-based assays. *Lab Chip*, 9(5):692–698, 2009.

[32] Andreas Hjarne Kunding, Louise Laub Busk, Helen Webb-Thomson, Markus Otto, Hans Klafki, Jörg P Kutter, and Martin Dufva. Micro-droplet arrays for micro-compartmentalization using an air/water interface. *Lab Chip*, 16(ii), 2018.

[33] D. F. Roberts and Robert Chester, editors. *Molecular Genetics in Medicine*. Palgrave Macmillan UK, London, 1991.

[34] Michael R. Speicher and Nigel P. Carter. The new cytogenetics: blurring the boundaries with molecular biology. *Nat. Rev. Genet.*, 6(10):782–792, sep 2005.

[35] John M.S. Bartlett and David Stirling. *PCR Protocols*, volume 226. Humana Press, New Jersey, aug 2003.

[36] Benjamin J. Hindson, Kevin D. Ness, Donald A. Masquelier, Phillip Belgrader, Nicholas J. Heredia, Anthony J. Makarewicz, Isaac J. Bright, Michael Y. Lucero, Amy L. Hiddessen, Tina C. Legler, Tyler K. Kitano, Michael R. Hodel, Jonathan F. Petersen, Paul W. Wyatt, Erin R. Steenblock, Pallavi H. Shah, Luc J. Bousse, Camille B. Troup, Jeffrey C. Mellen, Dean K. Wittmann, Nicholas G. Erndt, Thomas H. Cauley, Ryan T. Koehler, Austin P. So, Simant Dube, Klint A. Rose, Luz Montesclaros, Shenglong Wang, David P. Stumbo, Shawn P. Hodges, Steven Romine, Fred P. Milanovich, Helen E. White, John F. Regan, George A. Karlin-Neumann, Christopher M. Hindson, Serge Saxonov, and Bill W. Colston. High-Throughput Droplet Digital PCR System for Absolute Quantitation of DNA Copy Number. *Anal. Chem.*, 83(22):8604–8610, nov 2011.

[37] Monya Baker. Digital PCR hits its stride. *Nat. Methods*, 9(6):541–544, 2012.

[38] M. B. Eisen and P. O. Brown. DNA arrays for analysis of gene expression. *Methods Enzymol.*, 303:179–205, 1999.

[39] Martin Dufva, editor. *DNA Microarrays for Biomedical Research*. Methods in Molecular Biology. Humana Press, Totowa, NJ, 2008.

[40] F. Sanger, S. Nicklen, and A. R. Coulson. DNA sequencing with chain-terminating inhibitors. *Proc. Natl. Acad. Sci.*, 74(12):5463–5467, 1977.

[41] Olena Morozova, Martin Hirst, and Marco a Marra. Applications of new sequencing technologies for transcriptome analysis. *Annu. Rev. Genomics Hum. Genet.*, 10:135–151, 2009.

[42] Michael L Metzker. Sequencing technologies - the next generation. *Nat. Rev. Genet.*, 11(1):31–46, 2010.

[43] Chandra Shekhar Pareek, Rafal Smoczynski, and Andrzej Tretyn. Sequencing technologies and genome sequencing. *J. Appl. Genet.*, 52(4):413–435, 2011.

[44] Elaine R Mardis. Next-generation DNA sequencing methods. *Annu. Rev. Genomics Hum. Genet.*, 9:387–402, 2008.

[45] Timothy D. Harris, Phillip R. Buzby, Hazen Babcock, Eric Beer, Jayson Bowers, Ido Braslavsky, Marie Causey, Jennifer Colonell, James Dimeo, J. William Efcavitch, Eldar Giladi, Jaime Gill, John Healy, Mirna Jarosz, Dan Lapen, Keith Moulton, Stephen R. Quake, Kathleen Steinmann, Edward Thayer, Anastasia Tyurina, Rebecca Ward, Howard Weiss, and Zheng Xie. Single-molecule DNA sequencing of a viral genome. *Science*, 320:106–109, 2008.

[46] M J Levene, J Korlach, S W Turner, M Foquet, H G Craighead, and W W Webb. Zero-mode waveguides for single-molecule analysis at high concentrations. *Science*, 299(5607):682–686, 2003.

[47] Adam Ameur, Wigard P. Kloosterman, and Matthew S. Hestand. Single-Molecule Sequencing: Towards Clinical Applications. *Trends Biotechnol.*, 37(1):72–85, 2019.

[48] Yue Wang, Qiuping Yang, and Zhimin Wang. The evolution of nanopore sequencing. *Front. Genet.*, 5(DEC), 2014.

[49] Sarah Goldstein, Lidia Beka, Joerg Graf, and Jonathan L. Klassen. Evaluation of strategies for the assembly of diverse bacterial genomes using MinION long-read sequencing. *BMC Genomics*, 20(1), 2019.

[50] Shawn E. Levy and Richard M. Myers. Advancements in Next-Generation Sequencing. *Annu. Rev. Genomics Hum. Genet.*, 17(1):95–115, 2016.

[51] Catherine C Smith, Michael Brown, Wendy T Parker, Kimberly Lin, Kevin Travers, Susana Wang, Susan Branford, and Neil Shah. Single Molecule Real Time (SMRT (TM)) Sequencing Sensitively Detects the Evolution of Polyclonal and Compound BCR-ABL Mutations in Patients Who Relapse On Kinase Inhibitor Therapy. *Blood*, 120(21), 2012.

[52] Ruibao Ren. Mechanisms of BCR-ABL in the pathogenesis of chronic myelogenous leukaemia. *Nat. Rev. Cancer*, 5(3):172–183, 2005.

[53] Delphine Rea, Franck E. Nicolini, Michel Tulliez, François Guilhot, Joelle Guilhot, Agnès Guerci-Bresler, Martine Gardembas, Valérie Coiteux, Gaelle Guillerm, Laurence Legros, Gabriel Etienne, Jean Michel Pignon, Bruno Villemagne, Martine Escoffre-Barbe, Jean Christophe Ianotto, Aude Charbonnier, Hyacinthe Johnson-Ansah, Marie Pierre Noel, Philippe Rousselot, and François Xavier Mahon. Discontinuation of dasatinib or nilotinib in chronic myeloid leukemia: Interim analysis of the STOP 2G-TKI study. *Blood*, 129(7):846–854, 2017.

[54] National Comprehensive Cancer Network. NCCN Clinical Practice Guidelines in Oncology. Chronic Myelogenous Leukemia Version 2.2012. 10(1):64–110, 2012.

[55] Masaya Okada, Jun Imagawa, Hideo Tanaka, Hirohisa Nakamae, Masayuki Hino, Kazunori Murai, Yoji Ishida, Takashi Kumagai, Seiichi Sato, Kazuteru Ohashi, Hisashi Sakamaki, Hisashi Wakita, Nobuhiko Uoshima, Yasunori Nakagawa, Yosuke Minami, Masahiro Ogasawara, Tomoharu Takeoka, Hiroshi Akasaka, Takahiko Utsumi, Naokuni Uike, Tsutomu Sato, Sachiko Ando, Kensuke Usuki, Syuichi Mizuta, Satoshi Hashino, Tetsuhiko Nomura, Masato Shikami, Hisashi Fukutani, Yokiko Ohe, Hiroshi Kosugi, Hirohiko Shibayama, Yasuhiro Maeda, Toshihiro Fukushima, Hirohito Yamazaki, Kazuo Tsubaki, Toshimasa Kukita, Yoko Adachi, Toshiki Nataduka, Hiroto Sakoda, Hisayuki Yokoyama, Takahiro Okamoto, Yukari Shirasugi, Yasushi Onishi, Masaharu Nohgawa, Satoshi Yoshihara, Satoshi Morita, Junichi Sakamoto, and Shinya Kimura. Final 3-year Results of the Dasatinib Discontinuation Trial in Patients With Chronic Myeloid Leukemia Who Received Dasatinib as a Second-line Treatment. *Clin. Lymphoma Myeloma Leuk.*, 18(5):353–360.e1, may 2018.

[56] R. Hehlmann, A. Hochhaus, and M. Baccarani. Chronic myeloid leukaemia. *Lancet*, 370:342–350, 2007.

[57] Susan Branford, Zbigniew Rudzki, Sonya Walsh, Ian Parkinson, Andrew Grigg, Jeff Szer, Kerry Taylor, Richard Herrmann, John F. Seymour, Chris Arthur, David Joske, Kevin Lynch, and Tim Hughes. Detection of BCR-ABL mutations in patients with CML treated with imatinib is virtually always accompanied by clinical resistance, and mutations in the ATP phosphate-binding loop (P-loop) are associated with a poor prognosis. *Blood*, 102(1):276–283, 2003.

[58] Michele Baccarani, Michael W. Deininger, Gianantonio Rosti, Andreas Hochhaus, Simona Soverini, Jane F. Apperley, Francisco Cervantes, Richard E. Clark, Jorge E. Cortes, François Guilhot, Henrik Hjorth-Hansen, Timothy P. Hughes, Hagop M. Kantarjian, Dong Wook Kim, Richard A. Larson, Jeffrey H. Lipton, François Xavier Mahon, Giovanni Martinelli, Jiri Mayer, Martin C. Müller, Dietger Niederwieser, Fabrizio Pane, Jerald P. Radich, Philippe Rousselot, Giuseppe Saglio, Susanne Saußele, Charles Schiffer, Richard Silver, Bengt Simonsson, Juan Luis Steegmann, John M. Goldman, and Rüdiger

Hehlmann. European LeukemiaNet recommendations for the management of chronic myeloid leukemia: 2013. *Blood*, 122(6):872–884, 2013.

[59] Thomas O'Hare, Christopher A. Eide, and Michael W.N. Deininger. Bcr-Abl kinase domain mutations, drug resistance, and the road to a cure for chronic myeloid leukemia. *Blood*, 110(7):2242–2249, 2007.

[60] Simona Soverini, Caterina De Benedittis, Katerina Machova Polakova, Adela Brouckova, David Horner, Michele Iacono, Fausto Castagnetti, Gabriele Gugliotta, Francesca Palandri, Cristina Papayannidis, Ilaria Iacobucci, Claudia Venturi, Maria Teresa Bochicchio, Hana Klamova, Federica Cattina, Domenico Russo, Paola Bresciani, Gianni Binotto, Barbara Giannini, Alexander Kohlmann, Torsten Haferlach, Andreas Roller, Gianantonio Rosti, Michele Cavo, Michele Baccarani, and Giovanni Martinelli. Unraveling the complexity of tyrosine kinase inhibitor-resistant populations by ultra-deep sequencing of the BCR-ABL kinase domain. *Blood*, 122(9):1634–1648, 2013.

[61] David Erickson, Dongqing Li, and Ulrich J. Krull. Modeling of DNA hybridization kinetics for spatially resolved biochips. *Anal. Biochem.*, 317(2):186–200, 2003.

[62] Koji Hashimoto, Keiko Ito, and Yoshio Ishimori. Novel DNA sensor for electrochemical gene detection. *Anal. Chim. Acta*, 286(2):219–224, 1994.

[63] Henrik Bruus. *Theoretical Microfluidics*. Oxford University Press, 2008.

[64] COMSOL Multiphysics. The Finite Element Method (FEM).

[65] Axel E. Nkodo, Jean M. Garnier, Bernard Tinland, Hongji Ren, Claude Desruisseaux, Laurette C. McCormick, Guy Drouin, and Gary W. Slater. Diffusion coefficient of DNA molecules during free solution electrophoresis. *Electrophoresis*, 22(12):2424–2432, 2001.

[66] B. S. Fujimoto, J. M. Miller, N. S. Ribeiro, and J. M. Schurr. Effects of different cations on the hydrodynamic radius of DNA. *Biophys. J.*, 67(1):304–308, 1994.

[67] Gergely L. Lukacs, Peter Haggie, Olivier Seksek, D. Lechardeur, Neal Freedman, and A. S. Verkman. Size-dependent DNA mobility in cytoplasm and nucleus. *J. Biol. Chem.*, 275(3):1625–1629, 2000.

[68] Bernard Tinland, Alain Pluen, Jean Sturm, and Gilbert Weill. Persistence Length of Single-Stranded DNA. *Macromolecules*, 30(September):5763–5765, 1997.

[69] Brian J Kirby. *Micro- and Nanoscale Fluid Mechanics: Transport in Microfluidic Devices*. Cambridge University Press, 2010.

[70] Vincent Chan, Steven E. McKenzie, Saul Surrey, Paolo Fortina, and David J. Graves. Effect of hydrophobicity and electrostatics on adsorption and surface diffusion of DNA oligonucleotides at liquid/solid interfaces. *J. Colloid Interface Sci.*, 203(1):197–207, 1998.

[71] Yoshio Okahata, Masanori Kawase, Kenichi Niikura, Fuyuka Ohtake, Hiroyuki Furusawa, and Yasuhito Ebara. Kinetic Measurements of DNA Hybridization on an Oligonucleotide-Immobilized 27-MHz Quartz Crystal Microbalance. *Anal. Chem.*, 70(7):1288–1296, 1998.

[72] Frank F. Bier, Frank Kleinjung, and Frieder W. Scheller. Real-time measurement of nucleic-acid hybridization using evanescent-wave sensors: steps towards the genosensor. *Sensors Actuators B Chem.*, 38(1-3):78–82, 1997.

[73] Michael R. Henry, Priscilla Wilkins Stevens, Jason Sun, and David M. Kelso. Real-time measurements of DNA hybridization on microparticles with fluorescence resonance energy transfer. *Anal. Biochem.*, 276(2):204–214, 1999.

[74] Linan Song, D. Richard Lachno, David Hanlon, Adam Shepro, Andreas Jeromin, Dipika Gemani, Jayne A. Talbot, Margaret M. Racke, Jeffrey L. Dage, and Robert A. Dean. A digital enzyme-linked immunosorbent assay for ultrasensitive measurement of amyloid-β 1-42 peptide in human plasma with utility for studies of Alzheimer's disease therapeutics. *Alzheimer's Res. Ther.*, 8(1):1–15, 2016.

[75] Lei Chang, David M. Rissin, David R. Fournier, Tomasz Piech, Purvish P. Patel, David H. Wilson, and David C. Duffy. Single molecule enzyme-linked immunosorbent assays: Theoretical considerations. *J. Immunol. Methods*, 378(1-2):102–115, 2012.

[76] David Yu Zhang, Sherry Xi Chen, and Peng Yin. Optimizing the specificity of nucleic acid hybridization. *Nat. Chem.*, 4(3):208–214, 2012.

[77] Michael Salcius, Fang Zhou, Rhonda Bangham, Jaclyn Bonin, Hong Guo, and Michael Snyder. Analyzing antibody specificity with whole proteome microarrays. *Nat. Biotechnol.*, 21(12):1509–1512, 2003.

[78] E. TAUB, FLOYD, JAMES M. DeLEO, and E. BRAD THOMPSON. Sequential Comparative Hybridizations Analyzed by Computerized Image Processing Can Identify and Quantitate Regulated RNAs. *Dna*, 2(4):309–327, 1983.

[79] D. R. Call, D. P. Chandler, and F. Brockman. Fabrication of DNA microarrays using unmodified oligonucleotide probes. *Biotechniques*, 30(2):368–72, 374, 376 passim, feb 2001.

[80] Haukur Gudnason, Martin Dufva, Dang Duong Bang, and Anders Wolff. An inexpensive and simple method for thermally stable immobilization of DNA on an unmodified glass surface: UV linking of poly(T) 10-poly(C) 10-tagged DNA probes. *Biotechniques*, 45(3):261–271, 2008.

[81] Martin Dufva. Fabrication of high quality microarrays. *Biomol. Eng.*, 22(5-6):173–184, 2005.

[82] Nathalie Zammatteo, Laurent Jeanmart, Sandrine Hamels, Stéphane Courtois, Pierre Louette, Laszlo Hevesi, and José Remacle. Comparison between different strategies of covalent attachment of DNA to glass surfaces to build DNA microarrays. *Anal. Biochem.*, 280(1):143–150, 2000.

[83] Y H Rogers, P Jiang-Baucom, Z J Huang, V Bogdanov, S Anderson, and M T Boyce-Jacino. Immobilization of oligonucleotides onto a glass support via disulfide bonds: A method for preparation of DNA microarrays. *Anal. Biochem.*, 266(1):23–30, 1999.

[84] Anne Marie Caminade, Clément Padié, Régis Laurent, Alexandrine Maraval, and Jean Pierre Majoral. Uses of dendrimers for DNA microarrays. *Sensors*, 6(8):901–914, 2006.

[85] Paul Peluso, David S. Wilson, Duc Do, Huu Tran, Maanasa Venkatasubbaiah, David Quincy, Bettina Heidecker, Kelli Poindexter, Neil Tolani, Michael Phelan, Krista Witte, Linda S. Jung, Peter Wagner, and Steffen Nock. Optimizing antibody immobilization strategies for the construction of protein microarrays. *Anal. Biochem.*, 312(2):113–124, 2003.

[86] life technologies Invitrogen. Dynabeads ® M-270 Epoxy, 2012.

[87] Thermo Fischer. His-tagged Proteins – Production and Purification.

[88] Guoliang Zhen, S. Zurcher, D. Falconnet, Fei Xu, E. Kuennemann, and M. Textor. NTA-Functionalized Poly(L-lysine)-g-Poly(Ethylene Glycol): A Polymeric Interface for Binding and Studying 6 His-tagged Proteins. *2005 IEEE Eng. Med. Biol. 27th Annu. Conf.*, pages 1036–1038, 2005.

[89] Jacques Blümmel, Nadine Perschmann, Daniel Aydin, Jovana Drinjakovic, Thomas Surrey, Monica Lopez-Garcia, Horst Kessler, and Joachim P. Spatz. Protein repellent properties of covalently attached PEG coatings on nanostructured SiO2-based interfaces. *Biomaterials*, 28(32):4739–4747, 2007.

[90] R. Benters, C. M. Niemeyer, and D. Wöhrle. Dendrimer-activated solid supports for nucleic acid and protein microarrays. *ChemBioChem*, 2(9):686–694, 2001.

[91] Paul Wingfield. Protein Precipitation Using Ammonium Sulfate. In *Curr. Protoc. Protein Sci.*, pages A.3F.1–A.3F.8. John Wiley & Sons, Inc., Hoboken, NJ, USA, sep 1998.

[92] F. G. Wouterlood and A. J. Boekel. Fluorescence Microscopy in the Neurosciences. In *Encycl. Neurosci.*, pages 253–260. 2010.

[93] A. M. Omary and H.H Patterson. Luminescence Theory. In *Encycl. Spectrosc. Spectrom.*, pages 1186–1207. 1999.

[94] Jurek W. Dobrucki and Ulrich Kubitscheck. Fluorescence Microscopy. In *Fluoresc. Microsc.*, pages 85–132. Wiley-VCH Verlag GmbH & Co. KGaA, Weinheim, Germany, may 2017.

[95] Jeff W Lichtman and José-Angel Conchello. Fluorescence microscopy. *Nat. Methods*, 2(12):910–919, dec 2005.

[96] Anthony K. Au, Wilson Huynh, Lisa F. Horowitz, and Albert Folch. 3D-Printed Microfluidics. *Angew. Chemie - Int. Ed.*, 55(12):3862–3881, 2016.

[97] Douglas B Weibel, Willow R Diluzio, and George M Whitesides. Microfabrication meets microbiology. *Nat. Rev. Microbiol.*, 5(3):209–218, 2007.

[98] Carl Fredrik Carlborg, Tommy Haraldsson, Kim Öberg, Michael Malkoch, and Wouter Van Der Wijngaart. Beyond PDMS: Off-stoichiometry thiol-ene (OSTE) based soft lithography for rapid prototyping of microfluidic devices. *Lab Chip*, 11(18):3136–3147, 2011.

[99] Formlabs. Creating Camera Lenses with Stereolithography.

[100] Weimin Zhou, Jing Zhang, Yanbo Liu, Xiaoli Li, Xiaomin Niu, Zhitang Song, Guoquan Min, YongZhong Wan, Liyi Shi, and Songlin Feng. Characterization of anti-adhesive self-assembled monolayer for nanoimprint lithography. *Appl. Surf. Sci.*, 255(5):2885–2889, dec 2008.

[101] David O'Hagan. Understanding organofluorine chemistry. An introduction to the C-F bond. *Chem. Soc. Rev.*, 37(2):308–319, 2008.

[102] Samira Hosseini, Patricia Vázquez-Villegas, Marco Rito-Palomares, and Sergio O. Martinez-Chapa. *Enzyme-linked Immunosorbent Assay (ELISA)*. SpringerBriefs in Applied Sciences and Technology. Springer Singapore, Singapore, 2018.

[103] David A. Giljohann and Chad A. Mirkin. Drivers of biodiagnostic development. *Nature*, 462(7272):461–464, 2009.

[104] Gunnar I. Berglund, Gunilla H. Carlsson, Andrew T. Smith, Hanna Szöke, Anette Henriksen, and Janos Hajdu. The catalytic pathway of horseradish peroxidase at high resolution. *Nature*, 417(6887):463–468, 2002.

[105] Magnus Sjögren, Pia Davidsson, Anders Wallin, Ann Kathrine Granérus, Eva Grundström, Håkan Askmark, Eugeen Vanmechelen, and Kaj Blennow. Decreased CSF-β-amyloid 42 in Alzheimer's disease and amyotrophic lateral sclerosis may reflect mismetabolism of β-amyloid induced by disparate mechanisms. *Dement. Geriatr. Cogn. Disord.*, 13(2):112–118, 2002.

[106] Mirko Bibl, Marion Gallus, Volker Welge, Hermann Esselmann, Stefanie Wolf, Eckart Rüther, and Jens Wiltfang. Cerebrospinal fluid amyloid-β 2-42 is decreased in Alzheimer's, but not in frontotemporal dementia. *J. Neural Transm.*, 119(7):805–813, 2012.

[107] Bob Olsson, Ronald Lautner, Ulf Andreasson, Annika Öhrfelt, Erik Portelius, Maria Bjerke, Mikko Hölttä, Christoffer Rosén, Caroline Olsson, Gabrielle Strobel, Elizabeth Wu, Kelly Dakin, Max Petzold, Kaj Blennow, and Henrik Zetterberg. CSF and blood biomarkers for the diagnosis of Alzheimer's disease: a systematic review and meta-analysis. *Lancet Neurol.*, 15(7):673–684, jun 2016.

[108] Mingyue He and Michael J. Taussig. Single step generation of protein arrays from DNA by cell-free expression and in situ immobilisation (PISA method). *Nucleic Acids Res.*, 29(15):e73, aug 2001.

[109] Thermo Fischer. Expressway ™ Cell-Free E. coli Expression System User Manual, 2011.

[110] Vinny R. Sastri. *Plastics in Medical Devices*. Elsevier, 2010.

[111] A. Nakajima, K. Hashimoto, and T. Watanabe. Recent studies on superhydrophobic films. In W.J. Blau, P. Lianos, and U. Schubert, editors, *Mol. Mater. Funct. Polym.*, volume 132, pages 31–41. Springer, 2001.

[112] Ville Jokinen, Pia Suvanto, and Sami Franssila. Oxygen and nitrogen plasma hydrophilization and hydrophobic recovery of polymers. *Biomicrofluidics*, 6(1), 2012.

[113] John Goldman and Junia Melo. Chronic Myeloid Leukemia — Advances in Biology and New Approaches to Treatment. *N. Engl. J. Med.*, 349(15):1451–1464, 2003.

[114] Abraham D. Stroock, Stephan K.W. Dertinger, Armand Ajdari, Igor Mezić, Howard A. Stone, and George M. Whitesides. Chaotic mixer for microchannels. *Science (80-.).*, 295(5555):647–651, 2002.

[115] H. Schwarzenbach, D. S. B. Hoon, and K. Pantel. Cell-free nucleic acids as biomarkers in cancer patients. *Nat. Rev. Cancer*, 11(6):426–437, 2011.

[116] T. M. Tran, F. Lan, C. S. Thompson, and A. R. Abate. From tubes to drops: droplet-based microfluidics for ultrahigh-throughput biology. *J. Phys. D. Appl. Phys.*, 46(11):114004, mar 2013.

[117] G. Grosveld, T. Verwoerd, T. van Agthoven, A. de Klein, K. L. Ramachandran, N. Heisterkamp, K. Stam, and J. Groffen. The chronic myelocytic cell line K562 contains a breakpoint in bcr and produces a chimeric bcr/c-abl transcript. *Mol. Cell. Biol.*, 6(2):607–616, 1986.

[118] B Yurke, A J Turberfield, A P Mills, F C Simmel, and J L Neumann. A DNA-fuelled molecular machine made of DNA. *Nature*, 406(6796):605–608, 2000.

[119] Ye Tian and Chengde Mao. DNAzyme amplification of molecular beacon signal. *Talanta*, 67(3):532–537, 2005.

[120] Shinya Yamahira, Yumi Takasaki, Satoshi Yamaguchi, Kimio Sumaru, Toshiyuki Kanamori, and Teruyuki Nagamune. Dynamic PhotoChemical Lipid Micropatterning for Manipulation of Nonadherent Mammalian Cells. *Methods Cell Biol.*, 120:131–144, 2014.

[121] Ahmed S. Mehanna. High Throughput Kinetic Assay for Screening Potential Inhibitors of Sickle Hemoglobin Polymerization. *Med. Chem. (Los. Angeles).*, 07(07), 2017.

[122] Edgar Davidson and Benjamin J. Doranz. A high-throughput shotgun mutagenesis approach to mapping B-cell antibody epitopes. *Immunology*, 143(1):13–20, 2014.

[123] Jing Lin and Hugh A. Sampson. IgE epitope mapping using peptide microarray immunoassay. *Methods Mol. Biol.*, 1592:177–187, 2017.

[124] Lajla Bruntse Hansen, Soren Buus, and Claus Schafer-Nielsen. Identification and Mapping of Linear Antibody Epitopes in Human Serum Albumin Using High-Density Peptide Arrays. *PLoS One*, 8(7), 2013.

[125] Stanislav S Terekhov, Ivan V Smirnov, Anastasiya V Stepanova, Tatyana V Bobik, Yuliana A Mokrushina, Natalia A Ponomarenko, Alexey A Belogurov, Maria P Rubtsova, Olga V Kartseva, Marina O Gomzikova, Alexey A Moskovtsev, Anton S Bukatin, Michael V Dubina, Elena S Kostryukova, Vladislav V Babenko, Maria T Vakhitova, Alexander I Manolov, Maja V Malakhova, Maria A Kornienko, Alexander V Tyakht, Anna A Vanyushkina, Elena N Ilina, Patrick Masson, Alexander G Gabibov, and Sidney Altman. Microfluidic droplet platform for ultrahigh-throughput single-cell screening of biodiversity. *Proc. Natl. Acad. Sci.*, 2017.

Appendix

A | Finite Element Simulations of DNA Hybridisation on Surfaces

A.1 Comparison Between Homogeneous and Patterned Capture Surfaces

This section describes the set up of the COMSOL simulations that investigate the absorption on a homogeneous and a patterned capture surface without considering a reaction rate. Two separate simulations were run and compared to evaluate the impact of surface patterning. The homogeneous surface was simulated as a two dimensional system relying on the symmetry in the y-direction, whereas the patterned surface had to be modelled as a three dimensional structure and split into smaller parts to decrease computation complexity.

The following set-up guides will go through the configuration of COMSOL node by node in the model builder.

A.1.1 *Setting Up the Simulation*

Homogeneous capture surface.

1. Model Wizard.
   (a) Select space dimension: 2D.
   (b) Select physics: Transport of Diluted Species (tds).
   (c) Select study: Stationary.
2. Parameters
   (a) Input the parameters listed in Table A.1.
3. Geometry
   (a) Right click the Geometry node and create a rectangle.
   (b) Enter "L" as the width and "H" as the height.
   (c) Click Build.

Table A.1: Parameters used in the simulation of a fully absorbing, homogenous surface.

Name	**Expression**	**Description**
H	100[μm]	Height of the channel
L	15[mm]	Length of the channel
W	1[mm]	Width of the channel
Q	1[μl/min]	Flow rate
c0	1[pM]	Bulk concentration
D	1e-10[m^2/s]	Diffusion constant

4. Transport of Diluted Species

   (a) In settings → Transport mechanisms, the checkbox "convection" should be enabled.

   (b) Transport properties:

      i. Add a user defined velocity field

x	6/H^3*W)*Q*(H-y)*y
y	0

      ii. Define the diffusion coefficient as D.

   (c) Right click the Transport of Diluted species node and add two concentration boundaries and an outflow boundary.

      i. Concentration 1: Set "species c" to 0 and select the reacting surface.

      ii. Concentration 2: Set "species c" to c0 and select the inlet.

      iii. Outflow 1: Select the outlet.

5. Mesh

   (a) In the Size node, set to extremely fine.

   (b) Right click the Mesh node and add a free triangular mesh node. Then add a Size node to that. Choose "Boundary" as the geometric entity level and select the reactive surface. Choose user defined size and set the maximum element size to 1 μm.

6. Study

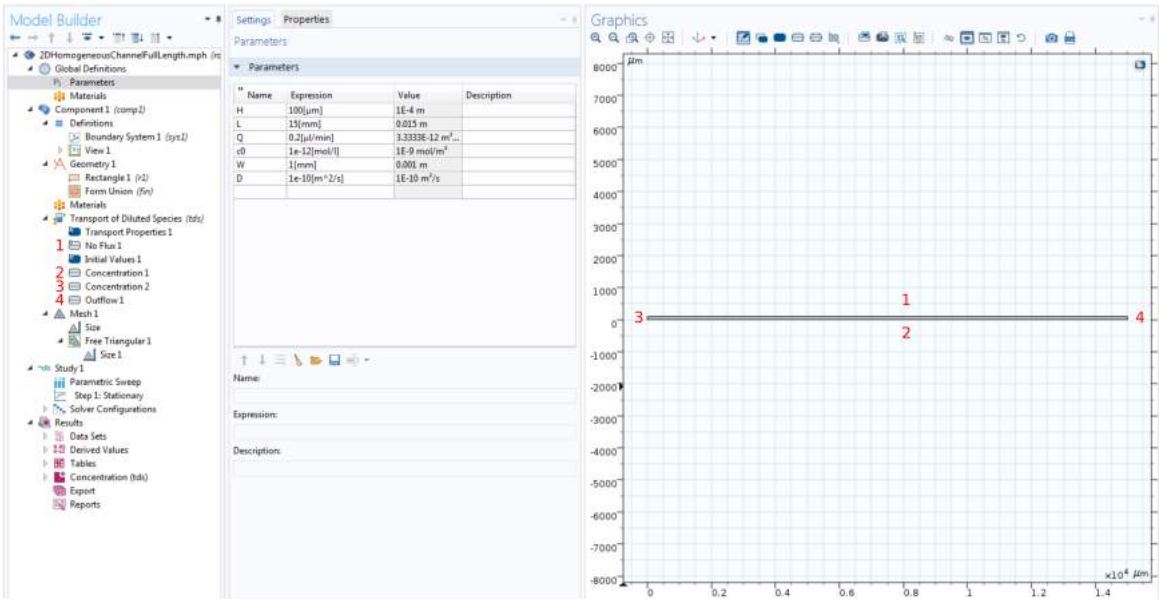

Figure A.1: COMSOL user interface after following the set up guide for the fully absorbing, homogeneous sensor.

(a) Right click the Study node and add a parametric sweep.

(b) Choose all combinations and add the parameters D and Q as the swept parameters.

(c) Set the values of Q as 0.05, 0.1, 0.5, 1, 2, and 5 μl/min.

(d) Set the values of D as 1e-10, 1e-11, 1e-12, and 1e-13 m^2/s.

(e) Click "Compute".

Figure A.1 shows how the interface of COMSOL should look like after setting up the simulation, including definition of the geometry.

Patterned capture surface.
The patterned capture surface was split up in pieces of 1 by 100 spots in order to reduce the complexity of the computation. If some of the steps are valid for some iterations only, this will be noted in the specific step.

1. Model Wizard.

   (a) Select space dimension: 3D.

   (b) Select physics: Transport of Diluted Species (tds).

Table A.2: Parameters used in the simulation of a fully absorbing, patterned surface.

Name	Expression	Description
H	100[μm]	Height of the channel
W	1[mm]	Width of the channel
Q	1[μl/min]	Flow rate
c0	1[pM]	Bulk concentration
D	1e-10[m^2/s]	Diffusion constant
n	100	Number of spots
s	2[μm]	Radius of spot
d	4[μm]	Diameter of spot

(c) Select study: Stationary.

(a) Input the parameters listed in Table A.2.

2. Definitions (only for iteration 2 and higher).

(a) Right click the definitions node and add an interpolation.

(b) Choose Local table as the data source and open the .csv file containing the output concentration profile from the previous iteration.

(c) The unit of the argument is μm, and the unit of the function is mol/m^3.

3. Geometry.

(a) Right click the geometry node and create a block.

(b) The width of the block is (s+d), the depth of the block is n*(s+d), and the height of the block is H.

(c) Right click the geometry node and add a Work Plane with the type Quick plane, Plane type xy-plane, off set from z by 0.

(d) Right click the plane geometry node to add a circle with radius s centered at x (s+d)/2 and y s/2+s.

(e) Right click the plane geometry to add an array located under transforms.

(f) Choose the circle as the input object, the array size as 1 by n, and the displacement as s+d in the y-direction.

4. Transport of Diluted Species (tds).

   (a) In settings → Transport mechanisms, the checkbox "convection" should be enabled.

   (b) Transport properties:

      i. Add a user defined velocity field

x	0
y	6/H^3*W)*Q*(H-z)*z
z	0

      ii. Define the diffusion coefficient as D.

   (c) Right click the Transport of Diluted species node and add two concentration boundaries (iteration 1 only), a periodic condition, and an outflow boundary. For iterations 2 and higher, add an inflow boundary in stead of one concentration boundary.

      i. Concentration 1: Set "species c" to 0 and select the reacting surfaces.

      ii. Concentration 2: Set "species c" to c0 and select the inlet (only iteration 1).

      iii. Inflow 1: Set the concentration to int1(z) and select the inlet (only iteration 2 and higher).

      iv. Periodic Condition 1: Select the two sides (yz-plane) of the block to create an open boundary, simulating that the channel continues in the x-direction.

      v. Outflow 1: Select the outlet.

5. Mesh

   (a) In the Size node, set to extremely fine.

   (b) Right click the Mesh node and add a free triangular mesh node. Then add a Size node to that. Choose "Boundary" as the geometric entity level and select all the spots. Choose user defined size and set the maximum element size to 0.1 μm.

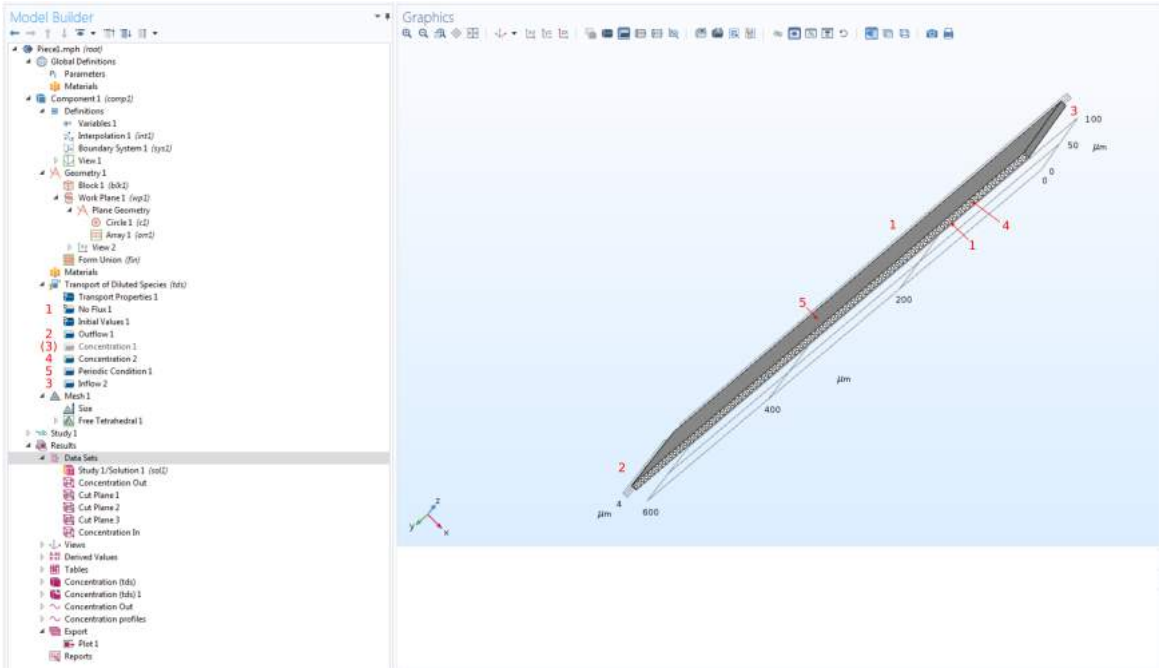

Figure A.2: COMSOL user interface after following the set up guide for the fully absorbing, patterned sensor.

6. Study: Press Compute

7. Results

   (a) After running the simulation locate the Data sets node in the Results and right click to create a 3D cut line.

   (b) Enter the coordinates for the cut line: (s+s/2, n*(d+s),0) and (s+s/2, n*(d+s),H).

   (c) Right click the results node and add a 1D plot group.

   (d) Right click the 1D plot group to add a line graph. Choose the 3D cut line in the data set and set the expression to c with unit mol/m^3.

   (e) Right click the export node and add a plot. Select the 1D plot group and choose a file location. Save the file as .csv and press export. The generated file is used in the next iteration as the input concentration profile (step 2b).

Figure A.2 shows the interface on COMSOL after following the set up guide for the patterned sensor surface.

Table A.3: Parameters used in the simulation of a homogenous surface using a first order rate equation.

Name	Expression	Description
H	100[μm]	Height of the channel
L	15[mm]	Length of the channel
W	1[mm]	Width of the channel
Q	1[μl/min]	Flow rate
c0	1[pM]	Bulk concentration
D	1e-10[m^2/s]	Diffusion constant
Gamma_s	20[nmol/m^2]	Probe surface concentration
k_ads	390e3[1/(M*s)]	On rate
k_des	0.1e-4[1/s]	Off rate

A.2 2D FEM Analysis of Homogeneously Covered Capture Surfaces

This section describes how to set up the simulations in two dimensions, utilising the symmetry in the y-direction to reduce the required dimensionality. These simulations investigated the capture of target molecules and the effect of the model parameters.

A.2.1 *Setting Up the Simulations*

1. Model Wizard.
   (a) Select space dimension: 2D.
   (b) Select physics: Transport of Diluted Species (tds) and General Form Boundary PDE (gb).
      i. In the settings for the general form boundary PDE, name the dependent variable cs, and define the unit for the dependent variable as mol/m^2, and the unit for the source term as mol/(m^2*s).
   (c) Select study: Time dependent.
2. Parameters
   (a) Input the parameters listed in Table A.3.
3. Definitions
   (a) Right click the definitions node and add two variables.

(b) Variables 1: For the entire domain define the variable v_lam with the expression 6/(H^3*W)*Q*(H-y)*y.

(c) Variables 2: For the reacting boundary define the variable R with the expression k_ads*c*(Gamma_s-cs)-k_des*cs.

4. Geometry

(a) Right click the Geometry node and create a rectangle.

(b) Enter "L" as the width and "H" as the height.

(c) Click Build.

5. Transport of Diluted Species

(a) In settings → Transport mechanisms, the checkbox "convection" should be enabled.

(b) Transport properties:

i. Add a user defined velocity field

x	v_lam
y	0

ii. Define the diffusion coefficient as D.

(c) Right click the Transport of Diluted species node and add one concentration boundary, one flux boundary, and an outflow boundary.

i. Flux 1: Set "species c" to -R and select the reacting surface.

ii. Concentration 2: Set "species c" to c0 and select the inlet.

iii. Outflow 1: Select the outlet.

6. Mesh

(a) In the Size node, set to extremely fine.

(b) Right click the Mesh node and add a free triangular mesh node. Then add a Size node to that. Choose "Boundary" as the geometric entity level and select the reactive surface. Choose user defined size and set the maximum element size to 1 μm.

7. Study

   (a) Right click the Study node and add a parametric sweep. In the next section, the different parameter sweeps are elaborated.

   (b) In the time dependent study node, define the range of times for which the simulation computes solutions. These ranges are also elaborated in the next section for each parameter sweep.
   (c) Click "Compute".

Parametric Sweeps to Investigate the Impact of Model Parameters

Investigation of equilibrium times.
For the investigation of the time it takes the system to reach equilibrium, three simulations were run with varying c_0. For each concentration, a parametric sweep was performed, where the diffusivity, D, with values of $1 \cdot 10^{-10}$ m^2/s, $1 \cdot 10^{-11}$ m^2/s, and $1 \cdot 10^{-12}$ m^2/s. For $c_0 = 1$ fM and 1 pM, the time dependent study was calculated from 0 hours to 5000 hours in steps of 100 hours, whereas for the 1 μM bulk concentration the results were calculated from 0 seconds to 180 seconds in steps of 10 seconds (0 to 90 s with steps of 5 s for $D = 1 \cdot 10^{-10}$ m^2/s).

For all of the following simulations, solutions were obtained at times 1 hour, 2 hours, 3 hours, 4 hours, 12 hours, and 24 hours.

Investigation of the effect of the rate constants.
Two parametric sweeps were performed for investigating the effect of the rate constants on the number of bound molecules. First, k_{des} was kept constant at $0.1 \cdot 10^{-4}$ s^{-1} and k_{ads} was varied with the values 50, 100, 150, 200, 250, 300, 350, and 390 m^3/(mol s). Next, k_{ads} was kept constant at 390 m^3/(mol s) while k_{des} was varied with the values 0.1, 1, 5, 10, 20, and 40 $\cdot 10^{-4}$ s^{-1}.

Varying the diffusion constant.
A parametric sweep varying the diffusion constant was performed next with the values of D = $1 \cdot 10^{-10}$ m^2/s, $1 \cdot 10^{-11}$ m^2/s, $1 \cdot 10^{-12}$ m^2/s, and $1 \cdot 10^{-13}$ m^2/s. This corresponds to the diffusivity of nucleic acids from short fragments to fragments several kb in length.

Varying the flow rate.
Lastly the flow rate was varied. Two parametric sweeps were performed for two values of D, namely $1 \cdot 10^{-10}$ m^2/s and $1 \cdot 10^{-12}$ m^2/s. The flow rate, Q, was varied with the values 0.01, 0.1, 0.5, 1, 2, and 5 μl/min in both cases.

B LabView Software for Controlling the Optomechanical Detection Platform

B.1 LabView Scripts

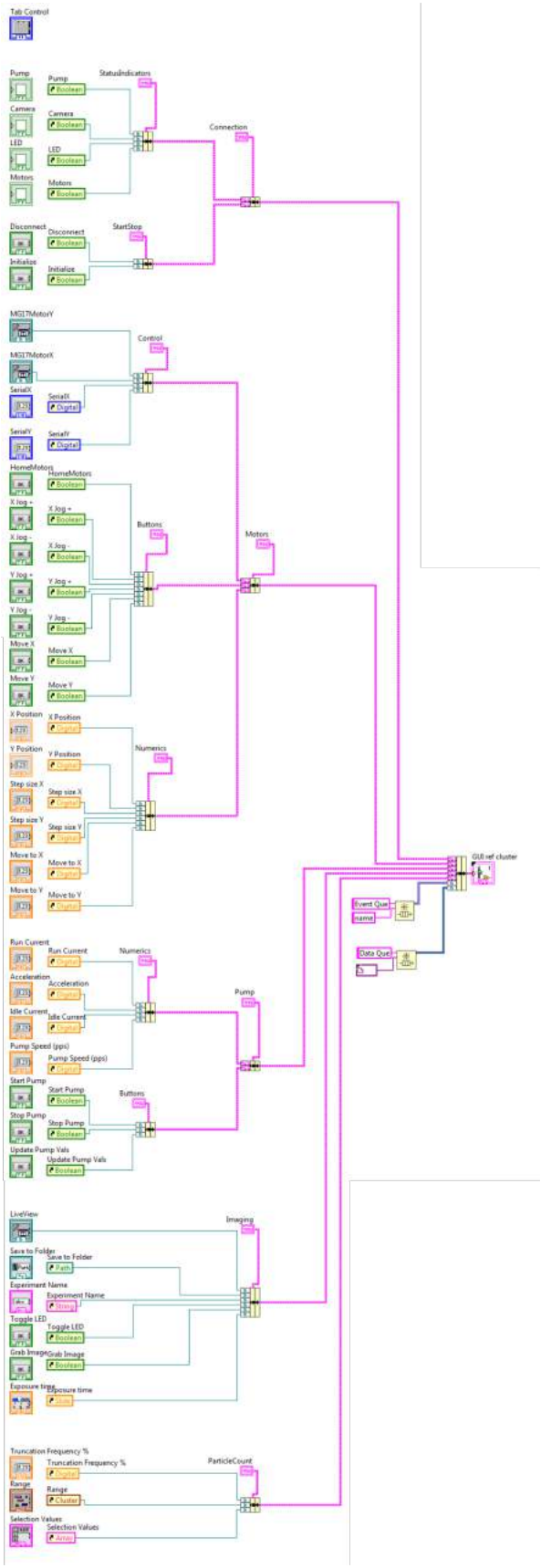

Figure B.1: The GUI Block diagram building the GUI reference cluster.

C | Standard Curves for the Detection of A-β_{1-42} and ApoE3

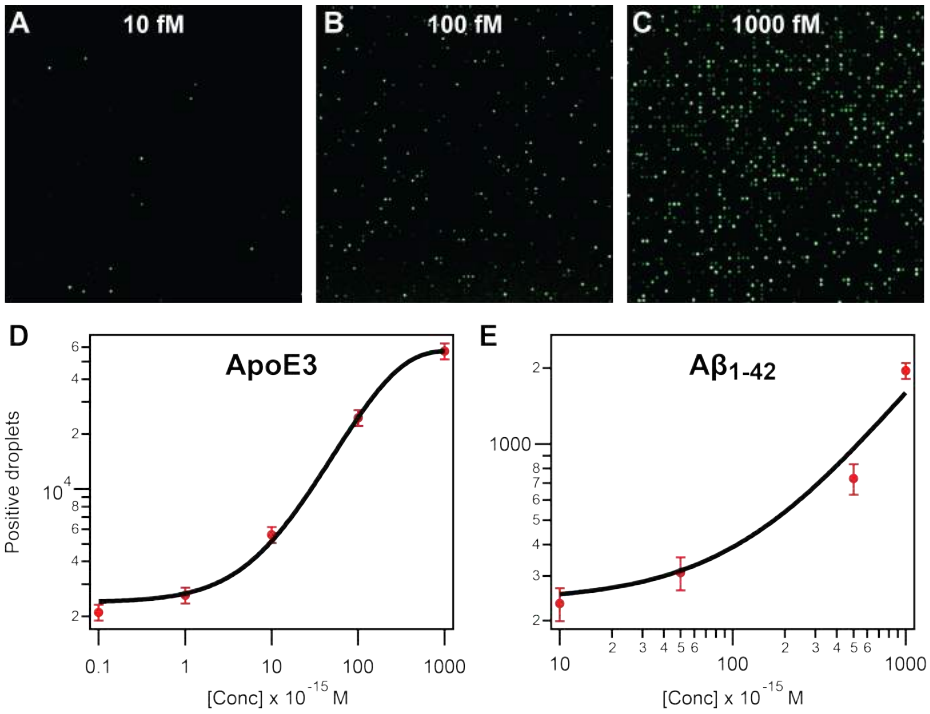

Figure C.1: Standard curves for the detection of ApoE3 and Aβ_{1-42} by digital ELISA. A) Fluorescence micrograph showing positive signals in the digital ELISA from 10 fM synthetic Aβ_{1-42}. B) Fluorescence micrograph showing positive signals in the digital ELISA from 100 fM synthetic Aβ_{1-42}. C) Fluorescence micrograph showing positive signals in the digital ELISA from 1000 fM synthetic Aβ_{1-42}. D) Standard curve for the protein ApoE3. E) Standard curve for the protein Aβ_{1-42}. This figure was produced by Andreas Hjarne Kunding.

D | Publications and Conference Contributions

D.1 Peer-reviewed Publication

Micro-droplet arrays for micro-compartmentalization using an air/water interface
Andreas H. Kunding, Louise L. Busk, Helen Webb, Hans W. Klafki, Markus Otto, Jörg P. Kutter and Martin Dufva. Lab Chip, 2018,18, 2797-2805.
https://pubs.rsc.org/en/content/articlelanding/2018/lc/c8lc00608c#!divAbstract

D.2 Conference Contribution - Micro- and Nano-engineering Copenhagen 2018

A Multistep Cell-free Protein Expression and Detection Assay on Microdroplet Arrays

Louise L. Busk [a], Martin Dufva [a]

[a] Dept. of micro- and nanotechnology, Technical University of Denmark, 2800 Kgs. Lyngby, Denmark.

E-mail: Martin.Dufva@nanotech.dtu.dk

Keywords: Droplet arrays, Cell-free protein expression, droplet microfluidics, water-in-air droplets, solid-phase droplet microfluidics, high throughput screening, protein arrays.

By conducting cell-free protein expression, capture, and detection on a microdroplet array (MDA) platform, we describe the ability to perform multi-step reactions in solid-phase microdroplets, a platform which have been used primarily for single-step reactions such as digital ELISA[1]. The aim of doing so is to advance the microdroplet platform towards high-throughput screening applications, e.g. protein arrays, for which the platform is highly suitable[2]. The problems which have limited this advancement include, but is not limited to: (i) droplet stability in the absence of a seal (oil or other); (ii) addition of reagents in multi-step experiments[2]; (iii) retrieval of positive hits in a (semi-)automated manner. On our droplet platform we have shown that droplets can remain stable in air for several hours, which allows us to perform incubations required for many multistep assays, and allows us to switch between reaction in bulk and in droplets several times. By immobilizing the molecules of interest on the surface, adding new reagents to the droplets become trivial. However, the problem of retrieving droplets containing molecules of interest remains to be solved. The combination of the microdroplet platform with cell-free protein expression furthermore offers the benefit of overcoming the comprehensive production of functional proteins for protein arrays while further reducing the reagent consumption compared to performing the protein array in microtiter plates[3].

Cell-free protein expression was carried out on a hydrophilic-in-hydrophobic droplet array embedded in a microfluidic channel. One droplet chip contains 16 fluidic channels, each with 400.000 droplets. Figure 1A shows a sketch of the cleanroom fabrication steps and the finished MDA. Droplets are generated in less than a minute by passing a plug of liquid through the fluidic channel, actuated by a peristaltic pump. Droplet evaporation was avoided by adding a small amount of liquid in the inlet and outlet without interfering with the array, and keeping the chip in a humid environment. To capture expressed proteins on the surface, the glass spots were functionalized with polyethylene glycol (PEG) carrying a poly-l-lysine (PLL) in one end and a nitrilotriacetic acid (NTA) group in the other end, allowing poly-His-tagged proteins to be captured. A commercially available coupled transcription and translation kit was used to express proteins inside the femto-liter droplets from trapped double stranded DNA consisting of a linear oligonucleotide containing a T7 promoter, a ribosomal binding site, a His(6) encoding sequence, and a sequence of interest. Two peptide sequences were expressed in ratio 1:100 (target peptide to background peptide DNA), with the concentration of target peptide DNA corresponding to 0.1 molecules per droplet. As a positive control, target peptide DNA was added in a concentration corresponding to 10 molecules per droplet, and the negative control contained no target peptide DNA, only background peptide DNA. Figure 1B describes the two-step process of expressing, binding, and detecting the proteins. After expression in the droplets, it was verified that the surface had not been fouled due to high protein content, and was still able to support droplets (see Figure 2A). Droplets with bound target peptides were detected with an anti-target antibody-HRP conjugate, which produce a strongly fluorescent product from a non-fluorescent substrate. Figure 2B-D displays fluorescence micrographs of B) the background signal of the antibody-HRP conjugate (no target DNA present during expression), C) the antibody-HRP bound to proteins expressed in the droplets with 0.1 molecules of target template per droplet, and D) the antibody-HRP bound to proteins expressed in the droplets with 10 molecules of target template per droplet. These results show that two independent operations, each requiring portioning, is possible and is a step towards HTS applications.

[1] D. M. Rissin et al., *Nature Biotech.* 28(6) (2010) 595-599.
[2] W. Feng, E. Ueda, P. A. Levkin, *Adv. Mater.* (2018) 1706111
[3] M. He, M. J. Taussig, *Nucl.Acids Res.* 29(15) (2001)

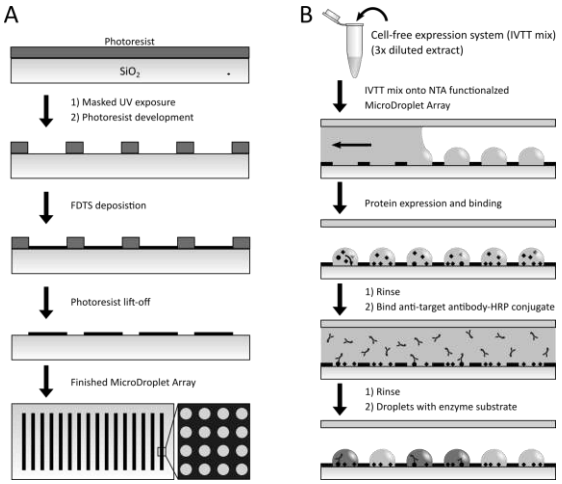

Figure 1 A) Cleanroom fabrication process resulting in hydrophilic SiO_2 spots surrounded by a hydrophobic FDTS coating. B) Protein expression assay in droplets followed by binding and detection with antibody-HRP conjugates. Darker droplets indicate fluorescent product due to target presence.

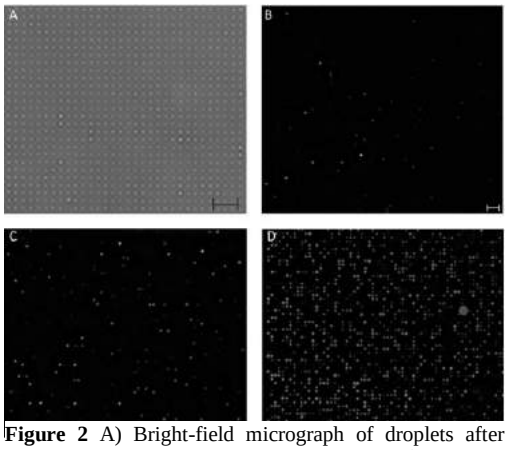

Figure 2 A) Bright-field micrograph of droplets after protein expression. B) Background binding of antibody-HRP conjugate. C) Peptide expression with 0.1 template copies per droplet. D) Peptide expression with 10 template copies per droplet. Scale bar is 20 µm.

DTU Nanotech
Department of Micro- and Nanotechnology

A Multistep Cell-free Protein Expression and Detection Assay on Microdroplet Arrays

Louise L. Busk, Martin Dufva

Background

Microdroplet arrays (MDAs) are used for compartmentalization of biochemical reactions. One application is single molecule ELISA, detecting biomarkers in sub-femtomolar concentrations.[1,2] Due to the need to seal the droplets to prevent evaporation, only single step reactions are commonly performed. Here we perform cell-free protein expression, binding, and detection on a droplet array, requiring two compartmentalization steps.

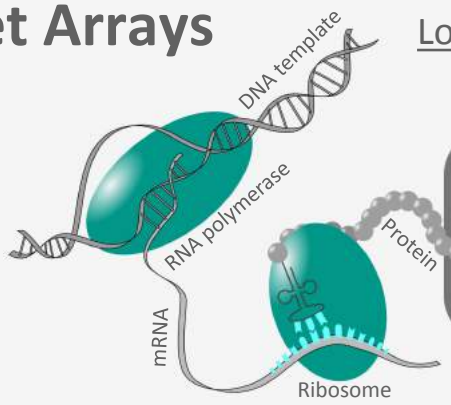

Aim

- Show a multi-step reaction on a solid-phase microdroplet array.

Fabrication

The MDA supporting glass slide is prepared in the cleanroom. Fig. 1 shows the fabrication steps. The hydrophobic FDTS coating sur-rounding the hydrophilic SiO_2 spots allow spontaneous formation of droplets. Microfluidic channels (COC polymer) are tape bonded to the glass slide

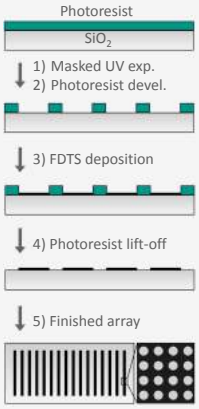

Fig. 1 Cleanroom process for the fabrication of MDAs. Glass patterned with photoresist is treated with FDTS using molecular vapour deposition.

Assay

The cell-free protein expression reaction steps are shown in Fig. 2. Two annealed, complimentary DNA oligo-nucleotides served as template. The structure and subunits of the template is shown below.

Fig. 2 Protein expression in droplets followed by binding and detection by antibody-HRP conjugates. Incubation in droplets with HRP substrate produce fluorescence (dark droplets) in droplets containing the target.

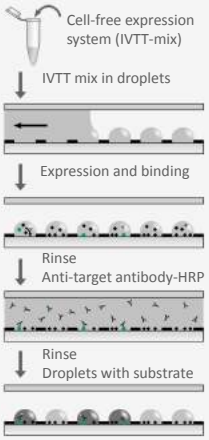

Results

Fig. 3 shows bright-field and fluorescence micrographs after expression and detection. The percentage of the measured droplets which fluoresced were recorded (see Tab. 1) and compared to the theoretical copy number.

	λ_{target}	$\lambda_{non\text{-}target}$	% exp.	% Theoret.
B	0	10	1.1%	0 %
C	0.01	10	0.9%	1 %
D	1	10	29%	63 %

Tab. 1 The percentage of fluorescing droplets (n=4000) counted from micrographs (fig.3 B-D) and the theoretical template copy number per droplet, λ. Background has been subtracted from C and D.

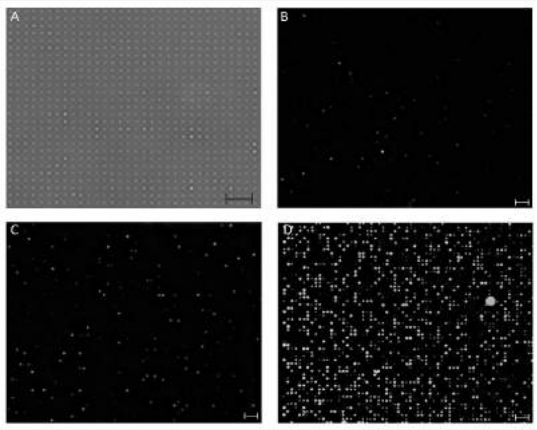

Fig.3 A) Bright-field micrograph of droplets after protein expression. B) Background binding of antibody-HRP conjugate in the absence of target. C) Peptide expression with 0.1 template copies per droplet. D) Peptide expression with 1 template copy per droplet. Scale bar is 20 µm.

Conclusion

Comparing our results to the theoretical number of droplets containing a target (Poisson statistics), fewer droplets fluoresced than expected. Some explanations include:

- Efficiency of oligo synthesis is not 100%
- Efficiency of annealing is not 100%

Conclusively, we have demonstrated a two-step reaction, and considering the known errors, it can be concluded that the efficiency of the expression of proteins was good.

[1] Rissin, D. M. et al. Nat. Biotechnol. 28, 595–599 (2010).
[2] Wang, T. et al. Lab Chip 13, 4190–7 (2013)

Contact

E-mail:
mallbu@nanotech.dtu.dk

Dept. of Micro- and Nanotechnology
Technical University of Denmark
2800 Kgs. Lyngby

Thanks to DTU Nanotech for supporting this research.

D.3 Conference Contribution - Lab-on-a-Chip and Microfluidics World Congress San Diego 2018

Cheap fabrication of solid phase droplet microfluidics chips for single molecule studies

Miniaturization offers great benefits in areas such as high throughput screening, single cell analysis, and molecular diagnostics, and particularly micro-scale compartmentalization has provided the ability to improve not only sensitivity and specificity but also the speed, cost and throughput.[1–3] Micro-scale compartmentalization has been achieved using physical wells in either polydimethylsiloxane (PDMS), silicon, glass or waveguides, or by partitioning using hydrophilic patches on a hydrophobic background, or a combination of both, and has been used for single cell analysis[4], single molecule counting[5], digital ELISA[6–8] and more. Here, we present the fabrication of a droplet array platform using a new and inexpensive photoresist using simple and fast fabrication methods, which is capable of supporting down to femtoliter droplets. We describe the parameters governing the thickness of the photoresist layer, as well as demonstrate the photo-patterning and droplet formation on the platform. The array is packaged in a microfluidic system where the droplets are protected from evaporation[9] without the use of an oil cover, as this has been shown to allow diffusion of small and large molecules.[10–12]

1. Kelly, B. T., Baret, J. C., Taly, V. & Griffiths, A. D. Miniaturizing chemistry and biology in microdroplets. *Chem.Commun.(Camb.)* 1773–1788 (2007). doi:10.1039/b616252e

2. Theberge, A. B. *et al.* Microdroplets in microfluidics: An evolving platform for discoveries in chemistry and biology. *Angew. Chemie - Int. Ed.* **49,** 5846–5868 (2010).

3. Griffiths, A. D. & Tawfik, D. S. Miniaturising the laboratory in emulsion droplets. *Trends Biotechnol.* **24,** 395–402 (2006).

4. Du, G. S. *et al.* Cell-based drug combination screening with a microfluidic droplet array system. *Anal. Chem.* **85,** 6740–6747 (2013).

5. Rissin, D. M. & Walt, D. R. Digital concentration readout of single enzyme molecules using femtoliter arrays and poisson statistics. *Nano Lett.* **6,** 520–523 (2006).

6. Rissin, D. M. *et al.* Single-molecule enzyme-linked immunosorbent assay detects serum proteins at subfemtomolar concentrations. *Nat. Biotechnol.* **28,** 595–599 (2010).

7. Wang, T., Zhang, M., Dreher, D. D. & Zeng, Y. Ultrasensitive microfluidic solid-phase ELISA using an actuatable microwell-patterned PDMS chip. *Lab Chip* **13,** 4190–7 (2013).

8. Kim, S. H. *et al.* Large-scale femtoliter droplet array for digital counting of single biomolecules. *Lab Chip* **12,** 4986–4991 (2012).

9. Kunding, A. H. *et al.* Micro-droplet arrays for micro-compartmentalization using an air/water interface. *Lab Chip* **16,** (2018).

10. Sakakihara, S., Araki, S., Iino, R. & Noji, H. A single-molecule enzymatic assay in a directly accessible femtoliter droplet array. *Lab Chip* **10,** 3355–3362 (2010).

11. Fletcher, P. D. I. & Parrott, D. The partitioning of proteins between water-in-oil microemulsions and conjugate aqueous phases. *J. Chem. Soc. Faraday Trans. 1* **84,** 1131–1144 (1988).

12. Huebner, A. *et al.* Static microdroplet arrays: a microfluidic device for droplet trapping, incubation and release for enzymatic and cell-based assays. *Lab Chip* **9,** 692–698 (2009).

DTU Nanotech
Department of Micro- and Nanotechnology

Cheap fabrication of solid phase droplet microfluidics chips for single molecule studies

Louise L. Busk, Martin Dufva - Dept. of Micro- and nanotechnology, Technical University of Denmark, 2800. Kgs. Lyngby

Introduction

Microdroplet arrays are used for compartmentalization of biochemical reactions. They enable single molecule detection with great sensitivity[1], which is particularly interesting in e.g. molecular diagnostics[2] and high-throughput screening. The availability of such platforms depend on price and ease of fabrication. Here, we present an easy to fabricate hydrophilic in hydrophobic droplet array chip for less than $10 per chip.

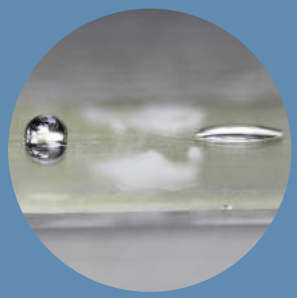

Properties of FluorAcryl 3298

CYTONIX FluorAcryl 3298 is a negative tone, hydrophobic photoresist based on fluorinated acrylate. The contact angle with water was measured to be 100° after UV curing and development (Figure 1). FluorAcryl 3298 is photopatternable through standard photo-lithographic methods. Besides being hydrophobic and oleophobic, FluorAcryl 3298 has good chemical resistance and is anti-fouling.

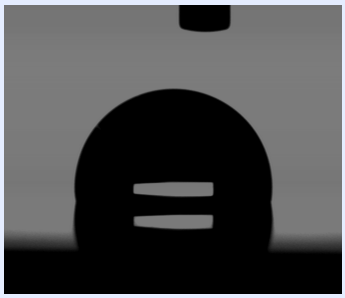

Figure 1: Photograph of a 2 µL droplet on FluorAcryl 3298 taken using a drop shape analyzer. The contact angle is measured to be 100°.

Fabrication of microdroplet arrays

Microdroplet arrays were produced by spin coating a thin film of FluorAcryl, then, the solvent was evaporated by heating the wafer to 80°C. Masked UV exposure produced a pattern in the FluorAcryl film, visible after dissolving the uncured resist in either ethyl acetate or butyl acetate (see Fig. 2).

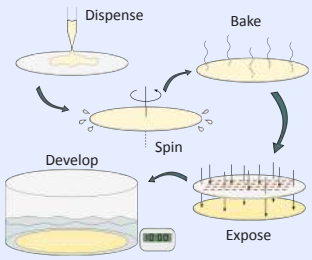

Figure 2: Fabrication steps for making FluorAcryl arrays on glass wafers

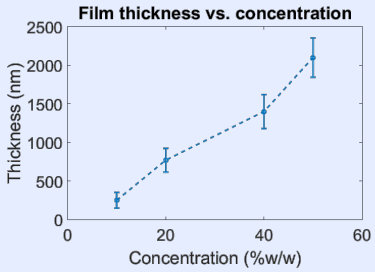

Figure 3: Film thickness vs. FluorAcryl concentration (30 s at 3000 rpm). Error bars represent std (n=3).

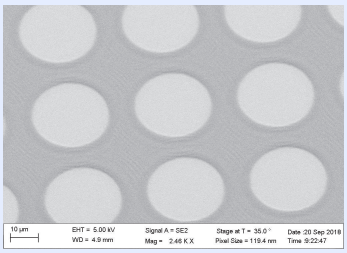

Figure 4: SEM micro-graph of 25 µm in diameter holes in a 175 nm thick film of FluorAcryl

Results

The thickness of the FluorAcryl film was primarily dependent on the concentration of FluorAcryl when spin coating the wafer. Dilution in ethyl or butyl acetate to between 10 and 50 %w/w produced films 200 to 2000 nm thick measured using a stylus profilometer (see Fig. 3). SEM inspection (see Fig. 4) in combination with topological measurements using a stylus profilometer revealed that photo patterning was complete, and microscope images of aqueous droplets supported this (see Fig 5).

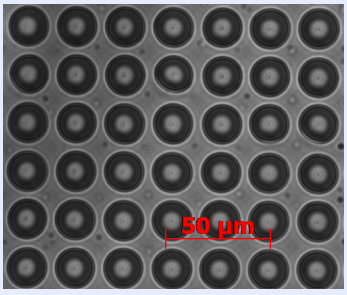

Figure 5: Aqueous droplets 25 µm in diameter on patterned Fluor-Acryl.

Conclusion

FluorAcryl 3298 has advantageous properties for fabricating microdroplet arrays. Other fluorinated polymers has been used for this purpose[3], however at a much higher price. Here we have shown that FluorAcryl 3298 is photopatternable using a single step lithographic process, and that arrays fabricated in this manner can support aqueous droplets.

[1] Y. Rondelez et al., Nat. Biotech., 2005, 23(3), 361-365
[2] D. M. Rissin et al., Nat. Biotech., 2010, 28(6), 595-599
[3] R. Iino et al., Lab Chip, 2012, 12, 3923-3929

Contact me

E-mail: mallbu@nanotech.dtu.dk

Dept. of Micro- and Nanotechnology
Technical University of Denmark
2800 Kgs. Lyngby

www.linkedin.com/in/louiselaubbusk

DTU Health Tech
Department of Health Technology
Danmarks Tekniske Universitet

Ørsteds Plads, Building 345C
2800 Kgs. Lyngby

www.healthtech.dtu.dk